Assessing the influence of environmental pH on algal physiology using a novel culture system

By

Rachel L. Golda

A DISSERTATION

Presented to the Division of Environmental and Biomolecular Systems
and the Oregon Health & Science University
School of Medicine
in partial fulfillment of
the requirements for the degree of

Doctor of Philosophy
in
Environmental Science and Engineering

August, 2017

School of Medicine
Oregon Health & Science University

CERTIFICATE OF APPROVAL

This is to certify that the PhD dissertation of
Rachel L. Golda
has been approved

_____
Mentor/Advisor: Tawnya Peterson
(Oregon Health & Science University)

_____
Mentor/Advisor: Joseph Needoba
(Oregon Health & Science University)

_____
Committee Chair: Paul Tratnyek
(Oregon Health & Science University)

_____
Member: Anne Thompson
(Portland State University)

TABLE OF CONTENTS

LIST OF TABLES

LIST OF FIGURES

APPENDIX A

APPENDIX B

LIST OF EQUATIONS

ACKNOWLEDGMENTS

This work supported by the United States Environmental Protection Agency (through a Science to Achieve Results (STAR) Graduate Fellowship to RLG) and Oregon Sea Grant (through a Robert E. Malouf Marine Studies Scholarship to RLG) and by NSF Cooperative agreement OCE-0424602 (the Center for Coastal Margin Observation and Prediction).

This work would not have been possible without the help, assistance, counsel, and advice of many people. I would like to first give my heartfelt thanks to my advisors, Drs. Tawnya Peterson and Joseph Needoba, for the guidance, support, advice, and opportunities they made available to me during my graduate studies, and whose mentorship and constructive criticism made this thesis what it is today. I would like to thank Dr. Rick Johnson, who provided his LabVIEW® expertise for pHstat programming, and Mr. Mark Golda, who provided electromechanical troubleshooting during the pHstat design and build phase. Thanks are also due to Dr. Michiko Nakano for her counsel and for answering my many questions with regard to the radioactivity work and the defense process. I also wish to thank my current and past committee members Drs. Paul Tratnyek, Anne Thompson, Kimberly Halsey, Tawnya Peterson, and Joseph Needoba for their careful review of my thesis. Great thanks to Bonnie Gibbs, Margaret Mascsak, Vanessa Green, Amy Johnson, Karen Camp, and Nievita Bueno Watts for helping me over many administrative hurdles along the way. Heartfelt thanks to my undergraduate interns over the years, for learning alongside me and for the grunt work they put in running countless pHstat tests (Jacqueline Hayes), microscopy counts (Maria Nunez), and SNARF EEMs (Lauren Roof). Thank you to my lab mates, who did life alongside me in the proverbial trenches: Estefania Llaneza Garcia, Michelle Maier, Claudia Tausz, Sheree Watson, and Brittany Cummings.

My last and best thanks are for the people who supported me behind the scenes. To my friends, who put up with random phytoplankton or ocean references in everyday conversation and cheer me on constantly. To my parents, Mark and Silvana Golda, thank you for being my biggest encouragers (tied with Galen!) and for keeping me grounded. Without your unflagging encouragement and support I could not have gotten this far. Period. Thank you so much for your faith in me, and for giving me the springboard to get this far. Finally, to my fiancé, Galen VanEeckhoutte, who has been my pit crew for the last mile of this long race, you've had incredible patience while I gave countless hours to writing and processing data instead of spending time with you. You have given me perspective, a (usually) willing audience, and never ending emotional support. Your love and pride in me have been an amazing gift through this process. Thank you.

ABSTRACT

Since the Industrial Revolution, surface ocean pH has declined due to the input of anthropogenically derived carbon dioxide, termed ocean acidification. Examinations of phytoplankton physiology in the face of changing pH are becoming more important as anthropogenically-driven pH decreases in the surface ocean progress (termed ocean acidification). Previous research has shown that phytoplankton response to acidification are highly variable, with some taxa showing improvement and some showing marked deterioration. The ability to maintain homeostasis of intracellular pH is an important adaptation for phytoplankton to continue to thrive under changing conditions; increased energy production has been shown to mitigate the negative effects of acidification. This dissertation examines the effect of steady state and changing pH environments on the internal pH, esterase activity, and photosynthetic efficiency (the latter two parameters are involved with energy production or utilization) of the marine phytoplankton species, *Isochrysis galbana*. To accomplish this, a novel pHstat system was developed for the culture of marine phytoplankton, capable of maintaining both steady state and dynamic pH environments autonomously over extended periods. The pHstat system was used to grow phytoplankton at three steady state pH levels (pH 7.5, 8.0, and 8.5), as well under two separate dynamic conditions. The dynamic conditions were differentiated by coupling or decoupling light cycles from their natural relationship with pH (i.e., pH increases during the day due to photosynthetic uptake of inorganic carbon and decreases at night due to carbon addition through cellular respiration) in an effort to determine if intracellular pH changes were driven by changes in external pH or by changes in internal pools of dissolved inorganic carbon (DIC) availability due to carbon fixation and cellular respiration. To determine intracellular pH using a rapid, reliable method, I explored the efficacy of the fluorescent

intracellular pH indicator for phytoplankton work, SNARF, and its suitability for use in phytoplankton cultures. Three methods of fluorescence detection (fluorescence spectroscopy, flow cytometry, and laser scanning microscopy) were compared as methods of fluorescence detection. Fluorescence detection was found to be dependent on the loading concentration of the fluorophore for flow cytometry; higher sensitivities were achieved using fluorescence spectroscopy and microscopy, which enabled the use of lower concentrations of the dye. Because of the greater flexibility in choice of excitation and emission wavelengths, fluorescence spectroscopy was found to be the superior method for pH measurement, with lower percent error and more reliable calculations of pH_i. However, the use of flow cytometry with SNARF has the added advantage of providing viability data for individual cells, as SNARF only accumulates within live, intact cells. Using the novel culture system and the pH sensitive dye, SNARF, I determined that intracellular pH changes in *I. galbana* fluctuated in response to changing external pH, not light:dark cycles. Esterase activity was highest in cells with the lowest photosynthetic efficiency, suggesting a link between esterase activity and energy production/demand, as cells can use esterases to access energy stored in the form of lipids. This work presents new links between cellular energy balance in phytoplankton and environmental pH response, providing valuable data regarding microalgal adaptation to changing ocean pH as ocean acidification progresses.

CHAPTER 1

Introduction

1.1 Ocean acidification and aquatic carbon chemistry

Since the commencement of the Industrial Revolution, land-use changes and anthropogenic use of fossil fuels have caused a massive increase in the amount of CO_2 present in the atmosphere. This has resulted in a concurrent reduction in surface ocean pH, termed ocean acidification (OA). Surface ocean pH has dropped globally by an average of approximately 0.1 units (Doney, Fabry, et al. 2009). OA is caused by changes in seawater carbonate chemistry resulting from the increased air-sea flux of carbon dioxide into the upper ocean. This flux is driven by the steady rise in anthropogenic atmospheric CO_2 since the early twentieth century. As more CO_2 gas enters the atmosphere, more CO_2 dissolves in the surface ocean.

pH and aquatic carbon partitioning are intimately linked. Aqueous CO_2 combines with water to form the transition species carbonic acid (H_2CO_3). Carbonic acid reversibly dissociates to form bicarbonate (HCO_3^-) and an H^+ ion. Bicarbonate in turn dissociates to form another H^+ ion and a carbonate (CO_3^{2-}) ion:

$$CO_2 + H_2O \rightleftharpoons H_2CO_3^* \rightleftharpoons H^+ + HCO_3^- \rightleftharpoons H^+ + CO_3^{2-} \qquad \textit{Equation 1.1}$$

As ocean pH decreases, the speciation of inorganic carbon in the water shifts to make bicarbonate (HCO_3^-) more abundant, reducing the alkalinity of the system (Fig. 1.1).

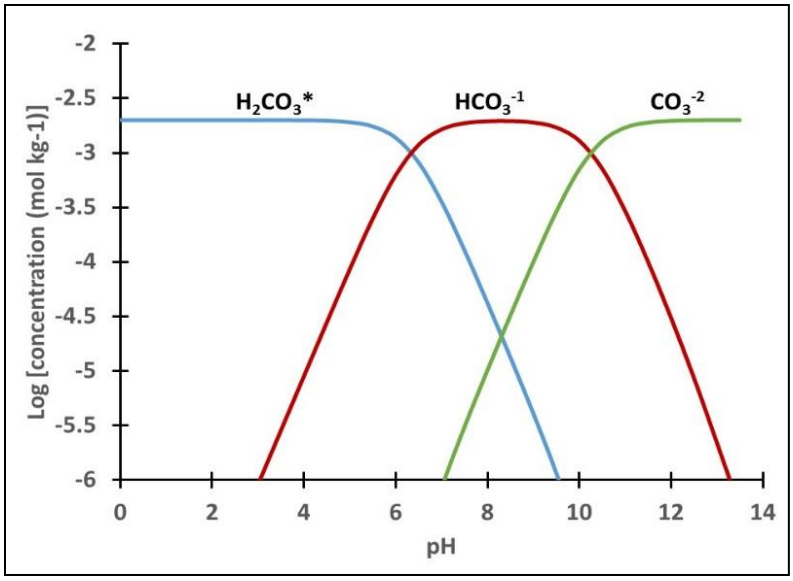

Figure 1.1: Aquatic inorganic carbon speciation as it relates to pH. Shown are carbonic acid ($H_2CO_3^*$), bicarbonate (HCO_3^-) and carbonate.

Dissolved carbon dioxide is necessary for aquatic photosynthesis; thus, changes to concentration and partitioning of DIC may influence these organisms. At a seawater pH of 8.2, carbon speciation is as follows: 1% of total DIC is present in the form of CO_2, 90% as HCO_3^-, and 9% as CO_3^{2-} (Steeman Nielsen 1975). The key enzyme that is responsible for biological fixation of inorganic carbon into organic compounds (Ribulose-1,5-bisphosphate carboxylase/oxygenase; RuBisCO) uses CO_2 as a substrate for carbon fixation (Palmer 1996). Higher environmental pH favors the dissociation of carbonic acid, diminishing the amount of CO_2 available for carbon fixation. Under these conditions, photosynthetic activity would be expected to decline. To combat this, many phytoplankton have carbon concentrating mechanisms (CCMs) for concentrating inorganic carbon to the extent that photosynthesis may continue with minimal impedance regardless of carbon speciation (Moroney and Somanchi 1999; Nimer et al., 1999). Most commonly, HCO_3^- is converted to CO_2 by the enzyme carbonic anhydrase (CA),

either within the chloroplast (intracellular CA) or in the periplasm of the outer cell membrane (extracellular CA; Badger and Price 1994; Moroney and Somanchi 1999; Trimborn et al. 2008)

CO_2 is the most energetically favorable carbon species, since no CA conversion is necessary for aquatic photosynthesis. Surprisingly, Rubisco has a competitive binding relationship with both oxygen (which useless for photosynthesis) and CO_2 (Palmer 1996; Moroney and Somanchi, 1999), making it remarkably inefficient in the presence of excess oxygen. Thus, the increasing amount of anthropogenic CO_2 in the surface ocean should theoretically stimulate photosynthesis in phytoplankton, as it provides more CO_2 molecules to the promiscuous binding sites on Rubisco. However, algal responses to pH conditions reflective of ocean acidification are varied, with some marine phytoplankton responding positively to increased pCO_2 and decreased pH (Doney et al. 2009a; Kranz et al. 2009; Iglesias-Rodriguez et al. 2008), and some responding negatively (Kim et al. 2006; Hurd et al. 2009; K. Gao and Zheng 2010; Kroeker et al. 2010). It is unclear if this effect is due to the phytoplankton response to speciation of inorganic carbon in the water, or some regulatory role that pH may play on cell dynamics/energetics.

1.2 pH as an independent, ecologically significant variable

The chemistry of pH and its radiating effects on marine biota are intricate and complex. Simply put, pH is a measure of the concentration of hydrogen ions (H^+) present in a solution.

$$\mathrm{pH} = -\log[H^+] \qquad \textit{Equation 1.2}$$

However, pH in aquatic systems is not simple. It is influenced by physical, chemical and biological parameters. The primary driving factors of ocean pH are DIC concentration and alkalinity. Alkalinity is the capacity of the water to neutralize acid, based on the amount of

chemical bases present in ionized form in the water, as well as their relative strength. This can also be thought of as the buffering capacity of the water, keeping the pH from drifting in an acidic direction. Physical factors like salinity and temperature have been shown to have a significant influence on alkalinity due to the influence of these factors on ion availability (Lee et al. 2006). Biological processes such as calcification changes alkalinity as carbonate ions are consumed by the consumption of $CaCO_3$ (Cai et al. 2010). In shallow waters, total alkalinity of the water can be increased by anaerobic processes, specifically denitrification and sulfate reduction in sediments (Thomas et al. 2009). Due to these processes, as well as the mixing of water masses such as upwelling, river outflow, or precipitation, alkalinity can vary according to location. One of the principal drivers of alkalinity and pH in aquatic systems is the amount and partitioning of dissolved inorganic carbon (DIC) present in the water. DIC concentration is a direct result of the amount of carbon dioxide (CO_2) gas dissolved in the water. CO_2 content is generally modified in seawater in one of three ways: (1) direct atmospheric input by equilibration with air; (2) addition of water with a higher/lower CO_2 concentration (e.g., rain, upwelling of deep water, addition of river water); (3) biological input through respiration, biological consumption (systemic deficit) through photosynthesis.

pH and partitioning of CO_2 are intimately linked; however, their respective influences are not inextricably bound. Due to the ability of many organisms to modify internal reservoirs of inorganic carbon through the use of physiological adaptations such as CCMs, the emphasis of the effect of OA on phytoplankton becomes less of a question of the effect of pH on aquatic partitioning of DIC, and shifts to a focus on pH as the master variable (Ying et al. 2014). A growing body of research demonstrates that pH is an important parameter in phytoplankton physiology independent of its relationship with ocean carbon chemistry.

Eberlein et al. (2014) showed that non-calcareous dinoflagellates showed no response to changing pCO_2 when pH remained constant. Havskum and Hansen (2006) suggest that in a nutrient replete environment, it is pH that limits algal growth. Dason and Colman (2004) also found that suppression of growth occurred concurrently with changing internal pH of the phytoplankton cells. This occurred even in the presence of increased pCO_2. Chen and Durbin (1994) demonstrated that growth of multiple species of the marine diatom, *Thalassiosira*, responded to changing environmental pH independently of changing alkalinity.

Even organisms such as coccolithophores that are well documented for demonstrating significant responses to OA appear to respond to pH semi-independently from DIC concentration. Kottmeier *et al.* (2016) showed that inorganic carbon uptake changed, with uptake being preferential for HCO_3^- or CO_2, depending on environmental acidification. McCulloch et al. (2012) found that a number of calcifying phytoplankton have the ability to actively resist the detrimental effects of OA on calcification by controlling the pH of the calcifying fluid $pH_{(cf)}$. This process is very energetically efficient, resulting in an extra energy requirement of less than 1% the total energy produced by the cell during photosynthesis. Organisms that were able to successfully regulate pH of the calcifying fluid were far less sensitive to changes in seawater aragonite saturation state (Ω_{ar}). However, contrary to the deliberate control $pH_{(cf)}$ of the cells, cytosolic pH in coccolithophores is passively regulated and independent the controls on $pH_{(cf)}$ (Mackinder et al. 2010). Thus, changes in the pH of the cytosol are more detrimental to calcification processes (and possibly overall cellular energetic balance) than the aragonite saturation state of the surrounding water (Cyronak et al., 2015)

1.3 Homeostasis of intracellular pH

Regulation of intracellular pH (pH_i) is critical to cell function, and is usually kept under tight biochemical control (Frohnmeyer et al., 1998). Changes in pH can affect growth indirectly by altering the availability of trace metals, as well as DIC carbon partitioning and availability, thus affecting metabolism, photosynthesis, and reproduction (Chen and Durbin 1994). Transitory changes in pH_i are also used to signal the genesis or regulation of cellular processes (Taylor et al., 2012), including cell cycle progression, life cycle changes, cellular dormancy, and developmental transitions (Busa and Nuccitelli 1984; W. Busa and Crowe 1983; Karagiannis and Young 2001). Essentially all proteins are sensitive conformationally to pH, with significant changes to structure occurring when pH_i deviates too far outside the range usually maintained by homeostasis for optimal metabolic efficiency (Chen and Durbin 1994; Casey et al., 2010). Cellular energetics also rely heavily on proton motive force, which can be influenced both directly by pH (Nimer et al., 1994; Casey et al., 2010), and indirectly through conformational changes to proteins and/or enzymes that are part of maintaining the electrochemical gradient (Casey et al., 2010).

pH homeostasis is primarily maintained through three mechanisms: (1) buffering using weak acids and bases, (2) modification of DIC partitioning and concentration, and (3) upregulating acid/base loader and transporters (Roos and Boron, 1981; Boron, 2004; Casey et al., 2010). A possible cause for the differences in algal physiological responses to pH may lie in the ability of the cells to maintain internal pH homeostasis. Previous work has shown that phytoplankton show a range of homeostatic capabilities in this area; some organisms exhibit the ability to survive with cytoplasmic pHs far from neutral (Table 1.1). This may be due to differences in how different taxa regulate pH. For instance, proton channels are the major

exporter of excess H^+ ions in many unicellular algae. However, these channels are not universal, with prasinophytes and certain macroalgae lacking this regulatory mechanism (Taylor et al. 2011). CO_2 diffusion and modification of partioning is the "preferred" method for regulating pH_i, as the response of pH_i is far more rapid with changing DIC than in response to weak acid/base addition (Thomas 1974; Roos and Boron 1981), this process is energetically expensive for extended pH perturbations (Casey et al., 2010); for long-term acclimation to pH changes, the cell upregulates acid/base loaders and transporters (Boron 2004; Taylor et al., 2012).

Physiological changes such as energy balance, mechanisms of photosynthesis, and actual pH_i will likely differ between organisms acclimated long-term to steady state or dynamic pH environments, as the cells have adapted to totally different pH environments, and will exhibit physiological responses reflective of that.

Table 1.1: Survey of literature showing change in pH_i due to changing external triggers

Organism	Class	Internal pH	Environmental pH	Irradiance	Reference
Euglena	Euglenophyceae	5.0–8.0	3.0-8.0	--	(Lane and Burris 1981)
Chlorella	Chlorophyceae	6.4	3.0	--	(Gehl and Colman 1985)
Thalassiosira	Bacillariophyceae	6.7-7.5	6.5-8.5	--	(Herve et al. 2012)
Plectonema boryanum	Cyanophyceae	8.5	--	High light	(Masamoto and Nishimura 1977)
Synechococcus	Cyanophyceae	8.5	--	High light	(Masamoto and Nishimura 1977)
Coccolithus pegalicus	Prymnesiophyceae	-0.2 pH_i[1]	pH_e decreased from 8.0 to 6.5	--	Taylor et al., 2011
Trichodesmium	Cyanophyceae	-0.4 pH_i[1]	pH_e decrease from 8.1 to 7.8	--	(Hong et al. 2017)

[1] Indicates change in pH_i after pH_e perturbation.

1.4 Esterase activity and cellular energetics

Increased esterase activity has been used as an indicator of environmental stress in phytoplankton (Agusti & Sanchez, 2002; Agusti et al., 1998; Regel et al. 2002). However, esterases are ubiquitous enzymes among living creatures and have been shown to have an important role with a normal life cycle in various organisms, and when they are in abeyance, to be associated with decreased metabolism (Yang and Kong 2011; Jiao et al. 2015).

Esterases are used by cells to access stores of energy stockpiled as lipids or short-chain fatty acids (Fojan et al. 2000; Johnson and Alric 2013). Because carbohydrates are easier to break down, lipids are not the preferred energy source for healthy phytoplankton cells; however, lipids have a higher energy density than carbohydrates, and are a good source of energy when the cells experience a sudden energy deficit (Johnson and Alric 2013; Obata et al., 2013). Thus, esterase activity is an important indicator of energy need by the cell. This is an important factor when looking at effects of OA on phytoplankton physiology, as demonstrated by Hong et al. (2017), who showed that increased ATP production allowed the colonial cyanobacterium, *Trichodesmium,* to partially moderate the negative effects of environmental acidification.

1.5 Ecological impact: potential effects of ambient pH on phytoplankton ecology

Although OA is likely to influence nearly all regions of the surface oceans in the coming decades, there are already measureable effects in many coastal ecosystems due to the influence of upwelling (Gruber et al. 2012). Nutrient rich, low pH water is upwelled from the deep ocean into the euphotic zone by coastal upwelling. This low oxygen water already has a high load of dissolved carbon dioxide, and is far more vulnerable to even small changes in pCO_2 and pH than open ocean waters. While the main driver of this interaction is carbon load of the water being

brought up from depth to above the continental shelf, the high nutrient concentrations of this water can also be a secondary driver of pH changes. The nutrients injected into coastal ecosystems by upwelling feed phytoplankton blooms. The majority of algal blooms are benign or even beneficial rather than deleterious, generating oxygen and contributing to productive food webs in both marine and freshwater environments. A regional example occurs in the Columbia River estuary, which is host to numerous species of the photosynthetic ciliate, *Mesodinium*, which form recurrent blooms each summer, dominating phytoplankton biomass and estuarine primary productivity during upwelling season when high DIC waters enter the estuary (Herfort *et al.*, 2011; Peterson *et al*., 2013). Estuaries can act as incubators for phytoplankton blooms. This semi-isolated environment also exposes the phytoplankton present to the impacts that such intense biological activity (i.e., photosynthesis and respiration) can have on local pH dynamics. It is important to understand how highly dynamic systems like this affect algal physiology and productivity under fluctuating pH regimes.

As stated earlier, effects of pH on phytoplankton growth are sometimes conflicting, and can be as individualized as the organisms studied (Kim et al. 2006). However, it is broadly recognized that OA conditions have the potential to drive species progression and phytoplankton community composition through changing pH or DIC concentration (Tortell et al. 2008; Beaufort et al. 2011; Collins et al., 2013). It has been well established that OA has negative impacts on the growth of calcifying phytoplankton (Doney et al. 2009a; Kroeker et al. 2010), as well as on other calcareous organisms such as pteropods and molluscs, particularly juvenile shellfish, which require aragonite and calcite to be in a supersaturated state (Talmage and Gobler 2010; Waldbusser et al. 2013). However, OA may also drive the loss of biological diversity of non-calcareous organisms due to species shifts in phytoplankton communities. This may be due

to the direct effect of low pH (Kroeker et al. 2010), or it may occur via secondary drivers such as increased growth of macrophytes, resulting in less light penetration in coastal or estuarine regions (Kroeker *et al.,* 2010; Fabricius *et al*, 2011).

The reduction in growth of phytoplankton may accompany changes in the availability of trace nutrients such as iron or copper in the water due to a reduction in pH. Trace metal nutrients are essential for growth and metabolism, with these metals often serving vital roles in essential enzymes (e.g., iron in ferredoxin, copper in cytochrome c oxidase, which are essential for photosynthesis and respiration, respectively; Tagawa and Arnon 1962; Sunda 2012; Sunda and Huntsman 1997). pH directly and significantly impacts the availability of OH^- and CO_3^{2-} ions, which complex easily with divalent trace metals (Baes and Mesmer 1976; Millero and Hawke 1992). At environmentally relevant pH, changes in proton concentration may impact ion complexation and micronutrient availability, and thus growth rate.

Growth may also be influenced by the impact of pH on metal/ligand complexation (Millero et al. 2009; Krachler et al. 2015). Iron, zinc, and cobalt availability has been shown to decline under ocean acidification conditions due to pH-sensitive changes in metal/ligand binding (Shi et al. 2010; Millero et al. 2009; Gledhill et al. 2015; Xu et al. 2012). However, availability of copper has been shown to increase with increasing acidity (Campbell et al. 2014; Lewis et al. 2016; Gledhill et al. 2015; Avendaño et al. 2016). These changes in trace metal availability may have important impacts on growth and species composition of phytoplankton communities, in addition to the more direct effects of changing pH described above.

Dinoflagellate growth has been shown to be retarded at low pH, with inorganic carbon acquisition—and consequently photosynthetic CO_2 fixation—becoming inhibited at pH 7.5 (Dason and Colman 2004). Controlled mesocosm experiments using natural phytoplankton

assemblages showed that phytoplankton population composition shifted from favoring photosynthetic microflagellates (nearly 60% of population by count) to less than 20% at decreased pH, with diatoms gaining dominance over population dynamics (Kim et al. 2006). Some organisms are better suited for low pH, high DIC environments due to biochemical differences; as ocean carbon inventories and pH continue to change, phytoplankton diversity and community taxon composition can be expected to follow suit. This may have cascading effects on higher trophic levels, some of which rely on prey specificity and quality (Rossoll et al. 2012).

1.6 Summary and research needs

A great deal of research has been accomplished regarding ocean acidification and phytoplankton physiology and ecology. Advances in our collective knowledge of aquatic carbon chemistry and dynamics has provided us with valuable evidence that pH is a regulatory environmental variable independent from DIC concentration. Designs for systems that can maintain static pH and/or DIC (termed "pHstats") are available for a variety of macro- and microbiota. However, no system is available that is able to maintain a dynamic pH environment. To this end, a system is needed that allows phytoplankton to be cultured in a controlled environment that isolates pH as the sole changing variable.

In comparison with the amount of literature available regarding calcifying phytoplankton, there is a shortage of available literature that addresses the response of non-calcifying microflagellates to ocean acidification (Miller, 2004). Because these organisms can make up a significant portion of phytoplankton biomass, it is important to examine the effect of changing pH on them. To this end, it is necessary to choose a model organism that will fill the gap in knowledge regarding microflagellate physiology, and that can be compared to existing literature.

One of the best-characterized clades of phytoplankton is Haptophyta (sometimes called Prymnesiophyta), given the obvious negative effects of OA on coccolithophores, which are a calcifying, non-motile subset of this group. However, the non-calcifying marine flagellate, *Isochrysis galbana*, is also included in this clade, and as such may serve as an excellent model non-calcifying microflagellate for examining the effect of changing external pH, with the potential for reliable cross-taxa comparisons of physiological responses. Also, *I. galbana* – unlike some other microflagellates such as chrysophytes – has been shown to contain carbonic anhydrase and thus should not be carbon limited at the pH levels relevant to this work (Maberly et al. 2009; Ores et al. 2016).

To effectively examine how environmental pH influences cellular parameters, it is necessary to first determine how intracellular pH and photosynthesis are influenced by changes in external pH. Research is needed to examine the differential effects of steady state and dynamic pH environments on phytoplankton physiology in order to extrapolate how phytoplankton assemblage and community structure may change between the open ocean (a relatively steady state environment) and a dynamic system like an estuary or an active phytoplankton bloom. There is also a need for research that examines the combined effect of regular, diel fluctuations in pH with the small, long term changes to base pH that will be seen in future oceans as OA worsens. This can give us valuable information on the more subtle effects of OA on dynamic systems such as estuaries or coastal ecosystems.

1.7 Dissertation overview

Effectively all previous research on pH and phytoplankton physiology has been accomplished with short-term experiments in a steady-state environment. Up to this point, the

availability of a system capable of simulating the regular pH changes of a dynamic system was lacking. To resolve this problem, Chapter 2 describes a novel, laboratory-based microalgal culture system for studying phytoplankton in both steady state and dynamic pH environments.

Methods abound for determining intracellular pH in cells, including NMR, pH microprobes, partitioning of radioactive carbon compounds between intra- and extracellular environments, and fluorescent probes. Of these, the use of fluorescent probes has proven to be the most accurate and least expensive method of determining pH_i. The indicator principally used to date 2',7'-Bis-(2-carboxyethyl)-5-(and-6-) carboxyfluorescein 4 (BCECF) in phytoplankton is a single peak indicator that is vulnerable to minute changes in both cell and dye concentration, as well as photobleaching, and leakage. The use of a ratiometric fluorescent indicator that utilizes the ratio in emission intensity of two fluorescent peaks to calculate pH vastly reduces or eliminates these problems; however literature demonstrating the used of the primary fluorescent probe for this purpose, seminaphtharhodafluor (SNARF), is rare. In Chapter 3 I developed the methods necessary to calculate in vivo pH_i in phytoplankton using SNARF as a pH_i indicator. We also conducted a survey of the efficacy of three different fluorescence methods for SNARF detection, and determined the latter's efficacy as an accurate pH_i indicator in a number of phytoplankton taxa.

Chapter 4 addresses the impact of both steady-state and dynamic pH environments on phytoplankton physiology using *Isochrysis galbana* as a model organism, in combination with the pHstat system of Chapter 2 and the SNARF methodology of Chapter 3. The physiological parameters of pH_i, esterase activity, photochemical efficiency, and growth rate were measured and the data used to construct a hypothesis regarding the effect of changing environmental pH on cellular energetic balance.

Finally, Chapter 5 provides a summary and overall conclusions regarding the research conducted and presented in Chapters 2–4. Supporting information for Chapters 2 and 3 are presented in Appendices.

CHAPTER 2

Development of an economical, autonomous pHstat system for culturing phytoplankton under steady state or dynamic conditions[2]

Rachel L. Golda, Mark D. Golda, Jacqueline A. Hayes, Tawnya D. Peterson, Joseph A. Needoba

2.1 Abstract

Laboratory investigations of physiological processes in phytoplankton require precise control of experimental conditions. Chemostats customized to control and maintain stable pH levels (pHstats) are ideally suited for investigations of the effects of pH on phytoplankton physiology, for example in context of ocean acidification. Here we designed and constructed a simple, flexible pHstat system and demonstrated its operational capabilities under laboratory culture conditions. In particular, the system is useful for simulating natural cyclic pH variability within aquatic ecosystems, such as diel fluctuations that result from metabolic activity or tidal mixing in estuaries. The pHstat system operates in two modes: (1) static/set point pH, which maintains pH at a constant level, or (2) dynamic pH, which generates regular, sinusoidal pH fluctuations by systematically varying pH according to user-defined parameters. The pHstat is self-regulating through the use of interchangeable electronically controlled reagent or gas-mediated pH-modification manifolds, both of which feature flow regulation by solenoid valves.

[2] Reproduced (with edits) with permission from Golda, R., Peterson, T., Needoba, A. Reference: Development of an economical, autonomous pHstat system for culturing phytoplankton under steady state or dynamic conditions. (2017). *Journal of Microbiological Methods*. 136:78-87.

Although effective pH control was achieved using both liquid reagent additions and gas-mediated methods, the liquid manifold exhibited tighter control (±0.03 pH units) of the desired pH than the gas manifold (±0.10 pH units). The precise control provided by this pHstat system, as well as its operational flexibility will facilitate studies that examine responses by marine microbiota to fluctuations in pH in aquatic ecosystems.

2.2 Introduction

Controlled laboratory conditions are essential for conducting experiments that examine the physiological responses of phytoplankton to environmental stimuli. This is particularly important when investigating the potential effects of variables in which long-term exposure to relatively small changes may lead to significant physiological consequences, as is the case with environmental pH. The increase in atmospheric carbon dioxide levels since the Industrial Revolution due to fossil fuel consumption and changes in land use (Ciais et al. 2014) has resulted in the emerging problem of ocean acidification (OA), defined as the global decrease in ocean pH. Although pH changes associated with OA appear small, with a global average decrease of 0.1 pH units to date (Doney 2010), they are significant in their effect on aquatic dissolved inorganic carbon (DIC) partitioning. While particular attention has been paid to the effect of OA on certain marine organisms (most notably calcifiers; Hendriks et al., 2010; Kroeker et al. 2013), the consequences of OA on many non-calcareous marine phytoplankton populations remain poorly understood (Doney et al. 2009; Connell et al. 2013; Kroeker et al. 2013) due to the high variability in both physiological response and the ability of the organisms to adapt or acclimate to changes in pH, pCO_2, or both (Riebesell and Tortell 2011).

To determine the effects of changing environmental pH on phytoplankton physiology, environmental pH must be directly manipulated as an experimental variable in controlled

laboratory cultures. Two of the most relevant laboratory culture methods for algal physiology experiments are batch and continuous culture systems (i.e., chemostats; Droop 1975; Harrison et al., 1976; LaRoche et al., 2010). Batch cultures are most representative of "bloom" conditions where cell concentration increases and nutrients are depleted in the vessel over time. Cultures may be kept in exponential phase growth by transferring the culture prior to nutrient depletion and subsequent buildup of metabolic wastes (fed batch culture; Fischer et al. 2014). However this semi-continuous approach to phytoplankton culture still results in significant changes in water chemistry when nutrient consumption and waste production outpace the dilution rate of the culture, preventing the stable growth conditions necessary for physiological studies. Because of this instability it can be difficult to determine whether physiological responses are truly due to experimental stressors or stimuli or to nutrient deprivation and waste buildup resulting from algal metabolism and growth.

Chemostats are a type of continuous culture system that feature a continuous influx and efflux of media (Monod 1950; Novick and Szilard 1950; MacIntyre and Cullen 2005). This creates a steady-state environment that maintains constant biomass and nutrient concentration while minimizing waste buildup. Because exponential growth rates can be maintained indefinitely under these conditions (Jannasch 1974), chemostats are representative of the steady-state conditions found in open-ocean environments. In chemostat systems, environmental variables (either singly or in combination) can be manipulated more precisely while other variables are held constant, allowing for finer control of growth and environmental chemistry than in batch cultures.

Fully automated continuous culture systems tend to be costly and involve complex technical details, making them difficult to implement for small-scale experimentation (Fay and

Kulasooriya 1973; Whiteley et al., 1997). However, the recent surge in OA research has led to the development of relatively inexpensive chemostat systems that are better suited to OA research than their predecessors, bringing focus on carbonate chemistry and pH growth conditions (McGraw et al. 2010; Hoffmann et al. 2013; Olariaga et al. 2014; Ying et al., 2014; Wynn-Edwards et al. 2014; MacLeod et al., 2015). These adapted chemostats are termed pHstats (Garcia-Arrazola et al. 2005) for their ability to maintain pH at a desired level. The fine control of external pH achieved by using a pHstat allows for precise manipulation of pH as an experimental variable, providing a useful tool in physiological studies.

A particular challenge for phytoplankton physiology experiments that involve pH is the direct addition and removal of dissolved inorganic carbon (DIC) as a result of photosynthesis and cellular respiration. These metabolic processes create relatively large changes in external pH at daily or shorter time periods (LaRoche, 2010). This problem spans experimental scales, providing challenges for both benchtop methods such as batch cultures or chemostats (LaRoche et al., 2010) as well as studies in coastal waters (Duarte et al. 2013). The latter environments can experience high diel variability in pH, sometimes changing more than one pH unit over the course of a few hours (Duarte et al. 2013). This is due in part to tidal cycles (Dai et al. 2009; Wang et al. 2014), but principally is a result of the high variability in primary productivity within coastal waters (Li et al., 2016). Variability in pH within the surface ocean is projected to increase as ocean acidification worsens owing to the reduced buffering capacity of waters that are undersaturated with respect to aragonite (Feely et al. 2010; Egleston et al., 2010; Wang et al. 2014). Therefore it is imperative that culturing conditions can mimic small changes in the average pH (for example, due to ocean acidification) while also incorporating large daily fluctuations that are typical of many aquatic habitats.

Here we describe the design, construction, optimization, and validation of a simple pHstat system that is designed for small-scale, benchtop experiments and customizable to set and maintain constant or fluctuating pH levels using liquid reagents or gases to modify pH. Both mean pH and pH fluctuations are maintained at a user-set frequency; this provides additional functionality over existing systems, which have focused on maintaining a static pH level. The inclusion of pH fluctuations provides a means to simulate either changes in water mass characteristics (for example, during tidal exchange), or diel changes in DIC associated with photosynthesis and respiration.

2.3 Materials and Methods

pHstats have additional requirements above those of a nutrient-based chemostat system. These requirements include precise pH monitoring and modification capabilities that maintain culture conditions within a target pH range. The high resolution necessary for this approach requires autonomous operation of the pHstat, which includes a culturing component (i.e., the growth chamber, which will contact the culture directly), an electronic component, an electromechanical component, and a programmatic component. Our pHstat includes all of the components necessary for high-resolution, in situ pH monitoring and autonomous pH adjustments (Table 2.1; Fig. 2.1).

Table 2.1: Major pHstat system components, supporting instruments, and system functions.

Component	Instrument	Function
Electronic	pH sensor	Measure pH within growth chamber
Electronic	Digital I/O device	Interface between computer and relay system
Electronic	Go!Link	Adapts signals from the pH sensor to be compatible with LabVIEW®
Electronic	GEORG	Solid state relay array; controls and boosts voltage pulses to pH-modification manifolds
Electromechanical	Reagent manifold	pH modification manifold; features solenoid pinch valves to control flow of reagents
Electromechanical	Gas manifold	pH modification manifold; features solenoid valves to control flow of gases
Electromechanical	Adjustable-rate peristaltic pump	Transports media from sterile media reservoir into the culture vessel
Biological	Culture vessel	Sterile vessel in which organisms will be grown

GEORG = conditionin**G** **E**lectronically **O**perated **R**elay **G**rouping

2.4 Major System Components

2.4.1 System Overview

The pH of the culture vessel is continuously monitored by an in situ pH sensor interfaced to a computer program (described below; Fig. 2.1). The user sets acceptable maximum and minimum pH thresholds (Note: for the pH cycling function maximum and minimum thresholds are programmed into the virtual instrument (VI) at ±0.03 pH units resolution). The pH sensor communicates through a USB interface with a LabVIEW® computer program that monitors and controls pH in the culture vessel. When the measured pH deviates outside of the set thresholds, it activates the electromechanical portion of the pHstat (i.e., the pH modification manifolds). This is accomplished by sending a digital signal to a set of solid state relays through a digital input/output (I/O) board. The solid state relay array is connected to the pH modification manifold, which utilizes solenoid valves to add reagents or gasses to the culture vessel to modify the pH. When the pH returns to the acceptable thresholds the system deactivates and remains on standby until the next pH deviation occurs.

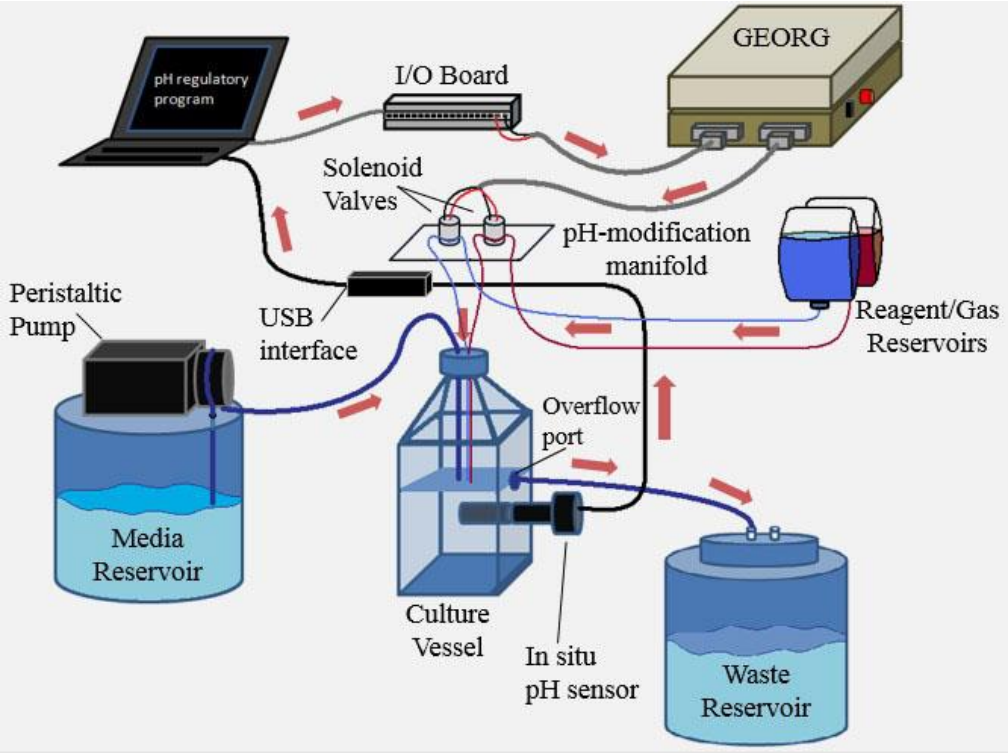

Figure 2.1: Schematic of pHstat system, showing spatial relationships and connections between components. Universal chemostat components are present (media reservoir, pump, culture vessel, waste reservoir), as well as custom additions for autonomous pH monitoring and modification (computer program, digital I/O board, pH modification manifold, in situ pH sensor). Note the presence of only one pump, as this is an overflow chemostat.

2.4.2 Computer Program

The LabVIEW® (National Instruments, Austin, TX) graphical programming platform was used to create a virtual instrument (VI) that monitors and controls pH in the culture vessel using either the gas manifold or the liquid/reagent manifold. Two particular applications are demonstrated here:

1) Set point pH – Maintains a pH with a narrow range of acceptable thresholds, with the mean of the outer thresholds being the target pH. The user sets the desired sample rate and pH thresholds. When the system senses that the pH of the culture vessel has

deviated out of the set range, the solenoid valves of the appropriate pH modification manifold activate until the pH returned to the acceptable range.

2) pH cycle – Maintains a pH that follows regular daily cycling patterns. The program uses a sine wave to simulate the desired pH fluctuation, for example a diel cycle. The user sets the desired frequency (number of cycles per day), offset (average/starting pH for y-intercept of sine wave) and amplitude (magnitude of the peaks and troughs) of the sine wave. A programmed ±0.05 pH unit "buffer" for the sine wave allows for up to 0.05 pH unit deviation from the desired pH point at any given time before the system triggers the solenoid valves to activate and begin driving pH in the appropriate direction to achieve the desired pH.

Data from the pHstat regarding pH, timestamp and solenoid activity are recorded as .lvm files by the VI. The VI used to produce the results presented here is provided in graphical code format in (Golda et al., 2017). The provided VI requires all system components necessary for pHstat function to be connected in order to function fully; this minimizes the possibility of running the system with a defective component.

2.4.3 pH Sensor

The system includes a LabVIEW® compatible pH probe (Vernier Software & Technology, Beaverton, OR) to measure pH in the culture vessel. The pH probe was connected to a computer using a Go!Link (Vernier Software & Technology, Beaverton, OR) Universal Serial Bus (USB) sensor interface (Fig. 2.1). pH is measured according to the scale developed by the National Bureau of Standards (NBS). Although this scale is less accurate in ionic solutions than in pure water, conversion to the total proton scale is according to the equation put forth by Millero (2013):

$$10 - \mathrm{pH_{NBS}} = \mathrm{f_H}[\mathrm{H^+}]_\mathrm{F}(1 + \beta_{\mathrm{HSO_4}}[\mathrm{SO_4^{2-}}]_\mathrm{T} + \beta_{\mathrm{HF}}[\mathrm{F^-}]_\mathrm{T}) \qquad \textit{Equation 2.1}$$

2.4.4 Input/Output (I/O) Device

A digital input/output (I/O) device (USB-1024LS, Measurement Computing Corporation, Norton, MA) was used as an interface between the VI and the relay array. This device outputs digital signals from the computer using 5V direct current (DC) pulses to relay commands from the VI to the relay grouping.

2.4.5 GEORG – Conditioning Electronically Operated Relay Grouping

We constructed a solid state relay (SSR) voltage switching array (see Fig. A5 Appendix A) for the dual purpose of (1) converting/boosting the outputs from the I/O interface device from low-current 5V DC signals to the current-boosted 12V DC signals required to drive the solenoid valves, and (2) permitting precise computer control of solenoid valve activation times.

Specifications for the SSRs (Crydom Inc., San Diego, CA) used in GEORG were as follows: Input: 3.5–32V DC (normally-open, N.O.), Output: 60V DC @ 3A (maximum). It is essential that the SSRs that are used be of the normally open (N.O.) type, for which the relay's default/un-energized state is open.[3] If a normally-closed (N.C.) relay is used in the system, it will stop gas or reagent flow only when an activation signal is received from the computer and remain open at all other times, causing the system to malfunction.

The relay grouping was mounted in a heavy-duty acrylonitrile butadiene styrene (ABS) instrument case (Jameco Electronics, Belmont, CA). Holes were precision-cut into the sides for

[3] It is important to note that when speaking of valves, "open" indicates that the valves allow for the flow of reagents or gases. However, in the terminology of circuits, "open" indicates that the switch or relay is *not* activated, because electrons cannot flow through the gap in a circuit that is introduced by the open switch. Therefore an open relay stops electrical activity, while a closed relay allows electrical activity "downstream" from the relay.

the bulkhead mounting of two DB15 (D-subminiature) connectors. A 12V DC/1500 mA wall adapter provided power to GEORG, while a single-pole, single-throw (SPST) off/on switch controlled master power to the relays. A 250V AC/1A fuse was installed between the power supply and the switch.

Input/output cables connecting GEORG to the digital I/O device were modified 25-conductor shielded cables (Jameco Electronics, Belmont, CA). The input cable for GEORG from the computer and output cable to the pH modification manifolds were each separately routed through their own their respective DB15 connectors. We suggest that the DB15 connectors be opposite sex-keyed; that is, the input and output connectors should not both be male or both female, but one of each to prevent misconnections. The output cable from GEORG was additionally sub-divided into separate 2-pin Molex® connectors, one for each solenoid. Each of these Molex® connectors were in turn uniquely keyed to avoid misconnecting any given solenoid to the energizing signal of another solenoid, causing accidental erroneous solenoid activation.

2.4.6 Reagent Manifold

A liquid/reagent manifold was designed and constructed for dispensing acid or alkaline reagents into the culture vessel. The manifold consists of two solenoid pinch valves (2-way, normally closed (N.C.) type, 1/16 in inner diameter (ID); Cole-Parmer, Vernon Hills, IL) threaded with flexelene™ tubing (1/16in ID; Eldon James Corporation, Denver, CO). It is critical that any component of the valves in contact with any reagents be inert to caustic chemicals. Potential options for appropriate valves include solenoid valves constructed with Teflon® or vinyl wet portions. Another option (which this system uses) is the use of pinch valves, which operate by putting pressure on a length of tubing, effectively pinching the tube

closed. This avoids contact between the valve itself and the reagent, which reduces the risk of chemical or biological contamination and lowers the risk of leakage. Pinch valves are also more cost-effective than the aforementioned wet valves.

The reagents used to adjust the pH of the culture vessel were 0.1 N Na_2CO_3 or 0.1 N HCl in order to adjust the pH in an alkaline or acidic direction as needed. Both reagent solutions were made up in a 3.6% NaCl solution to match the salinity of the marine culture medium and to eliminate the problem of altering the salinity of the medium through reagent additions.

2.4.7 Gas manifold

The custom gas manifold consists of an array of computer-controlled solenoid valves (Sizto Tech Corporation, Palo Alto, CA) to regulate the flow of gases to the culture vessel. A custom gas mixture (0.50% CO_2, 20.50% O_2, 79% N_2; Airgas Inc., Radnor Township, PA) was used to bubble the culture vessel and lower the pH. This mixture was chosen because bubbling with pure carbon dioxide causes the system to respond too dramatically for fine-scale pH adjustments. A clean air mixture (zero grade air, Airgas part number: AI Z200; Airgas Inc., Radnor Township, PA) was used to adjust the pH in an alkaline direction. A condenser was added to the manifold upstream from the solenoid valves as a safeguard to prevent aerosols formed by bubbling from leaking back through the lines. The solenoid valves used for the gas manifold were gas solenoid valves (12V DC activation voltage, 6.5W, 0-115 pounds per square inch [PSI]). It is important to use solenoid valves that are able to maintain a heavy duty cycle (100% ED preferred) without damage or overheating. All tubing in the gas manifold were suitable for compressed gases, both for safety reasons and to prevent dilution/contamination of the compressed gas stream by diffusion of gases through the tubing wall (Oakley et al., 2012).

2.4.8 Culture Vessel

The culture vessel (Fig. 2.2) was a 1 L polycarbonate bottle (Nalgene, Rochester, NY, USA). The in situ pH sensor was installed by drilling a hole into the side of the bottle and inserting the stem of the pH probe through a 0.5 in ID (metric units, 1.27 cm) autoclavable silicone grommet fitted in the opening approximately 6 cm from the base of the vessel.

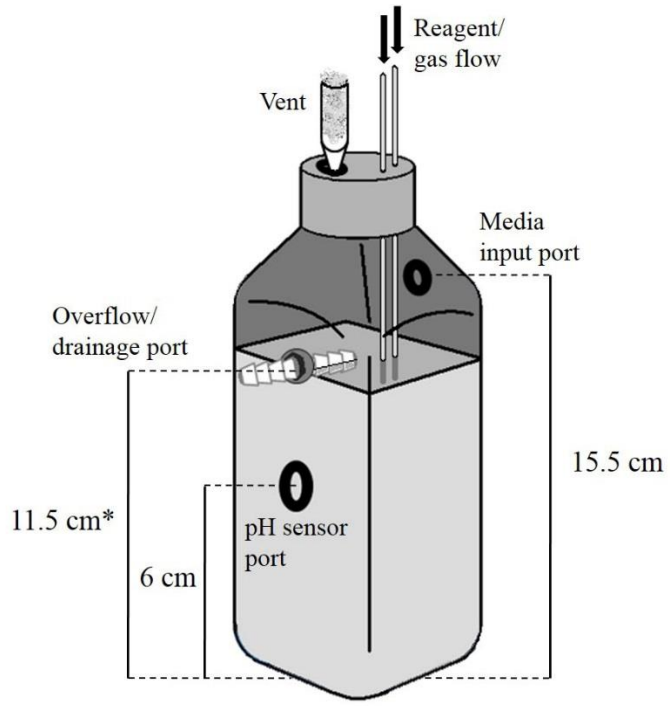

Figure 2.2: Diagram of culture vessel. Distances are measured from the base of the culture vessel to the center of the holes/grommets. The asterisk indicates potential variation from vessel to vessel; the drainage port should be placed at the point of desired maximum stable culture volume (900 mL for our vessel).

Overflow drainage was removed from the chemostat through a barbed bulkhead fitting installed in the bottle wall at the 900 mL water level (11.5 cm for our vessel). Input of media to the vessel came through a hole drilled in the slanted uppermost side of the flask and fitted with a 0.25 in ID (metric, 0.635 cm) silicone grommet. The tube from the pump (0.635 cm outer

diameter, OD) was inserted through this hole until the tip of the tube was submerged in the culture medium. This hole was located 4 cm above the drainage port, 15.5 cm from the base of the vessel. pH modification reagents/gas lines were fed through holes drilled in the lid of the bottle and fitted with appropriately sized autoclavable silicone grommets (for gas lines; reagent lines did not require grommets if the diameters of the holes were drilled to precisely match the reagent line OD). An additional silicone grommet was installed in the cap of the bottle, then fitted with a vent to allow air exchange in the system. The tip of a disposable 10 mL serological pipette filled with sterile glass wool serves as an excellent vent. Environmental conditions were controlled by placing the pHstat in a 15 °C cold room on a 12:12 light:dark cycle under full-spectrum, cool white fluorescent lighting (~100 µmol photons m^{-2} s^{-1}).

2.4.9 *Pump*

An adjustable-rate peristaltic pump (Stenner, Jacksonville, FL) was used to transport media from the sterile media reservoir to the culture vessel via autoclaved silicone tubing. For a chemostat to function properly, the system must reach steady state, which is determined by the concentration of a limiting nutrient (Droop 1975; Wood et al., 2005). Once the culture reaches steady state, the specific growth rate becomes synchronized to the dilution rate (due to the measured input of the limiting nutrient) according to the following equation:

$$\mu = \frac{\mathrm{F}}{\mathrm{V}} = \mathrm{D} \qquad \textit{Equation 2.2}$$

where F = flow rate of the culture medium, V = volume of the culture vessel, and D = dilution rate (Wood et al., 2005).

2.4.10 Culture Conditions

For the biotic experiments we cultured the marine flagellate, *Isochrysis galbana*, in triplicate to test the ability of the system to maintain a target pH in the presence of a photosynthesizing organism. Cells were acclimated to all growth conditions within the pHstat, with the exception of pH, for 8 generations (20-24 d) during which time fresh medium was supplied in calculated volumes semi-continuously to keep the cells growing exponentially. Once the cells were acclimated the pHstat experiments commenced, with the cells still in mid-exponential phase. Triplicates were performed in series rather than in parallel. Cells were grown in artificial seawater medium (ESAW; Harrison et al., 1980; Berges et al., 2001) at 20 °C in a climate-controlled growth chamber, on a 12:12 light dark cycle at an irradiance of 160 μE m^{-2} s^{-1}. The salinity was 34 PSU (practical salinity units), measured using a hand-held refractometer (Fisher Scientific, Waltham, MA). Major nutrient concentrations were 0.55 mM nitrogen as nitrate, 0.02 mM phosphorus as ortho-phosphate, and 0.11 mM silica as silicic acid, per Harrison *et al.* (1980) and Berges, *et al.* (2001). All the components of the media batches were combined except the major nutrients and the vitamin stock, and each batch of medium was bubbled for 24 h with ammonia-free air to equilibrate the carbonate system with the atmosphere. Then the major nutrients and vitamins were added and media was filtered using a 0.22 μm pore size Steritop filtration set (EMD Millipore, Darmstadt, Germany).

2.4.11 Measurements

Samples for the analysis of chlorophyll *a* were filtered onto 25 mm GF/F filters and stored frozen at -80 °C until extraction. Chlorophyll *a* was measured in duplicate fluorometrically using a Trilogy® laboratory fluorometer (Turner Designs, San Jose, CA)

following cold extraction in 90% acetone (Welschmeyer 1994). Chlorophyll fluorescence was measured on the Trilogy® fluorometer equipped with a non-acidification optical module.

Cell densities were determined using a Coulter Counter Model Z2 particle counter (Beckman Coulter, Indianapolis, IN) following 20 fold dilution in Isoton II® diluent (Beckman Coulter, Indianapolis, IN).

Samples for analysis of dissolved inorganic carbon (DIC) were collected by injecting 2 ml of filtered culture sample into 12 mL nitrogen-filled, septum-capped glass vials pre-filled with 1 mL concentrated (85%, or 14.8 M) phosphoric acid. Subsequently, DIC measurements were performed using a GasBench II infrared mass spectrometer (IRMS; Thermo-Scientific, Bremen, Germany) at the Stable Isotope Facility at University of California, Davis.

2.4.12 Performance Testing

System performance (i.e., ability to maintain target pH) was assessed for both steady state and fluctuating conditions, with cells (i.e., biotic) and without cells (i.e., abiotic). Each experiment to test performance was performed in triplicate. For abiotic perturbation experiments, the pH was perturbed artificially using 1N NaOH or 1N HCl to generate a large disturbance in the system at several maximum and minimum pH thresholds in order to determine the smallest sustainable spread between thresholds (i.e., precision of the system). For abiotic pH testing, 24 h triplicate runs were performed in series to establish a baseline for pH adjustment without cells present. For biotic pH testing, 72 h triplicate runs were performed in series using *Isochrysis galbana* to perturb pH biotically through respiration and photosynthesis, in order to evaluate how the pHstat system was able to control pH in the presence of an organism that actively changed pH through modification of the amount of free DIC available in the culture.

2.5 Results

In order to confirm that the pH modification manifolds successfully controlled pH, we designed a set of experiments to measure pHstat response to pH perturbations generated abiotically (i.e., programmed perturbations) and biologically (i.e., naturally driven by the consumption and release of CO_2 through photosynthesis and respiration). For the abiotic experiments, the pH of the system was artificially perturbed using 1N NaOH or 1N HCl in order to determine the resolution of the pH-modification manifolds (Figs 2.3 and 2.4).

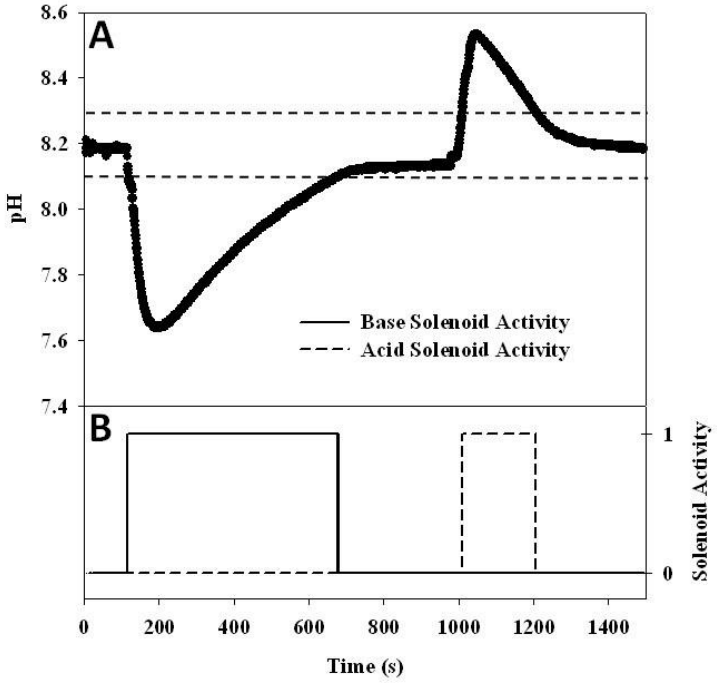

Figure 2.3: Abiotic pH perturbation test of gas manifold-mediated pH modification system. (A) pH over the course of the experiment. Dotted lines indicate pH thresholds (maximum pH threshold = 8.30, minimum pH threshold = 8.10). (B) Solenoid activity is recorded in digital bits; 1=on, 0=off; solenoids activate when the culture vessel pH deviates outside of threshold values.

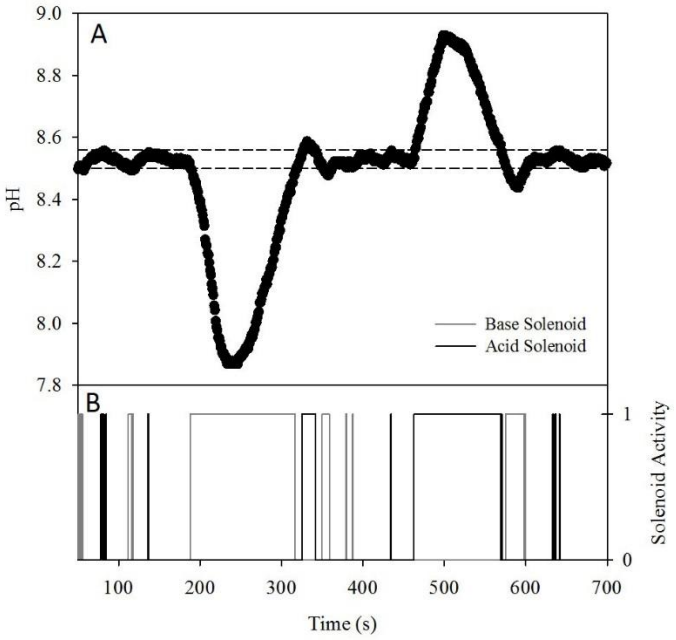

Figure 2.4: Abiotic pH perturbation test of liquid manifold-mediated pH modification system. (A) pH is shown, along with the pH thresholds (minimum = 8.50, maximum = 8.56). (B) Solenoid activity is recorded in digital bits; 1=on, 0=off; solenoids activate when the pH of the culture vessel deviates from the set range in an acidic or basic direction.

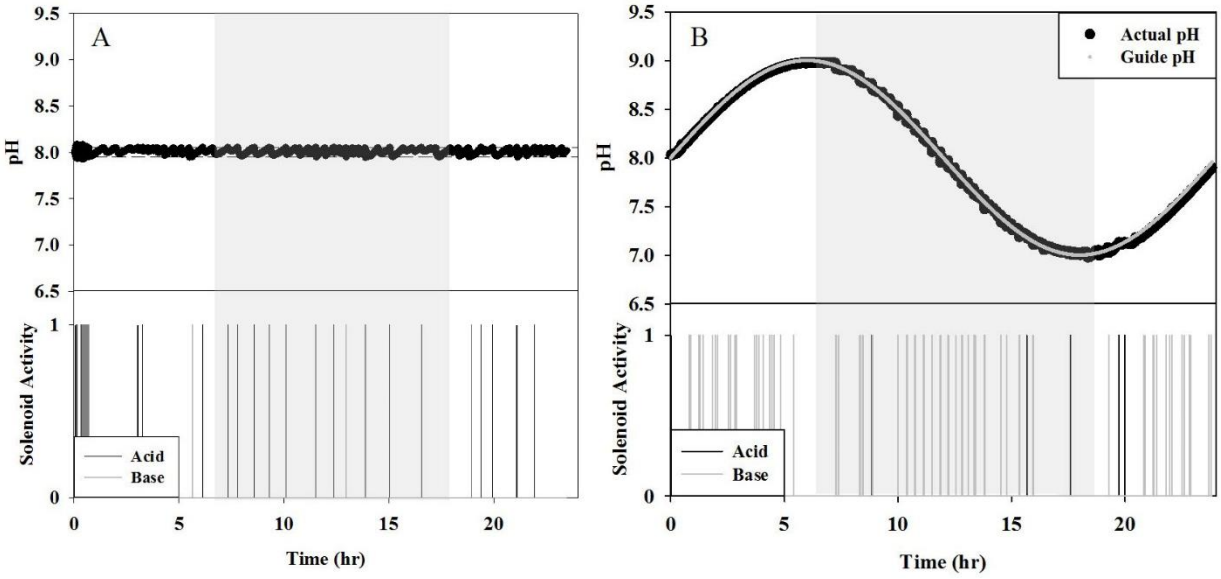

Figure 2.5: Representative data set of a pH time series from abiotic pHstat runs (n=3) with pH adjustment performed using the liquid manifold over 24 h.) Shaded areas show dark periods. (A) Static pH regime, mid point of 8.0. Horizontal dotted lines indicate pH thresholds (maximum = 8.05, minimum = 7.95) (B) Dynamic pH regime, mid point of 8.0, wave amplitude of 0.5. Gray line indicates guide pH, black line indicates measured pH. Activity of solenoid valves during the time series shown in bottom panels, with 0 = off and 1 = on.

The gas manifold used a custom gas mixture (including an elevated concentration of CO_2) and high purity air to adjust the vessel pH in an alkaline or acid direction, respectively; for the liquid/reagent manifold, Na_2CO_3 or HCl were used. The gas manifold had a precision of ±0.10 pH units (n=2), while the reagent manifold had a precision of ±0.03 pH units (n=3) at optimal reagent concentration. We determined the optimal reagent concentration for pH adjustments by examining rebound time as a function of reagent concentration and size of acidic and alkaline pH perturbations. Our goal was to use concentrated reagents (to reduce dilution of the culture by fluid addition), while avoiding overcompensation during pH adjustment, which can occur when the too much acid or base is added; for instance when reagents are too concentrated. High reagent concentrations above the suggested optima will cause the system to experience a slight loss of precision in the control of pH. In our experiments, the optimal reagent concentrations were determined to be 0.1 N HCl and 0.1 N Na_2CO_3 for acid and base reagents, respectively (Table 2.2). High reagent concentrations above the suggested optima will cause the system to experience a slight loss of precision in the control of pH. At the highest concentrations tested (0.12 N HCl, 0.20 N Na_2CO_3), pH precision was at best ±0.06 pH units, as opposed to the ±0.03 pH units at the optimal reagent concentrations, and required more reagent volume to stabilize the pH. Still higher reagent concentrations required further widening of the pH thresholds to avoid overcompensation and eventual loss of pH control. Thus, the gas manifold was able to control pH within 1.3% of the target value, and the liquid manifold was able to control pH within 0.04% of the target value.

Table 2.2: Results from determination of optimal reagent concentration for the reagent manifold. Data was obtained by measuring the time it took the system to bring the pHstat back into range after a 1.5 pH unit perturbation (rebound time). All tests were performed in triplicate. The acid reagent used was HCl, and the base reagent used was Na_2CO_3.

Concentration	Acid rebound time (s)	Base rebound time (s)	pH precision
0.20 N (n=3)	--	368 (S.D. = 23)	±0.06
0.12 N (n=3)	364 (S.D. = 22)	--	±0.06
0.10 N (n=3)	344 (S.D. = 45)	425 (S.D. = 56)	±0.03
0.05 N (n=3)	394 (S.D. = 22)	673 (S.D. = 32)	±0.03

The 72 h biotic perturbation experiments were performed in triplicate using cultures of the marine haptophyte flagellate, *Isochrysis galbana*, to test the ability of the system to maintain a target pH in the presence of a photosynthesizing organism. This organism was chosen based on its short generation time (approximately 1.75–2.0 d under the growth conditions described above) and its ability to achieve high cell densities in culture in order to place substantial stress on the capacity of the pHstat to maintain a given pH regime in the presence of high biological activity. System performance (i.e., ability to maintain target pH) was assessed for both steady state and fluctuating conditions (Figs. 2.6 and 2.7).

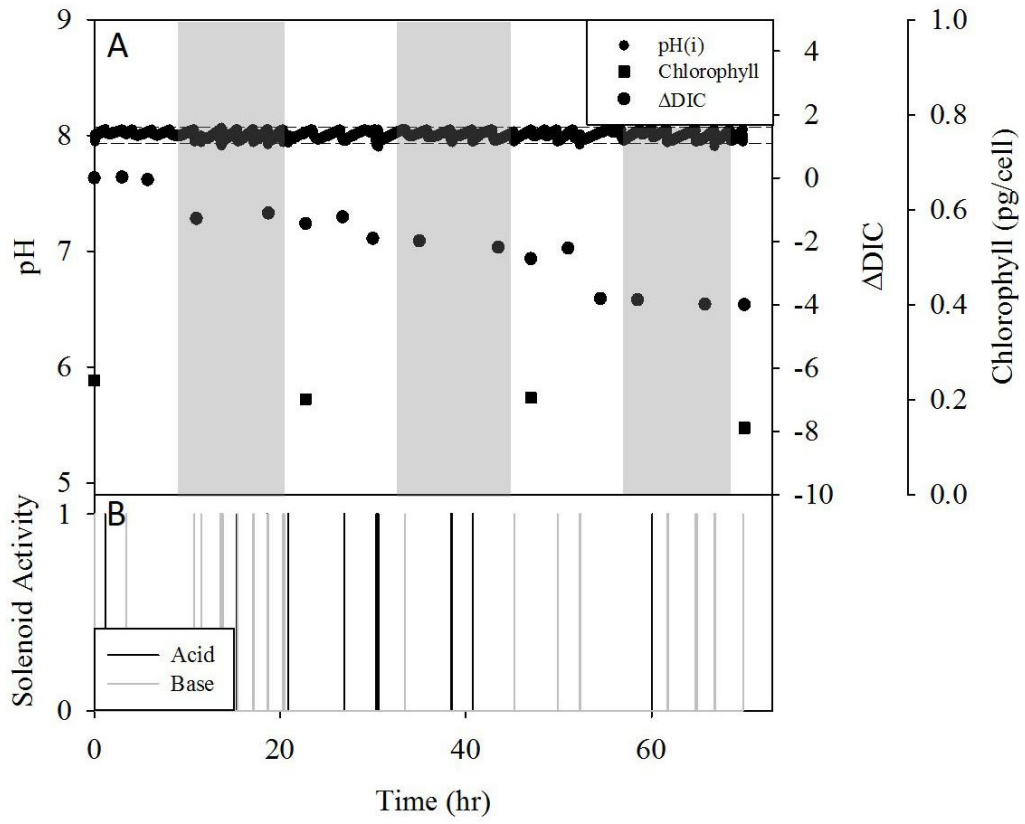

Figure 2.6: Representative data set from tests to determine deviations from a single target pH (8.0, static pH regime) in the presence of phytoplankton (*Isochrysis galbana*) with pH adjustment performed using the liquid manifold over 72 h (n=3). Shaded areas showing dark periods. (A) Time series of pH measured by the in situ sensor within the culture vessel. Horizontal dotted lines indicate pH thresholds (maximum = 8.05, minimum = 7.95). Black free circles indicate the change in DIC relative to initial concentration. Black squares show chlorophyll content per cell, with error bars representing standard deviation (error bars too small to be seen). (B) Activity of solenoid valves during the time series, with 0 = off and 1 = on.

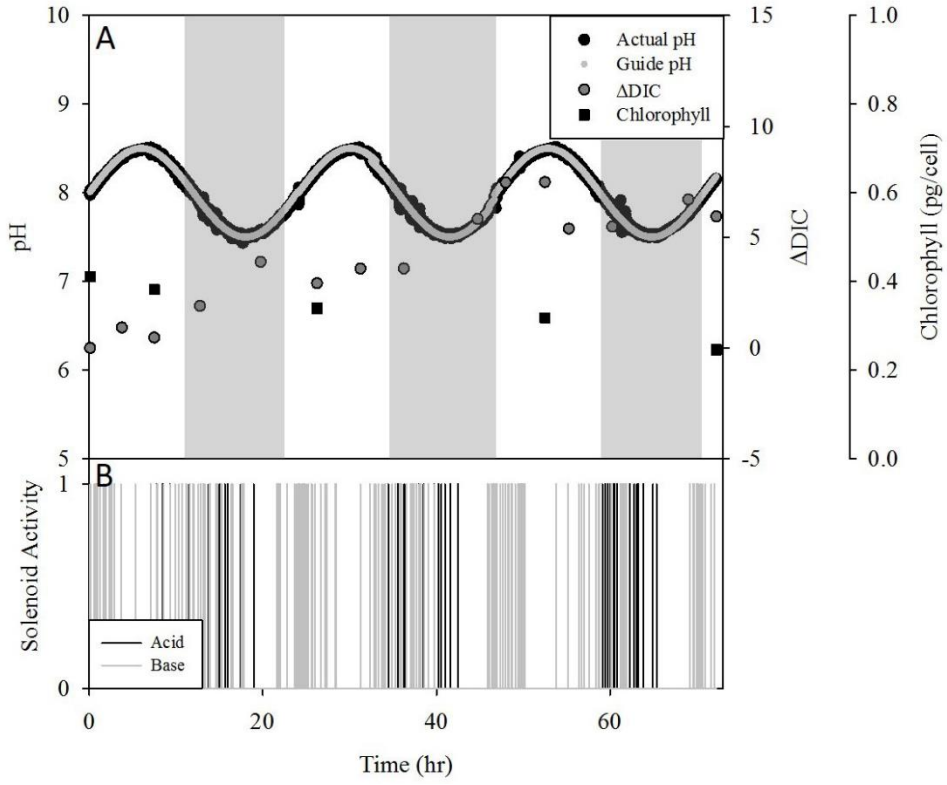

Figure 2.7: Representative data set from tests to determine deviations from cyclic fluctuations of target pH in the presence of phytoplankton (*Isochryrsis galbana*) pH adjustment performed using the liquid manifold over 72 h (n=3). Shaded areas indicate dark periods. (A) Time series of pH measurements made by the in situ sensor within the culture vessel. Gray line is the computer generated guide pH, black shows measured pH. Gray circles indicate the change in DIC over the course of the experiment due to biological activity, as well as the input of carbon from the addition of the alkaline reagent Na_2CO_3 to maintain pH cycling. Black squares indicate chlorophyll content per cell, with error bars (too small to be seen) representing standard deviation of triplicate measurements. (B) Activity of solenoid valves during the time series, with 0 = off and 1 = on.

Table 2.3: Results from performance tests of the pHstat. Growth rate data for *I. galbana* are included since additional biomass-dependent stress to the system should occur in response to changes in CO_2 resulting from photosynthesis and respiration. Solenoid activity (in seconds per day) indicates how much the system has to work to keep pH level to within user-defined thresholds. Error ranges represent one standard deviation of the mean value.

Experimental condition	**Target pH**	**Programmed pH thresholds**	**Mean pH variability**	**Mean solenoid activity (s d^{-1})**	**Growth rate (d^{-1})**
Abiotic, steady state (n=3)	8.00	±0.03	-0.011 ± 0.025	246 ± 59	n/a
Abiotic, dynamic (n=3)	8.00	±0.05	-0.006 ± 0.017	851 ± 149	n/a
Biotic, steady state (n=3)	8.20	±0.03	+0.021 ± 0.054	588 ± 171	0.33 ± 0.11
Biotic, dynamic (n=3)	8.00	±0.05	-0.003 ± 0.017	1622 ± 298	0.26 ± 0.02

Specific growth rates for the steady state and dynamic pH regimes were 0.33 ± 0.11 d^{-1} and 0.24 ± 0.02 d^{-1}, respectively (Table 2.3). The slower growth rate observed under the dynamic pH regime suggests that higher pH variability had a negative effect on cell growth. We measured chlorophyll content per cell during the process of acclimation to culture conditions; under both the static and dynamic pH regimes there was an overall decline in cellular chlorophyll content (Figs. 2.6A, 2.7A) as the cells underwent acclimation. Despite the decline in cell chlorophyll content, however, the amount of DIC in the system during the steady state run decreased over time due to photosynthetic activity. In contrast, the amount of DIC in the system during the dynamic pH run increased despite photosynthetic DIC consumption due to the much higher input of carbon from the alkaline reagent (Na_2HCO_3) over the course of the day as the system maintained the programmed pH cycles. This was confirmed by using the volume and concentration of Na_2HCO_3 added to the culture vessel to calculate the amount of DIC added from reagent addition over the course of the experiments (data not shown). This difference in DIC input and overall concentration in the cultures for steady state versus dynamic pH regimes should

be taken into account when planning an experiment. High culture biomass for the dynamic regime will consume some of the excess DIC and should ameliorate this difference somewhat.

We performed 4 x 48 h runs to demonstrate that the pHstat can be set to produce any desired cycle amplitude and midpoint (beginning/end) by modifying the parameters of the sine wave generated by the computer as a pH guide (Fig. 2.8). We also demonstrated that the pH cycles can be decoupled from light/dark cycles (Fig. 2.8A vs. Figs. 2.8B,C,D).

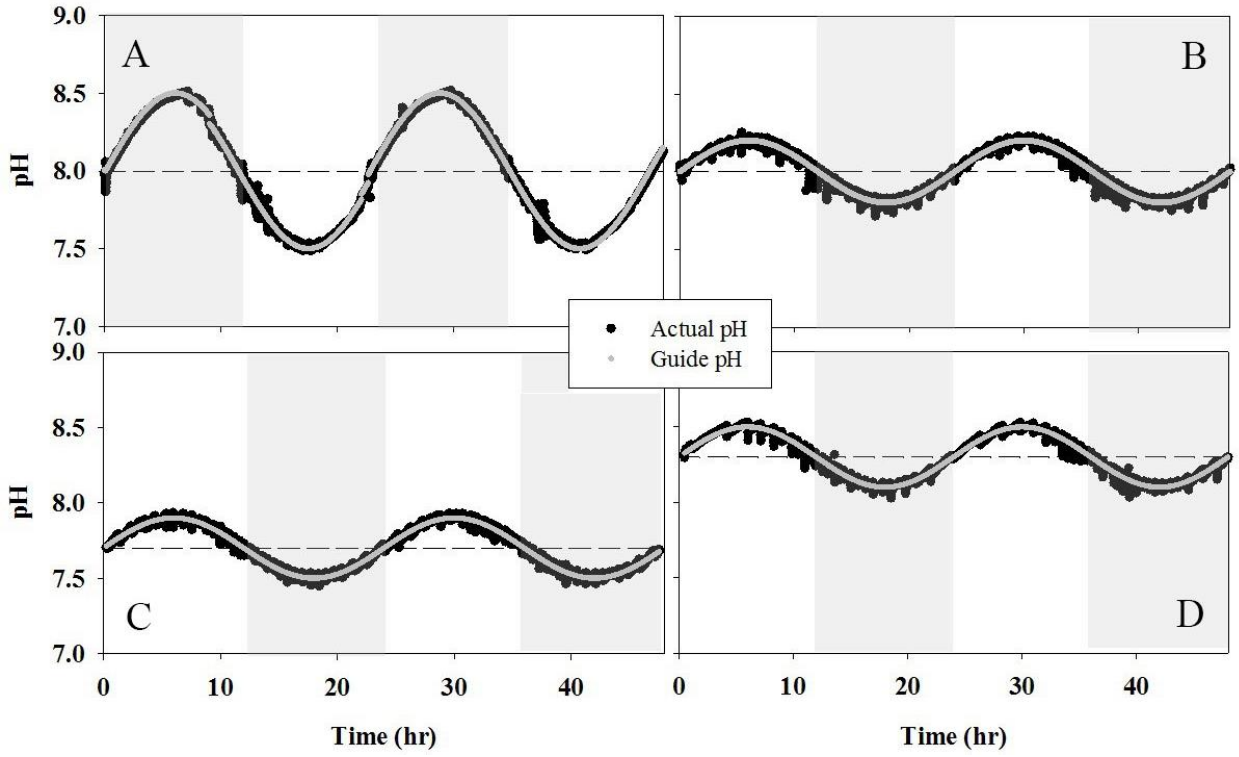

Figure 2.8: Demonstration showing the system's ability to track programmed pH variations of different amplitude and set point (mid-point) around which variations occur. (A) Amplitude = 0.5 pH units, mid-point pH (dotted line) of 8.0 units; (B) Amplitude = 0.2, mid-point pH = 8.0; (C) Amplitude = 0.2, mid-point pH = 7.7; (D) Amplitude = 0.2, mid-point pH = 8.3. Shaded gray areas indicate dark periods of day. Note the difference in diel pH vs light variations in A vs B, C, and D.

2.6 Discussion

Concern regarding ocean acidification has led to an increase in research on the effects of changing pH on marine organisms (Gattuso and Hansson 2011; Andersson and Mackenzie 2012; Ying et al., 2014; Li et al., 2016). Physiological research requires a stable environment with minimal non-experimental variability, and ocean acidification research further requires a culturing system that both records fine-resolution pH measurements and makes precise pH adjustments. We addressed these needs by designing and constructing a programmable pHstat tailored to small-scale benchtop cultures with the flexibility to simulate steady state or fluctuating pH levels that reflect variations observed in natural systems. The system is relatively cost effective and can be built with a basic knowledge of electronics and programming for approximately $2000 for the initial unit, with the possibility of building up to two additional units for less than $1700 each (Table 2.4; at the time of publication, excluding labor and software licenses). Additional systems cost less because some of the hardware components can be shared between pHstats. The Appendix includes more detailed schematics. The pHstat autonomously monitors, records and controls pH using a system of solenoid valves that can be easily assembled, expanded or modified. The method of pH modification (gas or reagent driven) is chosen by the user and can be easily changed in minutes.

The user can program the pHstat system to either maintain a constant pH within a set of acceptable thresholds, or to maintain the culture in an environment that undergoes cyclic variations in pH. Dynamic pH regimes can be set to cycle at any desired frequency, at any desired cycle amplitude and midpoint (beginning/end) by modifying the parameters of the sine wave generated by the computer as a pH guide (Fig. 2.8). Use of the dynamic regime provides a

tool to explore the influence of circadian rhythms on pH and phytoplankton physiology, by decoupling pH from light/dark cycles in photosynthesis and respiration (Fig. 2.8A).

Table 2.4: Approximate cost (in USD) of separate components.

Instrument	**Approximate Cost (2017)**
pH Sensor	$90
Digital I/O Device	$90
Go!Link	$60
GEORG	$320
Reagent Manifold	$250
Gas manifold	$350
Adjustable-Rate Peristaltic Pump	$150
Culture Vessel	$100
Miscellaneous Components	$350

This pHstat system achieves fine-scale regulation of pH directly, rather than by monitoring and regulating DIC or alkalinity. Many pHstats described in the literature (Hoffmann et al. 2013; Wynn-Edwards et al. 2014; Bockmon et al. 2013) have focused on constraining and sometimes controlling DIC, alkalinity, or other parameters affecting pH, while pH is considered as an attending variable. While oceanic pH is overwhelmingly influenced by alkalinity and the buffering capacity of available inorganic carbon species, various strategies for carbon acquisition — mainly carbon concentrating mechanisms (CCMs) — can render the ambient concentration and speciation of DIC less important than pH itself. For example, Chen and Durbin (1994)

showed that the difference in growth of two species of the marine diatom *Thalassiosira* as related to pH had less to do with the means by which pH levels were achieved (i.e., by bubbling with various gasses (CO_2, air, N_2) versus the use of chemical reagents) than by the pH of the culture media itself. The fact that there was no appreciable difference in growth rate between pH adjustment using gas versus chemical reagents suggested that differences in alkalinity had little effect on growth, since the use of reagents changed alkalinity as well as pH, while bubbling resulted in a change in pH without a corresponding change in alkalinity. Similarly, Eberlein et al. (2014) found that growth of non-calcareous dinoflagellates were unaffected by changes in pCO_2 when pH was maintained at a constant level (8.0 pH units), and Cyronak et al. (2015) postulated that changes in cytosolic pH – which is passively regulated in coccolithophores (Mackinder et al. 2010) – are more detrimental to calcification than the calcium carbonate saturation state (Ω) of seawater. The processes modulating intracellular pH (pH_i) are independent from the active regulation of the pH of calcifying vesicles within the same alga (MacKinder et al., 2010). Thus, the effect of OA on phytoplankton may be less related to the aquatic partitioning of DIC than to pH itself, shifting the focus to pH as the master variable (Ying et al., 2014).

Maintaining a pH does not ensure stability of the other variables related to the marine carbonate system such as pCO_2 or alkalinity (Gattuso *et al*, 2010). The design of this pHstat system offers limited controls for these parameters through judicious choice of reagents; use of HCl and Na_2HCO_3 as acid and alkaline reagents, respectively, allows for the maintenance of constant total alkalinity (A_T), while simultaneously adjusting pH and DIC. When choosing an alkaline reagent, a choice must be made between achieving constant alkalinity (by using Na_2CO_3) and allowing the DIC to change over the course of the experiment, versus maintaining a constant DIC concentration and allowing alkalinity to fluctuate (by using NaOH). However, as

stated earlier this system does not actively constrain or measure either DIC nor A_T; this system is designed to function strictly as a pHstat, as there is a significant body of evidence to show that pH is critical variable to study in and of itself. The use of pH probes to monitor and control pH does not offer precise control of these other variables. Precise knowledge of the state of the carbonate system in the culture vessel, measurements of dissolved inorganic carbon (DIC) and A_T should be taken regularly according to accepted experimental protocols (LaRoche *et al.*, 2010) if desired.

Preventing contamination is a major consideration when working with chemostat systems. The current system is vulnerable to contamination, since pH-modifying liquids or gases may carry biological contamination (Fischer et al. 2014). There is also a possibility that some of the components used in a pHstat (e.g., the pH probe) are too delicate to be subjected to the same robust sterilization procedures (e.g., autoclaving) as the culture vessel or media tubing. We followed acceptable sterility protocols for algal culturing such as cleaning components with 70% ethanol followed by a 10% hydrochloric acid solution, and rinsing with ultrapure water (obtained using a Milli-Q® Integral Water Purification System; EMD Millipore Corporation, Darmstadt, Germany). The gas manifold cannot be cleaned this way due to the composition of the solenoid valves. However, in line filters may be used to prevent biological contamination through gas flow. These filters must be kept dry and checked regularly for dampness. In order to prevent contamination of the sterile media reservoir, the reservoir and peristaltic pump should be placed higher than the culture vessel, thereby preventing backflow of the culture. The tube delivering sterile media to the culture vessel should be withdrawn from the culture liquid before the peristaltic pump is turned off to avoid backflow into the lines if the pump slips backward. We monitored the culture for contamination through visual examination of the culture via light

microscopy using a Leica DMIL inverted contrasting light microscope (Leica Microsystems, Buffalo Grove, IL; 20x, 40x magnification), and using the Coulter Counter to count small particles (e.g., bacteria; size range 2-4 μm).

When using the gas manifold it is important that the vent is sufficiently far from the media surface that the churning action of the bubbles does not cause the surface of the water to contact the filter. Using a 0.22 μm glass fiber syringe filter attached to the vent port may be problematic, as water vapor and aerosols released during the bubbling period may cause the filter to become damp, making it much less penetrable by gases. Continued bubbling may cause the filter to detach explosively from the culture vessel. A 10 mL disposable pipette cut at the 8 mL mark and filled with sterile glass wool makes an excellent vent, as it can absorb water vapor without losing its effectiveness.

Because the bubbling generated by using the gas manifold is quite vigorous, it can create a significant amount of turbulence in the culture vessel. For this reason, the gas manifold is not recommended for pH modification when more delicate organisms are grown. For such organisms the reagent manifold should be used to modify the pH of the system, as it generates far less turbulence in the culture vessel. However, it is important when choosing a mixing regime to take into account the sensitivity of the test organism to turbulence. Our observations (data not shown) showed some organisms (*Isochrysis galbana*, *Thalassiosira* sp., *Dunaliella salina*) are quite resistant to shear and other stressors caused by turbulence from higher velocity magnetic stir bars (>100 rpm) and bubbling. Many organisms lack this resistance and require far gentler mixing. Dinoflagellates tend to be quite sensitive to turbulence (White 1976; Berdalet 1992; Barton et al., 2014); in our experience with multiple species of *Alexandrium*, the cells responded poorly to mixing at any speed above 30 rpm (data not shown). Because the reagent manifold requires a

significant amount of turbulence in order to properly mix the pH-modifying reagents with the culture media, larger paddles or blades (preferably with non-uniform blade profiles) available with low velocity overhead stirrers provide sufficient mixing at low rpm to resolve this issue satisfactorily.

Greater pH control was achieved using the liquid manifold, with a resolution of ±0.03 pH units. However, we advise not setting the maximum and minimum pH thresholds within 0.05 pH units of one another for extended periods of time, as this overtaxes the solenoids and can lead to overheating and solenoid failure. If the experiment requires a tighter pH control, modification of the reagents used, the size of the vessel, or the use of industrial strength solenoid valves may help alleviate this problem. We found that the mean pH adheres more closely to the target pH than the programmed pH thresholds (Table 2.3). However, because of the slight delay between reagent release into the culture vessel and the homogenous dissolution of said reagents by mixing, this programmatic "buffer" is necessary to prevent overcompensation by the solenoid valves.

Pinching and flushing the reagent lines once daily will prevent any buildup or precipitates from blocking the lines, and should be included in standard daily maintenance practices. Other daily maintenance practices should include recalibrating (and if necessary, cleaning) the pH sensor, checking and refilling reagent or sterile media reservoirs as needed, checking vent filters for signs of moisture, examining the media lines for signs of contamination, and emptying the waste reservoir as needed.

Daily withdrawal of samples from the chemostat should not exceed 10% of the culture volume to maintain steady state conditions (LaRoche et al., 2010). When growing organisms that exhibit a slow growth rate, the sample volume must be reduced further to avoid perturbing the

stability of the system. In general, cell densities should be kept lower in a pHstat than in most chemostats, as high cell densities can cause the chemistry of the media to shift significantly, even if pCO_2 and pH are held at a static level (Shi et al., 2009).

Care should be taken when growing organisms with a tendency to form biofilms, or otherwise adhere to the sides of the culture vessel, as this system is optimized for pelagic marine microbiota. Wall growth may become a problem with certain organisms. Bubbling or more vigorous mixing may deter wall growth of some organisms.

As when working with any electrical system, the user should take all precautionary measures when handling the electronic and electromechanical components, especially due to the proximity of a highly ionic water solution. A basic knowledge of electronics is necessary to build components of this system (e.g., the pH-modification manifolds and GEORG). For safety purposes, if the user does not possess this knowledge we suggest seeking out a more experienced individual to construct this portion of the system.

2.7 Conclusions

The pHstat system described here is novel in its ability to not only maintain a constant pH, but also to produce daily pH fluctuations that may be used to simulate diel variability in pH that is driven by biological processes (photosynthesis, respiration) or mixing of water masses (e.g., tidal exchange). The precise control of this system minimizes experimental variability, and facilitates the design and implementation of studies that will provide much needed information about the responses by marine microbiota to fluctuations in pH in aquatic ecosystems.

CHAPTER 3

Determination of intracellular pH in phytoplankton using the fluorescent probe, SNARF, with detection by fluorescence spectroscopy

Rachel L. Golda, Lauren T. Roof, Joseph A. Needoba, Tawnya D. Peterson

3.1 Abstract

The maintenance of pH homeostasis is critical for a variety of cellular metabolic processes. Although ocean acidification is likely to influence cellular metabolism and energy balance, the degree to which intracellular pH in phytoplankton differs from the external environment under varying environmental pHs is not well known. As a first step, we tested the performance of the fluorescent pH indicator seminaphtharhodafluor (SNARF) for measuring intracellular pH in a number of phytoplankton taxa in culture. SNARF detection was accomplished using fluorescence spectroscopy (FS), flow cytometry (FCM), and laser scanning microscopy (LSM). Of these, FS proved the most sensitive; FCM showed variably usable fluorescence for pH_i calculations. Since SNARF fluorescence is activated by cleavage of an ester group from the core fluorophore by non-specific esterases, we compared esterase activity in various phytoplankton taxa using the esterase activity indicator fluorescein diacetate (FDA). Specific esterase activity had a positive relationship with cell volume; this influenced SNARF detectability by FCM, since small cells had insufficient fluorescence to separate signal from noise. Since effectively all cells showed fluorescence in SNARF assays, it is unlikely that

enzyme specificity and differences in individual esterase profiles will adversely affect SNARF performance in phytoplankton at sufficiently high loading concentrations of SNARF.

3.2 Introduction

Intracellular pH (pH_i) is a key physiological parameter that influences signaling, cell cycle progression, enzyme conformation and ion transport within the cell (Busa and Crowe 1983; Liu et al., 2001; Taylor et al. 2012; Gibbin et al. 2014), making pH regulation a critical component of cellular physiology. pH_i homeostasis is maintained through the use of buffers (i.e., endogenous acids and bases) and active ion transport (Booth 1985), with steep gradients maintained between the cytosol and many organelles (for example, lysosomes and the Golgi apparatus) through a combination of passive and active proton transport (Wu et al. 2000; Demaurex 2002; Casey et al. 2010). Active transport of protons against a concentration gradient is thought to involve the use of voltage-gated ion channels to remove excess H^+ ions (Demaurex 2002; Taylor et al. 2011). In coccolithophores, this process occurs at the expense of calcification (Taylor et al. 2011). In general, marine phytoplankton are thought to couple proton export with Na^+ transport, due in part to the high availability of this ion in marine environments (Taylor et al. 2012); however, the mechanisms by which pH homeostasis is achieved—and the metabolic costs associated with maintaining pH homeostasis—remain poorly known and likely differ with the pH gradient between intracellular and extracellular environments (Gibbin et al. 2014).

A number of techniques have been developed for measuring pH_i *in vivo*, including the use of microelectrodes (Brauer et al. 1996), ^{31}P-nuclear magnetic resonance spectroscopy (Loiselle and Casey 2003), and the disequilibrium of the radio-labeled pH indicator, [2-^{14}C]5,5,-dimethyloxazolidine-2,4-dione (DMO), between intra- and extracellular environments (Espie and

Colman 1981; Gehl and Colman 1985). More recently, pH-dependent fluorophores have been developed, making pH_i measurements more sensitive, less invasive, and less dependent on specialized equipment than the techniques listed above (Loiselle and Casey 2003; Han and Burgess 2010). Fluorophores can be used in a variety of assays to rapidly interrogate an entire population of cells (e.g., when using fluorescence spectroscopy) or consider individual cells (e.g., when using microscopy or flow cytometry). Because of these attributes, fluorescent probes are ideal for studies of pH_i (Wray 1988; Loiselle and Casey 2003; Aymerich et al. 2009).

One of the most popular fluorophores for measuring pH_i is 2',7'-Bis-(2-carboxyethyl)-5-(and-6-) carboxyfluorescein 4 (BCECF; Rink, Tsien, and Pozzan 1982). BCECF has been widely used to measure pH_i in a variety of organic systems, from living tissues to individual organelles, and has been successfully applied to mammalian cell lines, plant tissues, and protists (Han and Burgess 2010; Taylor et al. 2011). BCECF has a single emission peak, the height of which corresponds to the pH of the solution it is suspended in. Dependence on the intensity of a single peak makes pH_i values calculated from BCECF fluorescence emission intensity vulnerable to error associated with variable dye loading, photobleaching, and instrument stability (Owen, 1992; Molecular Probes, 2003).

The use of ratiometric fluorophores such as the seminaphtharhodafluors (SNARF) addresses this limitation (Nakata et al. 2011). In SNARF, the ratio of fluorescence emission intensity at two different wavelengths is used to calculate pH_i. A solution of activated SNARF includes two ionic forms, the acidic SNARF(A), which has a series of attached phenolic groups, and the basic SNARF(B), which possesses phenolate ions (Nakata et al. 2014). The proportion of SNARF(A) to SNARF(B) is directly dependent on pH, since higher concentrations of H^+ ions increase their availability for bonding to the phenolate anion, producing phenol. The transition

from a phenol to a phenolate anion causes a spectral shift from 583 nm (SNARF(A)) to 627 nm (SNARF(B)). pH is calculated by taking the ratio between the intensity of emission peaks at 585 and 627 nm. This eliminates many of the problems associated with BCECF as a single peak indicator (Nakata et al. 2011). An additional benefit of SNARF is that it is excited by visible rather than ultraviolet light, which reduces both damage to the cell and intracellular autofluorescence.

The core fluorophore group distinctive to SNARF is ionic and water-soluble. In order to make SNARF useful for pH_i measurements, it must be able to enter the cell with minimal efflux. Since charged molecules cannot easily diffuse across the plasma membrane, SNARF is chaperoned into the cell using an acetate or acetoxylmethyl (AM) ester group that protects the phenolic group and renders it non-fluorescent and membrane-permeable (Nakata et al. 2010, 2014). Once inside the cell, AM esters are cleaved from the SNARF molecule by nonselective esterases after crossing the plasmalemma into a living cell (Han and Burgess 2010; Nakata et al. 2014). This renders the SNARF molecule, now charged and fluorescent, less likely to efflux from the cell (Breeuwer et al. 1994).

Despite its benefits, SNARF has rarely been used as a pH indicator in algal cells. SNARF has been used in conjunction with the acidophilic *Chlamydomonas acidophila* (Gerloff-Elias et al. 2006), the dinoflagellate *Prorocentrum micans* (Nimer, Brownlee, and Merrett 1999), and coral dinoflagellate symbionts (*Symbiodinium* sp., Venn et al. 2009). However, for these latter symbionts, SNARF was not found to penetrate the dinoflagellate cells, only showing fluorescence in the coral cells. Motivated by an interest to understand how changes in environmental pH (for example, ocean acidification) influence pH_i homeostasis in marine

phytoplankton, we set out to determine SNARF efficacy in a variety of phytoplankton taxa using fluorescence spectroscopy and flow cytometry.

3.3 Methods

3.3.1 Phytoplankton isolates and culture conditions

Table 1 shows of a list of the organisms used in this study. All isolates were purchased from the National Center for Marine Algae and Microbiota at Bigelow Laboratory for Ocean Sciences, with the exception of *Pyrocystis fusiformis* (purchased from Biological & Popular Culture, Inc., Carlsbad, CA), *Dunaliella salina* (gift from J. Case, UC Santa Barbara), *Aulacoseira ambigua* (gift from M. Kagami, Toho University), and *Chlorella vulgaris* (isolated from the Columbia River). Of these, six organisms (*Alexandrium tamarense, Alexandrium fundyense, Thalassiosira pseudonana, Thalassiosira weissflogii, Dunaliella salina, Isochrysis galbana*) were further assessed for performance of the pH_i measurement using fluorescence spectroscopy, flow cytometry, or both.

All organisms were grown in triplicate 25 cm^3 canted neck, untreated sterile cell culture flasks with vented caps (Corning™, Corning, NY) in semi-continuous batch culture on at 12:12 light:dark cycle in media listed in Table 1. Isolates were grown at 15°C while generating the initial SNARF calibration curves and at 20°C during experimental treatments. Irradiance was 250 μmol photons m^{-2} s^{-1} for all taxa except *I. galbana* (160 μmol photons m^{-2} s^{-1}).

Phytoplankton cells were harvested during mid-exponential phase (confirmed by daily cell counts) and concentrated by centrifugation at 12,500 x *g* for 3 min. *Alexandrium tamarense* were centrifuged at a slower speed (5000 x *g* for 5 min) to avoid disrupting the membrane integrity of the cells. Following centrifugation, the supernatant was removed and discarded, and

the cell pellet was resuspended in sterile growth media to remove ectoenzymes associated with the plasma membrane. Since *P. fusiformis* was too buoyant to be concentrated by centrifugation, the cells were captured on a GF/F filter using gentle vacuum pressure and then re-suspended in sterile media.

Cell densities were ascertained using a Coulter Counter Model Z2 particle counter (Beckman Coulter, Indianapolis, IN) to count phytoplankton cells following 20-fold dilution in Isoton II® diluent (Beckman Coulter, Indianapolis, IN). Cell volume was calculated by using measurements obtained from microscopic examination of the cells, in combination with formulae for phytoplankton cell volume provided by (Olenina et al. 2006)

Table 3.1. Organisms used in fluorescence assays. FS = fluorescence spectroscopy; FCM = flow cytometry; LSM = confocal laser scanning microscopy. All analyses were performed in triplicate.

Organism	**Class**	**Habitat**	**Growth Medium**	**FS**	**FCM**	**LSM**
Aulacoseira ambigua	Bacillariophyceae	Freshwater	WC	+	n/a	+
Thalassiosira pseudonana	Bacillariophyceae	Marine	ESAW	+	-	+
Thalassiosira weissflogii	Bacillariophyceae	Marine	ESAW	+	+	+
Chlorella vulgaris	Chlorophyceae	Freshwater	WC	+	n/a	+
Dunaliella salina	Chlorophyceae	Marine	L1-Si	+	-	+
Rhodomonas salina	Cryptophyceae	Marine	L1-Si	+	-	+
Isochrysis galbana	Chrysophyceae	Marine	f/2	+	-	+
Pyrocystis fusiformis	Dinophyceae	Marine	f/2	+	n/a	+
Alexandrium fundyense	Dinophyceae	Marine	L1-Si	+	+	n/a
Alexandrium tamarense	Dinophyceae	Marine	L1-Si	+	+	+

3.3.2 Fluorophore loading

Two fluorescent pH indicators were used: 5-(and-6)-carboxy seminaphtharhodafluor (SNARF)-1, acetoxymethyl (AM) ester, acetate (Life Technologies, Eugene, OR), and 2',7'-bis-(2-carboxyethyl)-5-(and-6)-carboxyfluorescein) (BCECF), acetoxymethyl (AM) (Life Technologies, Eugene, OR). SNARF was the principal fluorescent indicator used and tested;

BCECF was used to visualize fluorescence patterns for comparison to SNARF under the microscope. Stock concentrations (1 mM) of SNARF were made up in anhydrous dimethyl sulfoxide (DMSO; ≥99.9%) and frozen at -20°C until needed. Stock solutions (1 mM) of BCECF were made by dissolving the solid in 80.4 µL of anhydrous DMSO (≥99.9%) immediately before use.

The washed cells were loaded with fluorophore by adding 3 µL of 1 mM SNARF dissolved in DMSO or BCECF [3 µM final concentration), together with 3 µL of a 5% solution of the non-ionic surfactant Pluronic® F-127 (Molecular Probes, Eugene, OR), which disperses the nonpolar SNARF more evenly in an aqueous solution (Molecular Probes, 2003)]. The fluorophores were loaded into the cells through passive diffusion (to avoid compromising cell membrane integrity; Brauer et al., 1996) during an incubation period of 30–40 min. Since some phytoplankton pigments are autofluorescent at the excitation wavelength used to stimulate SNARF fluorescence (French and Young 1952; French et al. 1956; Maxwell and Johnson 2000), subtraction of a non-dyed blank was necessary to eliminate potentially contaminating signal that might influence interpretation of fluorescence data. The blank was treated the same way as the fluorophore-loaded cells (including adding Pluronic® F-127), but avoiding the addition of the fluorescent probes. After incubation, the cells were washed, concentrated twice via centrifugation as described above and resuspended a final time in fresh media prior to the measurement of fluorescence emission. All analyses were performed in triplicate unless otherwise indicated.

3.3.3 Fluorescence measurements

Three methods were used to measure SNARF fluorescence: (1) epifluorescence microscopy, (2) flow cytometry, and (3) fluorescence spectroscopy (spectrofluorometry). Of these, fluorescence spectroscopy and flow cytometry were used to determine intracellular pH; laser confocal microscopy was used to confirm fluorescence of SNARF and BCECF inside the cells, as well as to determine the percentage of fluorescent versus non-fluorescent cells in SNARF treatments.

3.4 Confocal Laser Scanning Microscopy

A confocal laser scanning microscope (LSM 5 PASCAL, Zeiss) was used for epifluorescence microscopy measurements. LSM 5 software (version 3.5) was used to control the microscope and to capture and analyze the images. SNARF-1 and BCECF were excited using the 488 nm channel of a 25 mW argon ion laser. The beam path was configured to pass through the main dichroic beam splitter HFT 488/543/633, and the secondary dichroic beam splitter, NFT 635 VIS to filter the excitation wavelengths. The emission wavelengths were filtered using the high pass filter, LP 650, for Channel 1 to allow all wavelengths above 650 nm to pass to the detector for chlorophyll *a* detection. Channel 2 was used for SNARF detection, and used the band pass filter BP 560–615 to detect all wavelengths between 560–615 nm. The 546 nm (Cy3) reflector was used for visual examination of the cells.

To prepare the cells for microscopic analysis, phytoplankton cells were incubated with SNARF as described above, up to the end of the incubation step. Instead of separating the cells via centrifugation, at this step the cells were gently vacuum filtered onto a 25 mm polycarbonate filter with a 0.2 μm pore size (EMD Millipore, Darmstadt, Germany). Slides were examined at

100x and 400x magnification. Cell density in each field of view (FOV) was determined by manual counting of cells exhibiting SNARF fluorescence. 5 FOVs were counted for each slide, and averages of percent SNARF-positive cells were determined for each organism.

3.5 Fluorescence spectroscopy

A HORIBA Scientific Jobin Yvon FluoroMax-4 spectrofluorometer equipped with a 150 W ozone-free xenon lamp was used to perform spectrofluorometric measurements on the cellular suspensions prepared with fluorescent probes [SNARF, fluorescein diacetate (FDA)]. FluorEssence™ 2.1 software was used to take measurements and process signals. The corrected signal (S1c) was divided by the corrected reference signal (R1c) to account for variations in lamp performance. Calibration of the instrument was confirmed before each run by checking excitation calibration of air at excitation wavelengths 200–600 nm, at increments of 1 nm, emission wavelength at 350 nm; main peak at 467 nm. Emission calibration checks were accomplished by performing a water-Raman scan on a quartz cuvette filled with Milli-Q water. The excitation wavelength was 350 nm and emission wavelengths were 365–450 nm at increments of 1 nm, with the maximum emission wavelength at 397 nm. Cuvettes were also checked for contamination before each run.

Product specifications for SNARF (Life Technologies) indicated that maximum emission should result from excitation at 480–530 nm; following excitation-emission scans, the optimal excitation wavelength was determined to be 520 nm (Fig. 3.1); this wavelength was used for fluorescence detection of SNARF in all subsequent measurements by spectrofluorometry. To account for any variations in cell densities in the suspensions, the fluorescence spectra were normalized to a peak at 683 nm. Autofluorescence was accounted for by subtracting normalized

fluorescence intensities determined in the absence of SNARF from corresponding wavelengths in the SNARF treatments.

Fluorescence emission was measured at two wavelengths: 585 nm (F1) and 630 nm (F2), as suggested by the manufacturer (Molecular Probes, 2003). pH_i was calculated using calibration curves by taking the quotient of F1 divided by F2 (defined as R) at individual buffer pH levels in triplicate samples according to:

$$R = F1/F2 \qquad \textit{Equation 3.1}$$

3.6 Flow Cytometry

A BD Accuri™ C6 Flow Cytometer® equipped with a C-sampler automated sampling platform was used for flow cytometry measurements. The SNARF-1 fluorophore was excited using a 488 nm argon-ion laser, and emission filter sets at 585 nm (Channel FL2) and 670 nm (Channel FL3) were used for detection of the resulting fluorescence signal. Autofluorescence was accounted for by subtracting fluorescence intensities determined in the absence of SNARF from corresponding wavelengths in the SNARF treatments. For each organism, the population of cells exhibiting fluorescence were gated using BD Accuri™ C6 Plus software (BD Biosciences, San Jose, CA) (Fig. B4) and the mean fluorescence readings from control samples were subtracted from the mean fluorescence readings obtained from the SNARF samples inside the gates in order obtain more accurate SNARF fluorescence values.

3.6.1 SNARF calibration curves

To construct the calibration curves, cells were incubated with SNARF as described above. After incubation, before the first of two post-incubation washes, 7.25 µL 6.7 mM

nigericin was added to the SNARF-treated cells and incubated for 10 min. Nigericin is an ionophore; it opens H^+ and K^+ ion channels within the cell membrane; this allows pH_i and external pH to equilibrate while maintaining membrane integrity (Negulescu and Machen 1990), allowing for calibration curves to be built. After equilibration, pH can be determined using a probe submerged in the external growth medium or buffer.

Calibration curves were built from the relationship between pH_i and mean *R* values calculated from fluorescence intensities of the two SNARF emission peaks (585 and 630 nm) using a spectrum of pHs maintained by buffers (Figs. A5, A6A, A7A).

3.6.2 Radioisotopic pH_i measurements

To check the accuracy of pH_i values calculated using SNARF, we used a radioisotopic method. Partitioning of the radio-labeled weak acid ^{14}C-dimethoxazolidine-2,4-dione (DMO) between the cells and the liquid medium was measured and used to calculate pH_i (Waddell and Butler 1959; Johnson and Epel 1981; Espie and Colman 1981; Gehl and Colman 1985; Dason and Colman 2004).

A 6 mL sample was taken from the cell culture and washed via centrifugation (12,500 x *g* for 1 min). Cells were resuspended in an ASW buffer pH-adjusted to 8.5 using K_2HPO_4 and KH_2PO_4. 1 mL was reserved at this point as a blank (i.e., no radioisotope was added). 3.88 μL of 0.02 μCi ^{14}C-DMO stock (American Radiolabeled Chemicals Inc., Maryland Heights, Missouri) were added per ml (19.4 uL in a 5 mL sample) to the remaining cells, and incubated for 30 min. Incubation time was determined through the construction of saturation curves (Fig. B1). At the end of 30 min, the culture was syringe filtered 1 ml at a time through separate 25mm GF/F glass fiber filters, then washed with 5 mL of ASW. Filtrate and wash liquid were captured in a

scintillation vial, where 10 mL of Ecoscint A scintillation fluid (National Diagnostics, Atlanta, Georgia) was added. Filters were placed in separate scintillation vials, and 10 mL of scintillation fluid was added to each. Radioactivity of both filters and filtrate were determined using a Beckman Coulter LS 6500 scintillation counter (Beckman Coulter, Brea, California).

Determination of intracellular volume and extracellular water left on the filter are necessary for the calculation of pH_i. These values are determined using tritiated water (^{3}HHO, Moravek Inc., Brea, California), and tritiated sorbitol (American Radiolabeled Chemicals Inc., Maryland Heights, Missouri), the latter of which is not absorbed by the organism, and thus shows the amount of extracellular water clinging to the cells after washing. For each tritiated radioisotope, 6 mLof culture was washed as described above. 1 mL was reserved as a blank, and 5 µL of 1 µCi ^{3}HHO or 1 µCi ^{3}H-sorbitol were added, and incubated for 30 min (uptake curve, Fig. B2). After incubation, the sample was syringe filtered through GF/Fs 1 mL at a time, with separate filters for each 1 mL. The filters were washed with 5 mL of ASW, and the filtrate was discarded. Filters were placed in scintillation vials, along with 10 mL of scintillation cocktail. Radioactivity was determined using a scintillation counter.

The following equation from Waddell and Butler (1959) was used to calculate intracellular pH:

$$\mathrm{pH(i)} = \mathrm{pK'} + \log\left\{\left[\frac{C_t}{C_e}\left(1 + \frac{V_e}{V_i}\right) - \frac{V_e}{V_i}\right] \mathrm{x}\left[10^{(\mathrm{pHe}-\mathrm{pK'})} + 1\right] - 1\right\} \qquad \textit{Equation 3.2}$$

Where pK' is 6.32 (Espie and Colman 1981; C. Johnson and Epel 1981), C_t is intracellular activity of ^{14}C-DMO, C_e is the activity of the filtrate, V_e is the activity of ^{3}H-sorbitol detected on the filters, and V_i is the activity of ^{3}HHO detected on the filters (Waddell and Butler 1959).

3.6.3 Esterase activity

The fluorescein diacetate (FDA) hydrolysis assay was used to determine total esterase activity (Agusti et al. 1998; Agusti and Sanchez 2002). FDA stocks were made by dissolving 2 mg FDA in 10 mL of 100% acetone and kept at -20°C until used.

Culture material (5 mL) was gently vacuum filtered onto a 25 mm GF/F filter, stored in 50 mL Corning tubes, and frozen at -20°C. To release cytosolic esterases, the filters went through freeze/thaw cycles after a minimum of 3 d initial freeze time (Mayerhoff et al., 2008), followed by immersion in 5 mL deionized water (Chisti and Moo-Young 1986; Byreddy et al. 2015; Kar and Singhal 2015) adjusted to pH 7.60 using the phosphate buffers, K_2HPO_4 (Fisher Scientific, Fair Lawn, NJ) and KH_2PO_4 (Fisher Scientific, Fair Lawn, NJ). After cell lysis, 100 μL 20 mM EDTA was added to the solution, followed by 100 μL 4.8 μM FDA (Invitrogen, Eugene, OR). The solution was vortexed for 5 s and incubated for 60 min at room temperature. After incubation, 5 mL of a 2:1 chloroform–methanol solution was added and the solution was vortexed for 10 s. The tubes were centrifuged at 7000 *x g* for 5 min and the aqueous layer was extracted for analysis by spectrofluorometry (excitation at 490 nm, emission at 515 nm).

It is important to note that the organisms examined in this study are of varying sizes and volumes. It is important to note that the organisms examined in this study are of varying sizes and volumes. Thus, esterase activity for each organism was normalized to cell volume by calculating esterase activity per unit volume to facilitate a more direct comparison of the data.

3.6.4 Statistics

To evaluate the accuracy of the SNARF measurements derived from the calibration curves, we ran a series of regression analyses on calculated pH as a function of observed pH from each individual calibration curve using SigmaPlot 13.0 (Systat Software, Inc., San Jose, CA), and compared the slopes to expected regression curves with a slope of 1. These slope comparisons were made using t-tests. The significance threshold for all analyses was set at $\alpha = 0.05$.

3.7 Results

We used the fluorophore, SNARF, to determine pH_i in several phytoplankton taxa using two detection methods: fluorescence spectroscopy and flow cytometry. Based on excitation-emission scans (EEMs), we identified the maximum excitation wavelength associated with SNARF to be 520 nm. (Fig. 3.1). Confocal laser scanning microscopy (LSM) was used to confirm SNARF fluorescence in individual cells, and to ensure even expression of fluorescence between cell populations and taxa. Observations using a confocal Laser Scanning Microscope showed that all photosynthetically active cells exhibited SNARF (Fig. 3.1) or BCECF fluorescence (not shown).

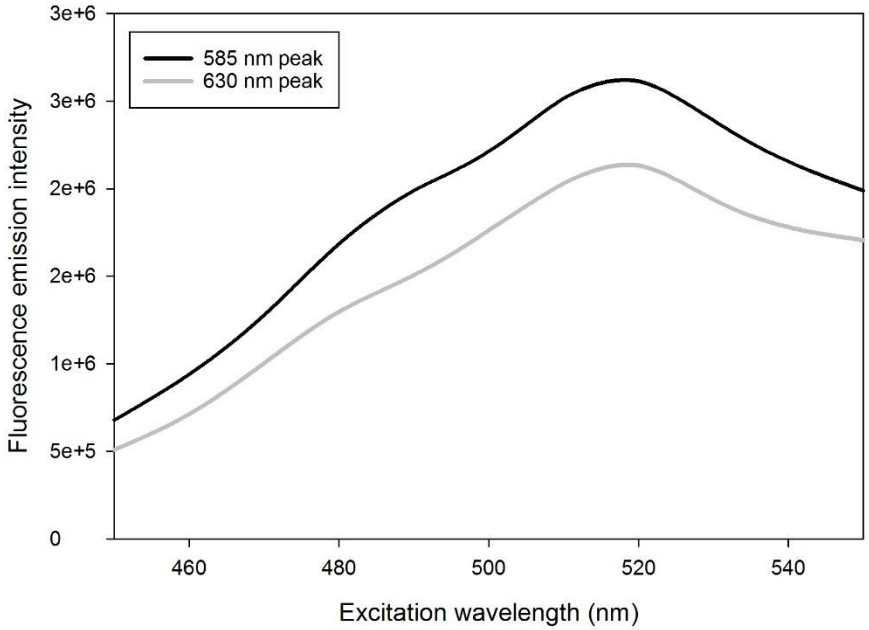

Figure 3.1: Spectra showing best excitation wavelength for maximum emission of SNARF at both fluorescence peaks (585 nm, black; 630 nm, grey).

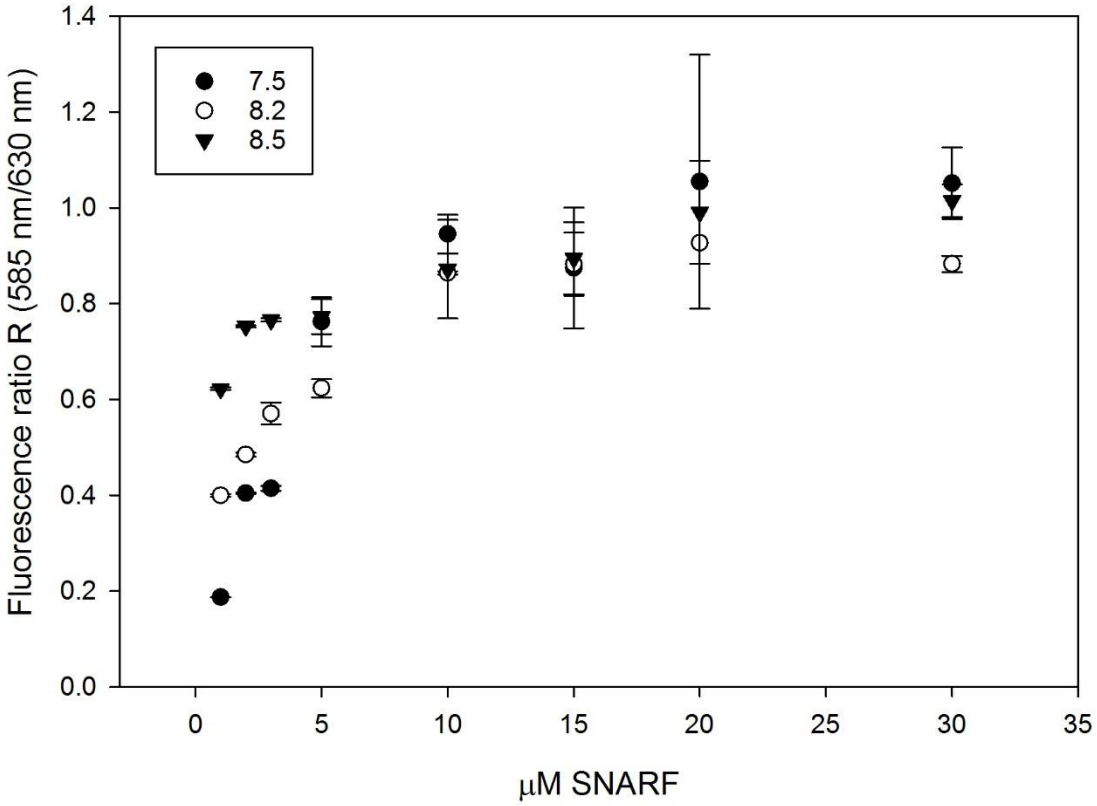

Figure 3.2: Saturation curves for SNARF concentrations during incubation, at different external pHs. Error bars indicate standard deviation. Y-axis is the fluorescence ratio R, determined by dividing SNARF fluorescence intensity at 585 nm by 630 nm.

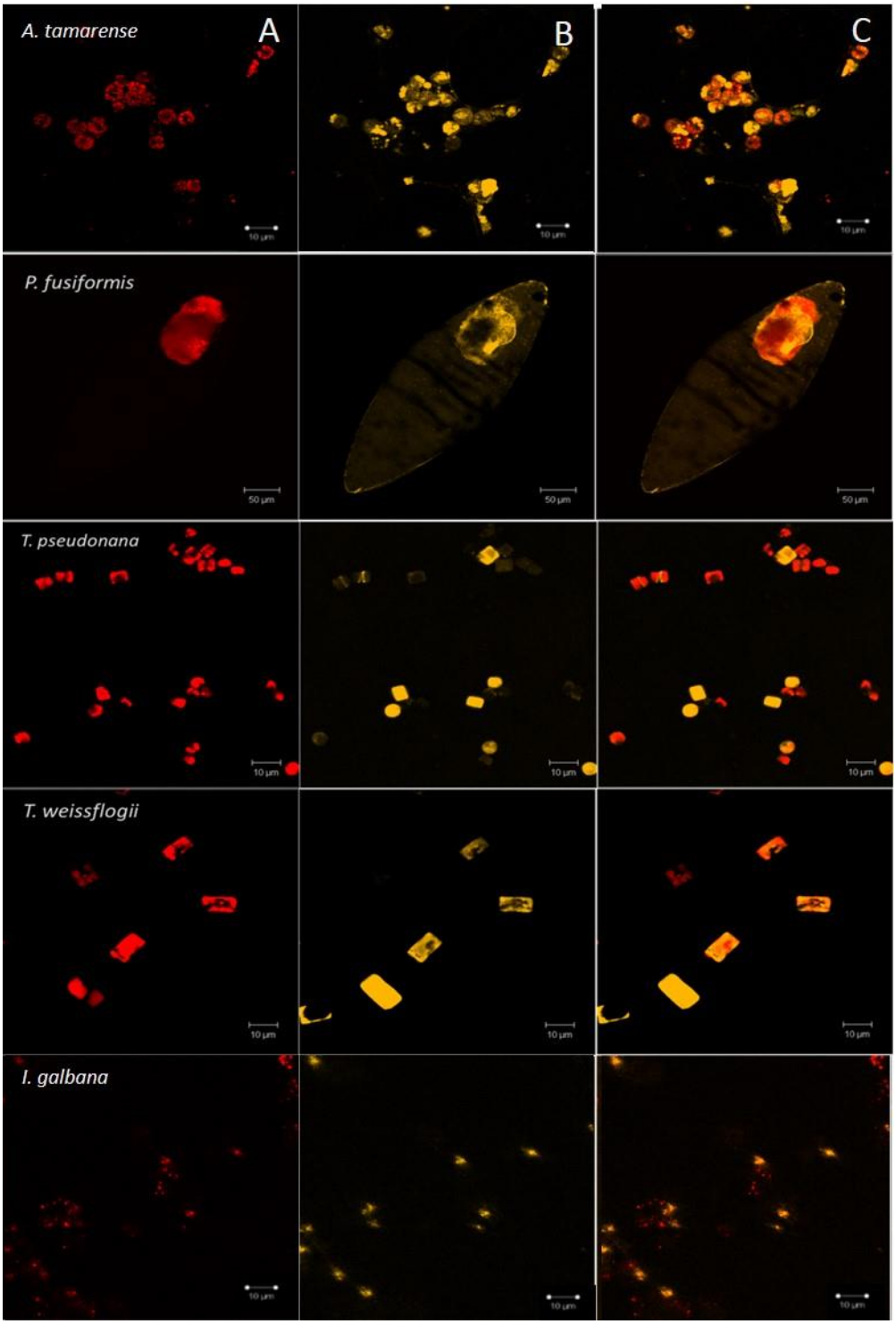

Figure 3.3: Laser confocal images of phytoplankton cells (taxa labeled by line). Column A) Channel 1, autofluorescence of chlorophyll; Column B) Channel 2, SNARF fluorescence; Column C) A + B. *P. fusiformis* image was taken at 100x magnification; all other images were taken at 400x. Scattered red fluorescence for *I. galbana* are chloroplasts from burst cells.

Of the organisms listed in Table 3.1, only two exhibited SNARF fluorescence that was usable for pH_i calculations using flow cytometry (FCM; *T. weissflogii* and *A. fundyense*). The percent error associated with calculated pH_i from FCM measurements was much larger for these two taxa compared to those derived from measurements made using fluorescence spectroscopy (Table 3.2).

Table 3.2: Calibration curve equations for the determination of pH_i in phytoplankton taxa using fluorescence spectroscopy and flow cytometry (FCM). Percent error (% Error) refers to the average percent error between calculated and measured pH values determined in each taxa.

Method	**Organism**	**Equation for calibration curve**	**% Error (n=3)**
Fluorescence spectroscopy	*T. pseudonana*	$y = 313.05e^{-0.831x}$	0.42
	T. weissflogii	$y = 54.119e^{-0.563x}$	1.02
	D. salina	$y = 1189.29e^{-0.752x}$	0.54
	I. galbana	$y = 81.012e^{-0.641x}$	1.10
	A. tamarense	$y = 58.855e^{-0.59x}$	0.47
Flow cytometry	*T. weissflogii*	$y = -0.0014x + 0.0249$	10.3
	A. fundyense	$y = -0.0475x + 0.6719$	4.40

There was good agreement between pH_i calculated from ratiometric fluorescence measurements and expected pH_i. With the exception of *Alexandrium tamarense,* there was no significant difference in slopes of the regressions between calculated and measured pH_i when fluorescence spectroscopy was used to detect SNARF fluorescence ($p > 0.05$; Fig. 3.5). In contrast, much larger error was observed when using FCM (Table 3.2). In addition, there was no difference between calculated pH_i values derived from SNARF and those determined using ^{14}C-DMO disequilibrium (Fig. 3.4, significance threshold of $p \leq 0.05$).

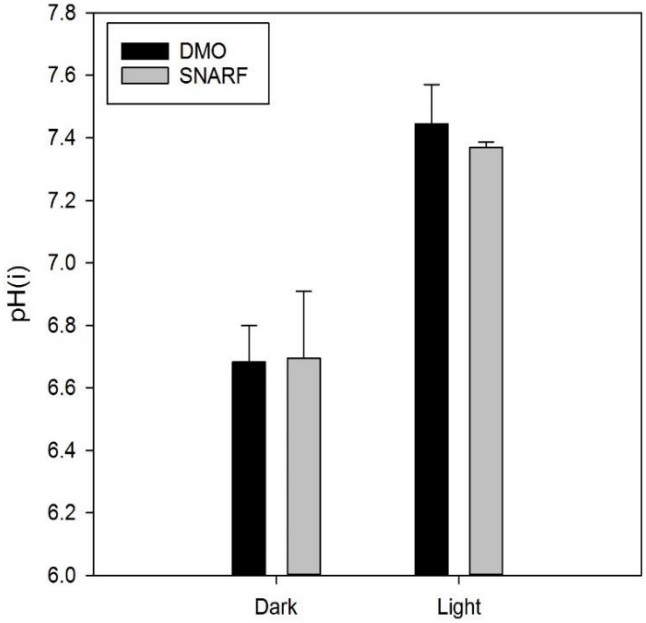

Figure 3.4: Comparison of pH_i calculated using ^{14}C-DMO (black) and SNARF (gray) methods. Error bars indicate standard deviation. No significant difference was found between the values derived for these methods.

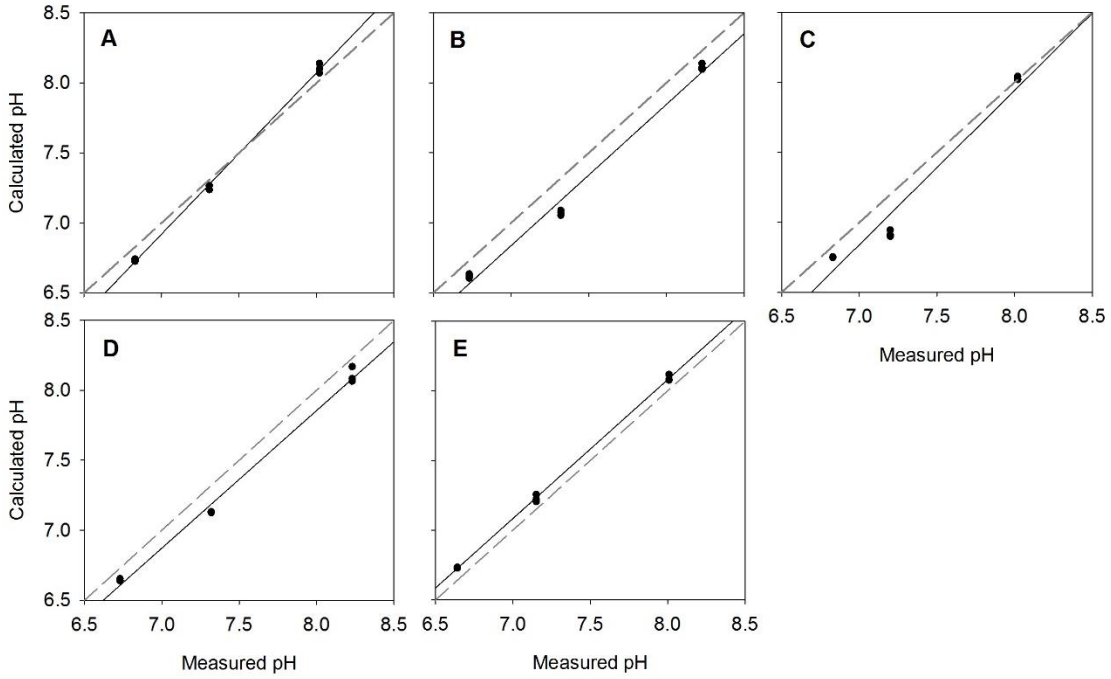

Figure 3.5: Calculated versus measured pH_i determined using fluorescence spectroscopy. 1:1 relationship between measured pH and calculated is indicated by the dotted gray line. Solid black line shows regression for pH values calculated from the individual calibration curves. A) *Alexandrium tamarense*, B) *Isochrysis galbana*, C) *Thalassiosira weissflogii*, D) *Dunaliella salina*, E) *Thalassiosira pseudonana*.

Esterase activity

Since SNARF fluorescence is activated by the cleavage of an AM ester by non-specific esterases, we measured esterase activity in various phytoplankton taxa to determine whether there is variability among taxa that might contribute to assay sensitivity. Esterase activity was normalized to cell density to yield average esterase concentration per cell in a population of cells. In addition, volume-normalized esterase activity was determined for each organism at mid-exponential phase of growth (Table 3.3). *R. salina* had the highest esterase activity among the taxa examined (10.1×10^{-3} fmol min^{-1} μm^{-3}), while the largest taxa, *T. weissflogii* (1.8×10^{-3} fmol min^{-1} μm^{-3}) and *A. tamarense* (0.75×10^{-3} fmol min^{-1} μm^{-3}), had the lowest. Values for volume-normalized cellular esterase activity for the latter two organisms did not differ significantly from each other ($p > 0.05$), but were significantly lower than *R. salina* and *D. salina* ($p < 0.05$). Interestingly, volume-normalized esterase activity in the small diatom, *T. pseudonana* was significantly higher than the larger diatom, *T. weissflogii* ($p < 0.05$; Table 3.3).

Table 3.3: Cell volume, cell-specific esterase activity, and esterase activity per unit volume for 7 phytoplankton taxa.

Organism	Cell volume* (μm^3)	Esterase activity (fmol min^{-1} $cell^{-1}$) (S.D.)	Esterase activity per unit volume ($\times 10^{-3}$ fmol min^{-1} μm^{-3})	
			Not corrected for vacuole volume	Corrected for vacuole volume
Rhodomonas salina	17	0.16 (0.032)	8.13 ±3.67	10.10 ±1.97
Dunaliella salina	20	0.17 (0.048)	8.26 ±2.44	8.70 ± 2.56
Isochrysis galbana	46	0.17 (0.029)	3.60 ±0.62	3.79 ± 0.76
Phytomonas sp.	45	0.16 (0.003)	3.63 ±0.064	3.82 ± 0.067
*Thalassiosira pseudonana***	45	0.17 (0.009)	3.70 ±0.22	5.29 ± 0.31
*Thalassiosira weissflogii***	750	0.75 (0.036)	1.00 ±0.048	1.81 ± 0.086
Alexandrium tamarense	4190	10.2 (0.058)	0.84 ±0.0048	0.842 ± 0.0048

*Cell volumes were calculated using formulae provided in Olenina *et al.* (2006).
**Indicates significant difference between EA per unit volume and EA per unit volume with vacuole volume subtracted.

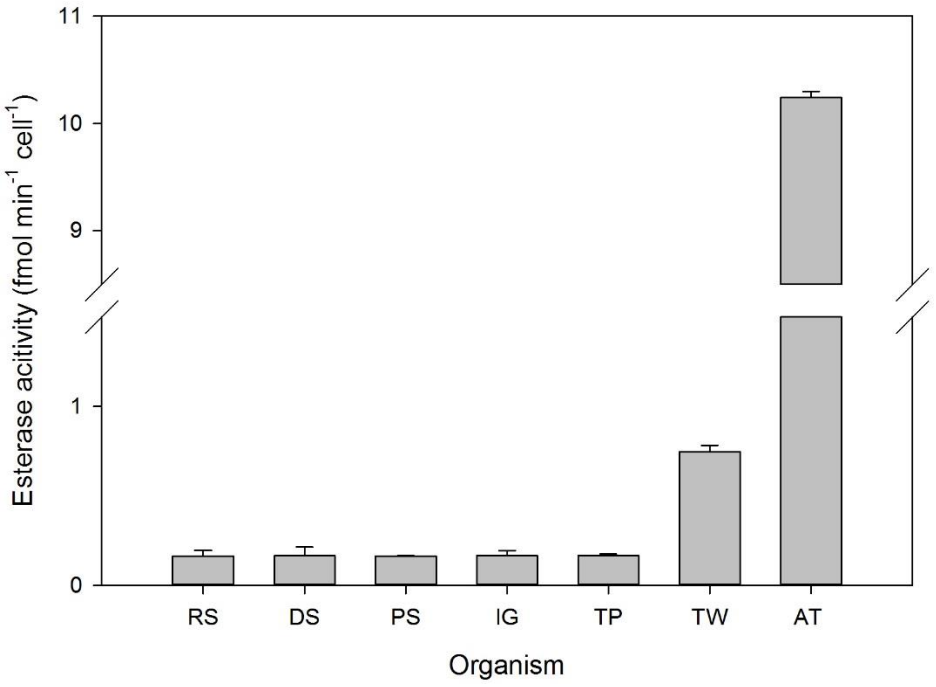

Figure 3.6: Esterase activity for 7 different phytoplankton taxa, indicating total esterase activity per cell (fmol min^{-1} $cell^{-1}$) at mid-exponential phase, with no known stressors. Error bars represent ± 1 standard deviation. RS = *R. salina,* DS = *D. salina,* PS = *Phytomonas* sp., IG = *I. galbana,* TP = *T. pseudonana,* TW = *T. weissflogii,* AT = *Alexandrium tamarense*.

3.7.1 Effect of salinity on esterase activity

Esterase activity varied among organisms grown at different salinities (Fig. 3.7). Significant changes in EA per unit volume ($p < 0.05$) were exhibited by *Phytomonas* sp., *T. pseudonana,* and *T. weissflogii* when salinity was reduced from 35 to 15 PSU. The largest and smallest differences in mean esterase activity were experienced by *T. pseudonana* (increase, 4.61 x 10^{-3} fmol min^{-1} μm^{-3}) and *A. tamarense* (decrease, 3.40 x 10^{-4} fmol min^{-1} μm^{-3}), respectively. However when looking at the percent change in EA, *A. tamarense* (control) showed the greatest change, with a 299% increase per unit volume. The smallest change was exhibited by *R. salina*, with a 7.79% increase in EA (Table 3.4).

Esterase activity increased significantly ($p < 0.05$) in *T. pseudonana, T. weissflogii*, and *Phytomonas* sp. when cells were acclimated to reduced salinity (i.e., 15 PSU) but not in the other

organisms. No cells showed a significant decrease in esterase activity on exposure to reduced salinity. Modifying salinity abruptly ("shock" experiment) and observing EA both immediately (0 min) and after 30 min showed that there was initially a significant difference between the EA for 0 PSU and that of 30 PSU at 0 min; however, this effect disappeared by the next sample time at 30 min, and there was no significant difference between treatments at this point.

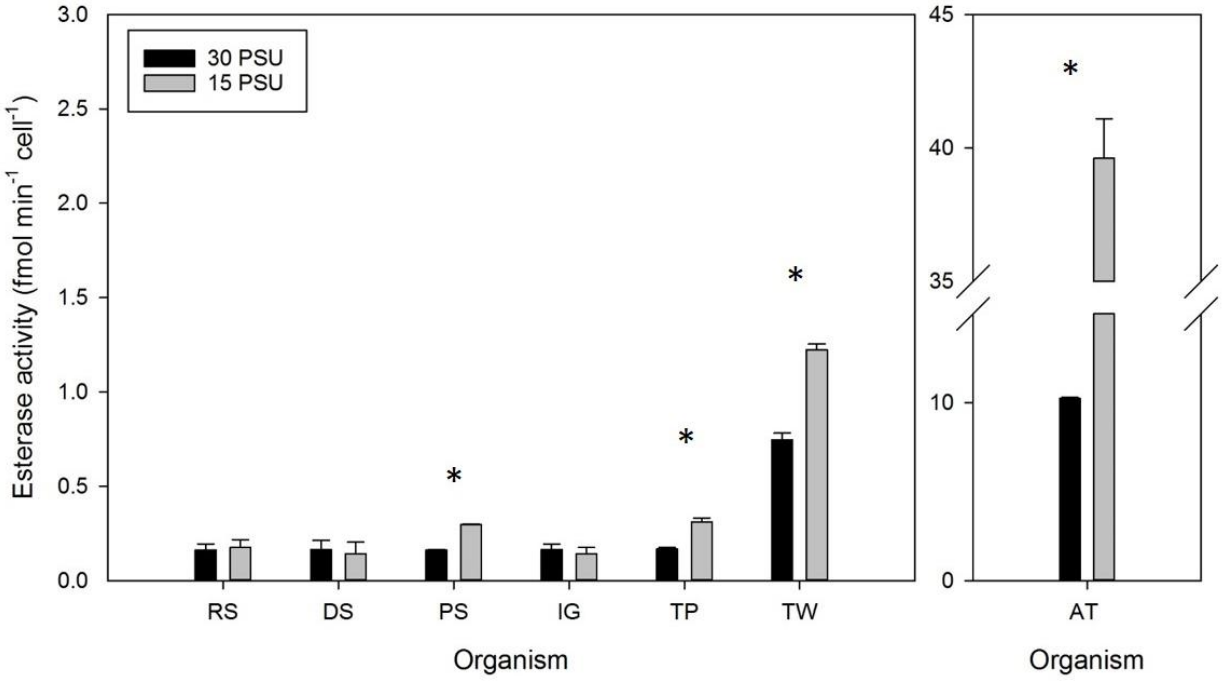

Figure 3.7: Comparisons of esterase activity per cell when exposed to varying salinities. Esterase activity. Column pairs with a (*) indicate organisms for which the esterase activity was significantly different ($p \leq 0.05$) between the 30 PSU and 15 PSU treatments. Error bars represent ± 1 standard deviation. RS = *R. salina,* DS = *D. salina,* PS = *Phytomonas* sp., IG = *I. galbana,* TP = *T. pseudonana,* TW = *T. weissflogii*

Table 3.4: Changes in esterase activity (EA) per unit volume when acclimated to salinities of 30 PSU (control) and 15 PSU. Both actual and percent change relative to 30 PSU of EA are presented.

Organism	**µEA (fmol min^{-1} $µm^{-3}$) (x 10^{-3})**	**Percent change**
Rhodomonas salina	0.79	+7.8%
Dunaliella salina	-1.13	-13.0%
Isochrysis galbana	-0.53	-13.9%
Phytomonas	3.10	+81.2%
Thalassiosira pseudonana	4.61	+87.2%
Thalassiosira weissflogii	1.16	+63.9%
Alexandrium tamarense	3.68	+299.0%
Alexandrium tamarense (high light)	-0.34	-80.3%

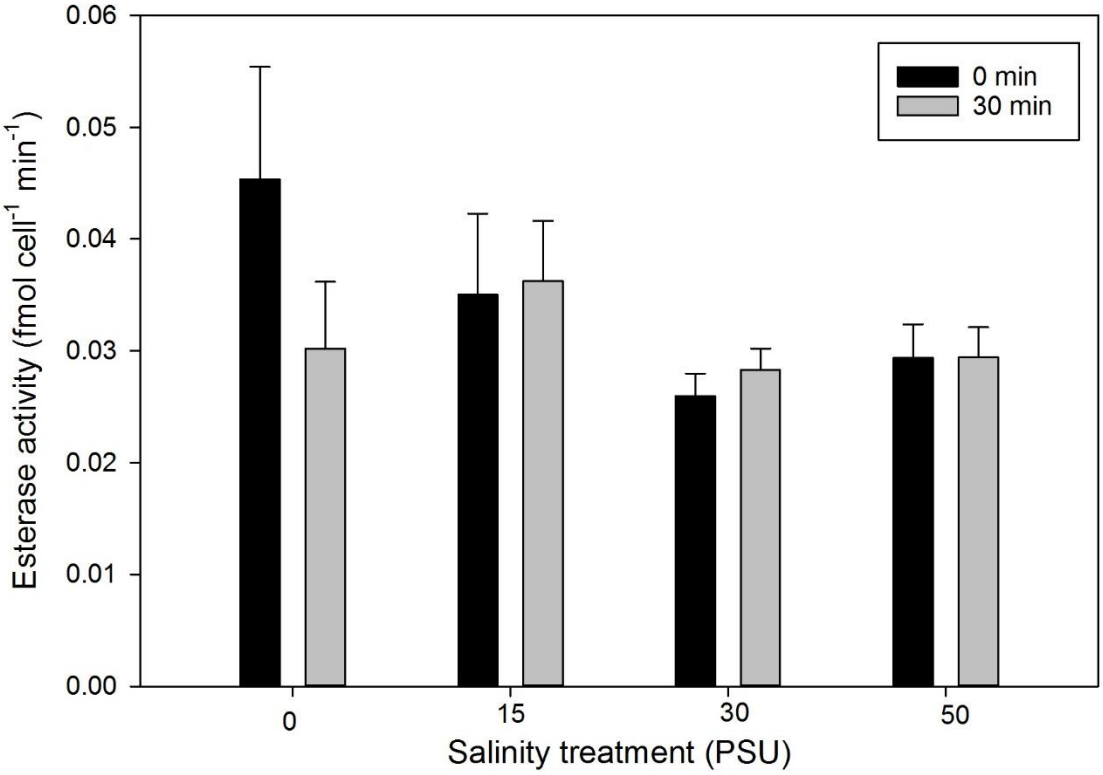

Figure 3.8: Esterase activity in response to acute change in salinity, both immediately (0 min), and 30 min after salinity modification. The esterase activity at 0 PSU at 0 min (t_0) was significantly different from that of the 30 PSU treatment; no other significant differences were observed. No significant difference exists between t_0 and t_{30} for individual treatments.

3.8 Discussion

An increasing interest in identifying ecological effects of ocean acidification motivated us to test the efficacy of a SNARF fluorescence-based assay for the determination of intracellular pH (pH_i) in different classes of phytoplankton. Fluorescence assays are desirable for their sensitivity, simplicity, and non-invasive approach (Loiselle and Casey 2003). Interestingly, a lack of SNARF fluorescence in certain phytoplankton has been observed in the literature, such as has been seen in the dinoflagellate symbiont of the coralline alga, *Stylophora pistillata* (Laurent *et al*., 2013). *S. pistillata* itself exhibited excellent cytosolic SNARF fluorescence, while its symbiont showed no SNARF fluorescence whatsoever. In another study, SNARF fluorescence was detected in *S. pistillata* and in the anemone, *Anemonia viridis*, but not in their respective algal endosymbionts (Venn *et al*., 2009). These observations suggested that SNARF fluorescence in algal cells might be difficult to detect, either because of problems with sensitivity (i.e., total cell fluorescence too faint to be detected using LSM or FCM methods), or that algal esterases were of insufficient concentrations or specific activities to cleave the AM esters from the parent molecule at the necessary rate to produce adequate fluorescence to be detected. We will address both of these issues in the following discussion.

Our LSM observations show that, contrary to the previous reports, SNARF fluorescence is observed in all cells loaded with dye. In this study, fluorescence microscopy showed higher sensitivity in detecting SNARF than FCM, due to greater flexibility in the choice of excitation and emission wavelengths compared to standard flow cytometers. The flow cytometer excites SNARF at the low end of the range recommended by the dye manufacturer (Molecular Probes, 2003) and over 30 nm lower than the excitation wavelength we found to elicit maximum emission (520 nm). In addition, only one of the emission peaks matched up well with the range

of one of the detectors (FL3, at 585 nm); the emission intensity of the second peak was measured at 670 nm (corresponding to the FL4 detector), which lies on the tail end of the second SNARF peak, and is contaminated by chlorophyll fluorescence evident in a peak located at 683 nm. Because of these mismatches, the sensitivity of the assay was likely reduced. However, our experiments show that detection of fluorescent cell populations using FCM could be improved by increasing the loading concentration of dye. For example, we found that increasing the concentration of SNARF during the dye loading process provided stronger fluorescence return for *T. pseudonana*; however, at low SNARF loading concentrations, this organism did not exhibit a change in SNARF fluorescence that was substantial enough to be useful for pH_i calculations. The increase in fluorescence noted at higher SNARF concentrations may make FCM fluorescence detection of SNARF usable for viability assays, even if it lacks the sensitivity for pH_i measurements. BCECF has the same mechanism of activation as SNARF (Loiselle and Casey, 2003; Molecular Probes 2003) as both indicators are activated by ubiquitous intracellular esterases. BCECF has use as a viability indicator(Lloyd et al. 2001; Loiselle and Casey 2003; Xu and Mutharasan 2011) as fluorescent BCECF only accumulates within live, intact cells. Based on this principal, we advance the concept that SNARF has multiple uses as not only a pH_i indicator (which was its primary design function), but can serve a secondary function as a viability indicator, similar to FDA (Garvey et al., 2007). Thus, SNARF has the potential for applications in all methods of fluorescence detection, as long as the limitations of each method and assay (i.e., pH_i, viability) are taken into account.

Optimum dye loading concentration was found to be 10 μM SNARF, as determined by building saturation curves based on the stabilization of the fluorescence ratio. There was no difference in dye loading at different environmental pH levels over a biologically relevant range

(7.5-8.5). It is important to note that accurate pH_i measurements can be obtained from lower concentrations of SNARF using fluorescence spectroscopy as a method of SNARF detection, as long as calibration curves are optimized for these lower concentration. Fluorescence spectroscopy can be used at these lower concentrations due to the high sensitivity of this method of fluorescence detection. Using a lower concentration than is optimum (based on the saturation curve) is desirable for several reasons, the primary of which is the cytotoxicity of the SNARF solvent, DMSO, at higher concentrations (Molecular Probes 2003). Another important consideration is the significant expense that such a high concentration of dye would entail for large-scale experiments.

In this study, only fluorescence spectroscopy of bulk culture material could be used reliably to determine pH_i. Fluorescence spectroscopy has the advantage of greater sensitivity of detection than either LSM or FCM, as well as the ability to interrogate entire populations of cells, which improves the signal-to-noise ratio. We confirmed that SNARF could reliably be used to accurately determine pH_i using fluorescence spectroscopy, which was corroborated by by comparing pH_i values calculated using our SNARF calibration curves to those obtained using the ^{14}C-DMO method, the latter of which is considered the "gold standard" of non-invasive pH_i measurement methods. Thus, SNARF is suitable for investigations of pH_i in algal cultures and field samples.

Because SNARF and BCECF fluorescence both depend on cellular esterases (Molecular Probes 2003; Nakata et al. 2011; Han and Burgess 2010; Nakata et al. 2014), it is important to understand how esterase activity varies among phytoplankton taxa, as this may affect the fluorescent intensity of the dye. This is especially important for small cells, which were harder to

detect using FCM at lower loading concentrations of dye due to the low concentration of total fluorescent molecules present within a smaller cell (and thus a lower signal).

We measured esterase activity in several phytoplankton taxa, including diatoms, nanoflagellates, and dinoflagellates in cultures harvested at mid-exponential phase of growth in order to determine esterase activity of the cells when measured at mid-exponential phase of growth, with no known factors that would cause significant metabolic perturbations. The results showed that EA was highly variable among organisms, and even between different species of the same genus, as observed in *T. pseudonana* and *T. weissflogii.* The significant variation that we observed in esterase activity among phytoplankton taxa agrees with previous work that shows a similar difference in esterase activity among varieties of brewing yeast, with certain taxa showing higher activity than others (Dufour et al., 2008). Similarly, Lund (1967) showed that the concentration of various individual types of esterases present in motile *Streptococcus* sp. differed significantly from those found in non-motile strains of the same serotype. Esterase activity may also vary with cell age, with gross hydrolytic efficiency and overall esterase expression changing over time (Frohlich 1990).

Variations in esterase activity among organisms may be due to differences in the abundance of specific esterases among individuals or organisms, or may be due to differences in the intracellular esterase profiles, or types of esterases present, within specific taxa. Esterase profiles have been shown to be sex-specific (Frohlich 1990), species-specific (Lund 1967; Inoue et al. 1979; Fu et al. 2015), and tissue-specific, with variations occurring among different tissues in the same organism (Paul and Fottrell 1961; Radic and Pevalek-Kozlina 2010). Esterases include any enzyme that can cleave an ester from a larger molecule (Riegman 2002; Lomolino et al. 2005). Some esterases have been found to be highly specific in terms of catalytic efficiency

with relation to various substrates. Koo et al. (2013) identified a highly substrate-specific methyl esterase in *Arabidopsis* that showed a 10-fold reduction in catalytic efficiency in the hydrolysis of other substrates. Another example is that a highly substrate-specific lysosome based esterase, that was exploited in the development of a fluorescent probe to visualize in situ lysosome activity (Gao et al. 2014). However, esterases generally do not display rigorous substrate specificity (Fojan et al. 2000), and those that do still maintain a significant degree of promiscuous activity (Gould and Tawfik 2005; Devamani et al. 2016). For this reason, individual esterases may have a higher enzymatic efficiency with certain substrates as compared to others (Goullet and Picard 1995; Lomolino et al. 2005). For example, in human pseudocholinesterases the rate of substrate hydrolysis can vary by an order of magnitude depending on which esterases are present in serum, due to substrate/enzyme specificity (Uete et al. 1985). Thus, variations in the relative amounts of specific esterases available in the esterase profiles of each phytoplankton taxa may have a significant impact on overall esterase activity, particularly if looking at the rate of hydrolysis of a specific substrate. Therefore, it is possible that some taxa possess esterases that are more efficient at cleaving ester bonds within the SNARF parent molecule. The density and specificity of intracellular esterases ultimately influence the intensity of fluorescence emission, since SNARF fluorescence depends upon the activity of cellular esterases to cleave esters from the parent molecule (Nakata et al. 2011; Han and Burgess 2010; Nakata et al. 2014).

An increase in esterase activity is often attributed to an acute stress response (Agusti et al. 1998; Devonshire and Field 1991; Haubner et al. 2014), which could therefore influence esterase-based fluorescence assays if experimental conditions result in stress to the cells. Although there was an immediate, significant increase in EA at 0 PSU when compared to 30 PSU in the halotolerant haptophyte, *I. galbana* (Kaplan et al. 1986, Pick 2002), there was no

difference between 0 and 30 PSU 30 min after the initial shock. Further, there was no difference in EA between salinity treatments when the difference was smaller. Interestingly, although most of the organisms we examined did not show a significant increase in esterase activity following long-term acclimation to reduced salinity of 15 PSU, the two diatoms, *T. weissflogii* and *T. pseudonana*, which are also considered tolerant of low salinity (Radchenko and Il'yash 2006, Baek et al. 2011), did show an higher esterase activity at 15 PSU compared to 30 PSU. This difference may be the result of increased metabolic demand involved in maintaining osmotic homeostasis. This is consistent with findings that EA increases in response to increased energy demands, as esterases break down the lipids and fatty acids where much cellular energy is stored (Johnson and Alric 2013; Obata et al. 2013; Levitan et al. 2015). Thus, caution must be exercised when using SNARF to determine pH_i if conditions influence EA.

In summary, SNARF is an excellent pH_i indicator when used in conjunction with fluorescence spectroscopy. Its limited efficacy as a pH_i indicator with other fluorescence detection techniques and small cells may somewhat improved when higher concentrations of dye are used during cell incubation. It has the additional advantage of being useful as a viability indicator. In the latter respect it may be more useful than current indicators used for this purpose, such as BCECF, as the ratiometric nature of SNARF reduces or eliminates the problems associated with bleaching, precise cell counts, and leakage (Grynkiewicz et al. 1985; Bright et al. 1989). However, care should be taken when using SNARF in experiments where esterase activity is perturbed by experimental parameters.

CHAPTER 4

Influence of extracellular pH on phytoplankton physiology and cytosolic pH homeostasis under steady state and dynamic conditions

Rachel L. Golda, Joseph A. Needoba, Tawnya D. Peterson

4.1 Abstract

Intracellular pH (pH_i) is a key physiological parameter, affecting protein conformation, enzyme activity, cell cycle progression, and ion transport within cells. Maintenance of pH homeostasis varies among phytoplankton taxa, meaning that pH_i can be influenced by external pH. However, few studies have examined the effects of pH fluctuations on phytoplankton physiology. We used a pHstat system to control external pH in two types of pH environments: (1) static, or steady state and (2) dynamic, or fluctuating. The goal was to determine the influence of external pH on internal pH and physiological parameters (photosynthetic efficiency, esterase activity, growth, and pH_i) at different levels of environmental pH under steady state conditions (7.5, 8.0, and 8.5), as well as under dynamic conditions produced by programmed diel fluctuations of pH around a set value. pH_i varied relatively widely in response to changes in external pH, adjusting inversely to external pH fluctuations. *I. galbana* exhibited lower growth rates for the dynamic coupled treatment and lowest static pH than the highest static pH examined. The changes observed in pH_i appear to affect photosynthetic efficiency, with a significant correlation between pH_i and maximum quantum yield of PSII at lower steady state pH levels. However, the loss of energetic yield from photosynthesis may be partially mitigated

by increased availability of energy from fatty acid hydrolysis due to increased esterase activity, at the expense of growth and reproduction.

4.2 Introduction

Since the commencement of the Industrial Revolution, surface ocean pH has declined by approximately 0.1 unit (Doney et al. 2009a) due to equilibration of anthropogenically derived carbon dioxide between the atmosphere and the ocean (Ciais et al. 2014), termed ocean acidification (OA). OA is predicted to continue to worsen (Gruber et al. 2012; Solomon et al. 2007), with serious consequences for calcifying organisms such as coccolithophores, mollusks, and corals due to complex interactions between pH, DIC speciation, and aragonite saturation state (Cyronak et al. 2015; Doney et al. 2009a; Doney et al. 2009b; Kroeker et al. 2010). Because they are unicellular, the changes that take place in an individual phytoplankton cell's immediate environment are real challengers to cell physiology and biochemistry (Kevin Flynn et al. 2012). Although a number of studies have described short-term physiological responses of phytoplankton to changing pH (Berge et al, 2010; Chen and Durbin, 1994; Dason and Colman, 2004; Nimer et al., 1994; Pancic et al., 2015; Siu et al., 1997), there is a scarcity of data regarding long-term physiological responses to decreasing pH (Pancic et al., 2015). The data that have been published suggest that phytoplankton responses to changes in pH vary among taxa. Iglesias-Rodriguez et al. (2008) showed that calcification and primary production in the coccolithophore, *Emiliania huxleyi*, increased in response to increased pCO_2; however, Feng et al. (2008) showed that the effect of increased CO_2 concentration on calcification and growth of the same organism changes when combined with variations of other physical parameters, such as irradiance and temperature, and in some cases results in decreased calcification rates. There is

also variability in the reported relationship between phytoplankton photosynthesis and pH, with some studies showing an increase in photosynthetic efficiency and primary production under OA conditions (Doney et al., 2009a; Iglesias-Rodriguez et al., 2008; Kranz et al., 2009), and others showing a decline (Doney et al., 2009b; Gao and Zheng, 2010; Kroeker et al., 2010; Riebesell et al., 2000; Russell et al., 2009). A better knowledge of the role of intracellular pH homeostasis on cell physiology is required to explain the variability observed in laboratory studies of phytoplankton response to changing pH (Taylor et al., 2011).

Due to the interrelationship between pH and DIC partitioning, many phytoplankton species are carbon-limited at higher pH, and have higher growth rates at lower pH (Rost et al., 2003). However, because many phytoplankton are equipped with carbon concentrating mechanisms (CCMs), they can continue to thrive in concentrations of carbon that would otherwise be limiting to growth (Nimer et al., 1999; Raven et al., 2011). An essential part of CCMs is the enzyme carbonic anhydrase (CA), which catalyzes the inter-conversion of HCO_3^- and CO_2 (Badger, 2003; Gee & Niyogi, 2017). Not all phytoplankton possess CCMs; for example, many chrysophytes appear to as a group lack a CCM, and thus cannot use HCO_3^- as an alternative carbon source under CO_2 limiting conditions (Maberly et al., 2009). owever for phytoplankton that possess CCMs, pH has been shown to have a greater independent impact on the phytoplankton that possess them than DIC concentration (Cyronak et al., 2015; Eberlein et al., 2014; Hansen et al., 2007; McCulloch et al., 2012), as DIC becomes limiting only at very high pH (Hansen et al., 2007).

Table 4.1: Phytoplankton internal pH (pH_i) with respect to environmental pH (pH_e) or changes in irradiance.

Organism	Class	Internal pH	Environmental pH	Irradiance	Reference
Euglena	Euglenophyceae	5.0–8.0	3.0-8.0	--	(Lane and Burris 1981)
Chlorella	Chlorophyceae	6.4	3.0	--	(Gehl and Colman 1985)
Thalassiosira	Bacillariophyceae	6.7–7.5	6.5–8.5	--	(Herve et al. 2012)
Plectonema boryanum	Cyanophyceae	8.5	na	High light	(Masamoto and Nishimura 1977)
Synechococcus	Cyanophyceae	8.5	na	High light	(Masamoto and Nishimura 1977)
Coccolithus pelagicus	Prymnesiophyceae	$\Delta pH = -0.2^*$	pH_e decreased from 8.0 to 6.5	--	Taylor et al., 2011
Trichodesmium	Cyanophyceae	$\Delta pH = -0.4^*$	pH_e decrease from 8.1 to 7.8	--	(Hong et al. 2017)

$^*\Delta pH$ = change in pH_i after pH_e environmental perturbation

Aquatic environments exhibit significant diel variations in pH due to biological processes—sometimes within hours—that often exceed projected changes due to OA (Flynn et al., 2012; Hinga, 2002; Santos et al., 2011; Waldbusser and Salisbury, 2014). Although pH should not be strongly affected by changes in external pH due to low permeability of the cell membrane to ions (Booth 1985), membrane ion channels permit passive diffusion of H^+ ions across the membrane (Boron 2004). For organisms that lack the ability to upregulate acid/base transporters, this can cause internal pH to track with external pH perturbations over time (Dason & Colman, 2004; Taylor et al., 2011; Table 4.1). These changes are usually curated by cellular machinery that allow cells to maintain a stable intracellular pH. Maintaining pH_i homeostasis puts significant energetic demands on the cell. Phytoplankton are equipped with acid/base transporters and chemical buffers that enable them to maintain pH homeostasis under fluctuating

conditions (Boron, 2004; Casey et al., 2010; Nimer et al., 1994). The manufacture and transport of buffers is used by cells as a short-term mechanism for adjusting pH_i during acute pH perturbations. This process not suitable in the face of sustained pH perturbations, as it is energetically expensive, and individual cells have finite buffer capacity (Boron, 2004; Casey et al., 2010). It is estimated that in mammalian cells the CO_2/HCO_3^- buffer pair make up 50-66% of total buffering capacity of the cell (Boron 2004). HCO_3^- is transported through the cell and across cell membranes using the energetically expensive V-ATPase complex (Dietz et al. 2001). V-ATPase uses ATP hydrolysis to drive active transport of ions, consuming significant energy(Dietz et al. 2001). When faced with sustained pH challenges, the cell will upregulate intrinsic regulatory processes, such as HCO_3^- transporters or acid exporters, to maintain pH homeostasis in response to sustained pH stress (Casey, Grinstein, and Orlowski 2010). While the use of Na^+/H^+ antiporters uses electrochemical gradients significantly reduces the cost moving hydrogen ions in or out of the cell (Taylor et al., 2012; Taylor et al., 2011), the majority of H^+ transport is thought to be facilitated using V-ATPase (Dietz et al. 2001; Kevin Flynn et al. 2012). Thus, while upregulation of intrinsic control systems is a more energetically efficient solution as compared to buffering, maintaining pH_i homeostasis is often a costly endeavor (Boron 2004).

Additional energy needs of the cell to maintain growth and metabolism under limiting conditions may be met by accessing energy stored in the form of lipids or fatty acids. This is accomplished using cellular esterases (Dorsey et al., 1989; Koussoroplis et al., 2017). Esterase activity has often been used as a biomarker for cellular (or for higher organisms, systemic) stress (Agusti and Sanchez, 2002; Li et al., 2007; Montella et al., 2012; Radic et al., 2010), as esterase activity can increase when an organism is subjected to environmental stressors. For land plants, this has been observed when the plant is subjected to treatments of herbicides, allelochemicals,

or pathogens (Li et al., 2007). Similar responses are seen in insects (Li et al., 2007; Montella et al., 2012) and mammals, the latter of which make ample use of esterases in their suite of hepatic enzymes as a method for detoxification and processing of toxins and pharmaceuticals (Kamendulis et al., 1996; Williams, 1985). However, increased esterase activity also accompanies increased growth and metabolism in healthy cells (Dorsey et al., 1989; Jiao et al., 2015; Yang and Kong, 2011). This can occur during natural stages of a cell's life span, including growth (Fojan et al. 2000), certain stages of the cell cycle (Chang et al., 2011), or in sync with circadian rhythms (Kouser et al. 2013). Esterases are used to hydrolyze lipids and fatty acids, both of which serve an important function in energy storage. Increased esterase activity allows the cell to access increased energy during times when growth or metabolism may otherwise be limited (Fojan et al., 2000; Johnson and Alric, 2013). Thus, esterase activity becomes less a question of stress, and more a matter of meeting the overall energetic demands, and as such serves as a useful indicator of the metabolic needs of the cell.

Although it is not known if esterase-mediated lipid hydrolysis is upregulated in phytoplankton under OA conditions, low pH, high pCO_2 conditions are associated with reduced lipid and fatty acid content of both phytoplankton and zooplankton. OA conditions have been shown result in reduced fatty acid content of diatoms in laboratory cultures; predatory copepods feeding on the diatoms were in turn negatively affected due to the inferior nutritional content of the diatoms, exhibiting reduced growth, metabolism, and egg production (Rossoll et al. 2012). Diet quality directly influences upregulation of lipase and esterase production in the zooplankton *Daphnia pulex* (Koussoroplis et al. 2017). Fatty acid content of copepods has also been found to decrease under high pCO_2, low pH conditions, making them in turn a less energetically rich food source for higher trophic levels (Garzke et al., 2016; Jayalakshmi, 2016) Thus, while increased

esterase activity may improve phytoplankton survival by providing extra energy to deal with environmental perturbations, the loss of stored energy at foundational trophic level may have cascading effects on ecosystem energy transfer.

We examined the effect of variations in external pH (pH_e) on pH_i of *Isochrysis galbana*, a cosmopolitan haptophyte species, as well as photosynthetic efficiency, growth rate, and esterase activity under steady state conditions (external pH of 7.5, 8.0, and 8.5) and non-steady state (dynamic) conditions using a custom pHstat. *I. galbana* is a good model microflagellate for examining the effect of pH_e, as it – unlike microflagellates such as chrysophytes – has been shown to possess carbonic anhydrase and thus should not be carbon limited at the pH levels relevant to this work. Since diel changes in photosynthesis and respiration influence pH_e, the pHstat system was programmed to control pH either in sync with typical day/night patterns (i.e., pH in the external medium decreases at night when respiration dominates over photosynthesis; "coupled") or out of sync with the diel pattern (i.e., pH in the external medium was set to increase at night and decrease during the day; "decoupled") in order to determine whether light or external pH were driving variables. There are few studies that address the influence of pH on the physiology of microflagellates, which often make up a significant proportion of phytoplankton assemblages in nature (Miller 2004). The goal of this work was to determine how pH_i varies with pH_e under steady state or fluctuating conditions, and to characterize physiological changes that accompany variations in pH, including efficiency of photosystem II, esterase activity, and growth rate to better predict how phytoplankton will respond to ocean acidification.

4.3 Methods

4.3.1 Cell culture

Cultures of the marine flagellate, *Isochrysis galbana*, were obtained from the National Center for Marine Algae and Microbiota (Bigelow Laboratory for Ocean Sciences, East Boothbay, ME) and acclimated to a series of different pH levels under steady state or fluctuating conditions (described in the next section). All treatments were grown in triplicate series using a custom pHstat (Golda et al., 2017a), under a 12:12 light:dark cycle in ESAW media (Berges et al. 2001; Harrison et al. 1980). Isolates were grown in an environmental chamber at 20°C, under full spectrum, cool white fluorescent lights at 160 μmol photons m^{-2} s^{-1}.

4.3.2 pH environments

Environmental pH was maintained at desired levels using the pHstat system detailed in Golda et al. (2017a). An in situ pH probe (Vernier Software and Technology, Beaverton, OR) was used to monitor pH within a customized 900 mL polycarbonate culture vessel. Environmental pH in the culture vessels was monitored, recorded, and modified using the LabVIEW® (National Instruments, Austin, TX) graphical coding platform described in Golda et al., (2017b) and the electromechanical components described in Golda et al. (2017a). pH was modified using reagents, with 0.1M HCl for acidic corrections and 0.1M Na_2HCO_3 for alkaline corrections.

Two sets of experiments were undertaken. First, *I. galbana* was grown at three pH levels (7.5, 8.0, 8.5) under steady state conditions to determine whether pH_i, photosynthetic efficiency, and esterase activity vary with external pH. Second, the response of pH_i, photosynthetic efficiency, and esterase activity to programmed fluctuations in external pH over the course of the

day was investigated under two different dynamic regimes: (1) pH of the external medium was programmed to increase over the course of the day and decrease at night (referred to as "coupled"), simulating effects of photosynthesis and respiration on ambient pH; and (2) pH of the external medium was programmed to decrease over the course of the day and increase at night (referred to as "decoupled"; Table 4.2). In both dynamic cases, pH varied in a sine wave pattern, with one full cycle every 24 h (one high, one low). The sine wave peak amplitude was 0.5 pH units, with a midpoint of 8.0 (lowest pH 7.5, highest pH 8.5). All pHstat experimental runs were performed in triplicate series and cells were acclimated to conditions for 8 generations.

Table 4.2: pH treatment conditions for test organisms. Programmed pH error was ±0.05 pH units. Amplitude indicates amplitude of the sine wave used to generate dynamic pH cycles.

External pH	*Isochrysis galbana*	Amplitude	Light cycle (Light/Dark)
7.5	n=3	-	12L/12D
8.0	n=3	-	12L/12D
8.5	n=3	-	12L/12D
Dynamic (coupled)	n=3	0.5	12L/12D
Dynamic (decoupled)	n=3	0.5	12L/12D

4.3.3 Determination of biomass

Duplicate chlorophyll *a* samples were filtered onto 25 mm GF/F filters and stored frozen at -80 °C until cold extraction in 90% acetone (Welschmeyer 1994). Chlorophyll *a* was measured fluorometrically using a Trilogy® laboratory fluorometer (Turner Designs, San Jose, CA) equipped with a non-acidification optical module.

Cell densities were determined using a Coulter Counter Model Z2 particle counter (Beckman Coulter, Indianapolis, IN) to count phytoplankton cells following 20 fold dilution in Isoton II® diluent (Beckman Coulter, Indianapolis, IN). Growth rates were calculated from cell counts.

$$\mu = \frac{\ln(m_2 - m_1)}{t_2 - t_1}$$ *Equation 4.1*

Where μ = growth rate, m_2 = cell count/biomass at time 2 (t_2), and m_1 = cell count/biomass at time 1 (t_1).

4.3.4 Measurement of photosynthetic efficiency

A Walz Water-PAM (pulse amplitude modulated) fluorometer (Heinz Walz GmbH, Germany) was used in conjunction with a PAM-Control unit (Heinze Walz GmbH, Germany), and WinControl-3 Software (v. 3.25) to measure efficiency of photosystem II (F_v/F_m). After sampling, 4 mL aliquots of sample were dark-adapted for 15–20 min, then exposed to a saturating pulse of light to obtain F_v/F_m values.

4.3.5 Intracellular pH measurements

The fluorescent pH indicator dye 5-(and-6)-carboxy seminaphtharhodafluor (SNARF)-1, acetoxymethyl (AM) ester, acetate (Life Technologies, Eugene, OR) was used to measure intracellular pH. Cells were prepared for dye loading by an initial centrifugation/washing step during which 1 mL of *I. galbana* culture was centrifuged at 13,000 x *g* for 3 min. The cells were then resuspended in sterile media taken from the same culture and filtered through a 25 mm GF/F filter. This was used in order to maintain the same external pH that the cells had been growing in at the moment of sampling. After resuspension, 3 μL of 1 mM SNARF (dissolved in dimethyl sulfoxide) was added to the cells, along with 3 μL of a 5% solution of the nonionic detergent, Pluronic® F-127 (Thermo-Fisher), which acts as a dispersant for SNARF to minimize clumping in aqueous solution (Molecular Probes 2003). The final concentration of SNARF in the culture vessels was 3 μM. Cells were incubated with SNARF for 30–40 min, then centrifuged

and washed twice in the filtered media. After the final wash step the cells were diluted in 4 mL of filtered media and fluorescence emission intensity of the cells was measured. pH_i was calculated by taking the ratio of F1/F2 and using it in combination with the SNARF calibration curve for *I. galbana* calculated in Chapter 2.

4.3.6 Determination of esterase activity

Total cellular esterase activity was measured in duplicate using the fluorescein diacetate (FDA) hydrolysis assay (Agusti & Sanchez, 2002; Agusti et al., 1998). FDA stocks were made by dissolving 2 mg FDA in 10 mL of 100% acetone; stocks were kept at -20°C until used. Five mL of sample was filtered using GF/F filters and frozen for a minimum of 3 d at -20°C pending analysis. Cell lysis was achieved by exposing cells to two freeze/thaw cycles (Mayerhoff et al., 2008) followed by immersion in 5 mL deionized water adjusted to pH 7.60 (Chisti and Moo-Young 1986; Byreddy et al. 2015; Kar and Singhal 2015) using the phosphate buffers, K_2HPO_4 and KH_2PO_4 (Fisher Scientific, Fair Lawn, NJ). After cell lysis, 100 µL 20 mM EDTA was added, followed by 100 µL 4.8 µM FDA stock (Invitrogen, Eugene, OR). The solution was vortexed for 5 s and incubated for 60 min at room temperature. After incubation, 5 mL of a 2:1 chloroform–methanol solution was added and the solution was vortexed for 10 s. The tubes were centrifuged at 7000 x *g* for 5 min and the aqueous layer was extracted for analysis by spectrofluorometry (excitation at 490 nm, emission at 515 nm).

4.3.7 Fluorescence measurements

A HORIBA Scientific Jobin Yvon FluoroMax-4 spectrofluorometer was used to measure fluorescence emission of SNARF and FDA in cells suspended in culture medium. SNARF was

excited at 520 nm, and emission intensities were measured at 585 nm and 630 nm. The ratio of these measurements was used to calculated pH_i as detailed in Chapter 2. Samples containing FDA were excited at 490 nm and emission intensity was determined at 520 nm. To account for autofluorescence of phytoplankton pigments, fluorescence associated with a blank (identical treatment and handling but without SNARF addition) was subtracted for each sample.

4.3.8 Gibbs calculations

The amount of energy needed to transport H^+ ions against the intra/extracellular concentration gradient was calculated using the equation to calculate the free-energy change for transport of an ion, ΔG_t:

$$\Delta G_t = RT\ln\left(\frac{C_2}{C_1}\right) + ZF\Delta\psi \qquad \textit{Equation 4.2}$$

where *R* is the universal gas constant, *T* is the temperature in Kelvin, and C_2 and C_1 refer to the concentration of ions outside and inside of the cell, respectively. *Z* is the charge on the ion, *F* is the Faraday constant (96,480 J V^{-1} mol^{-1}), and $\Delta\psi$ is the transmembrane potential in volts.

4.4 Results

Using a pHstat system, external pH (pH_e) was maintained at different levels under both steady state (pH_e of 7.5, 8.0, and 8.5), and dynamic (coupled and decoupled from light cycles) conditions (Figs. 4.1 and 4.2). The physiological responses of *I. galbana* to pH_e under steady state and dynamic conditions are described in the following sections.

4.4.1 Steady state conditions

Under steady state conditions, pH_i remained between 6.5 and 7.3, regardless of pH_e (Fig. 4.1 and 4.2). However, the average pH_i of cells grown at pH_e 7.5 (pH_i = 7.02) was significantly higher ($P < 0.05$) compared to that of cells grown at either pH_e 8.0 (pH_i = 6.83) or pH_e 8.5 (pH_i = 6.84), which did not differ from each other (Fig. 4.2). In addition, the range of pH_i values measured for pH_e 7.5 (range of 1.03; 6.67–7.70 pH units) was larger than observed for either pH_e 8.0 (range of 0.88; 6.35–7.24) or pH_e 8.5 (range of 0.86, 6.38–7.24).

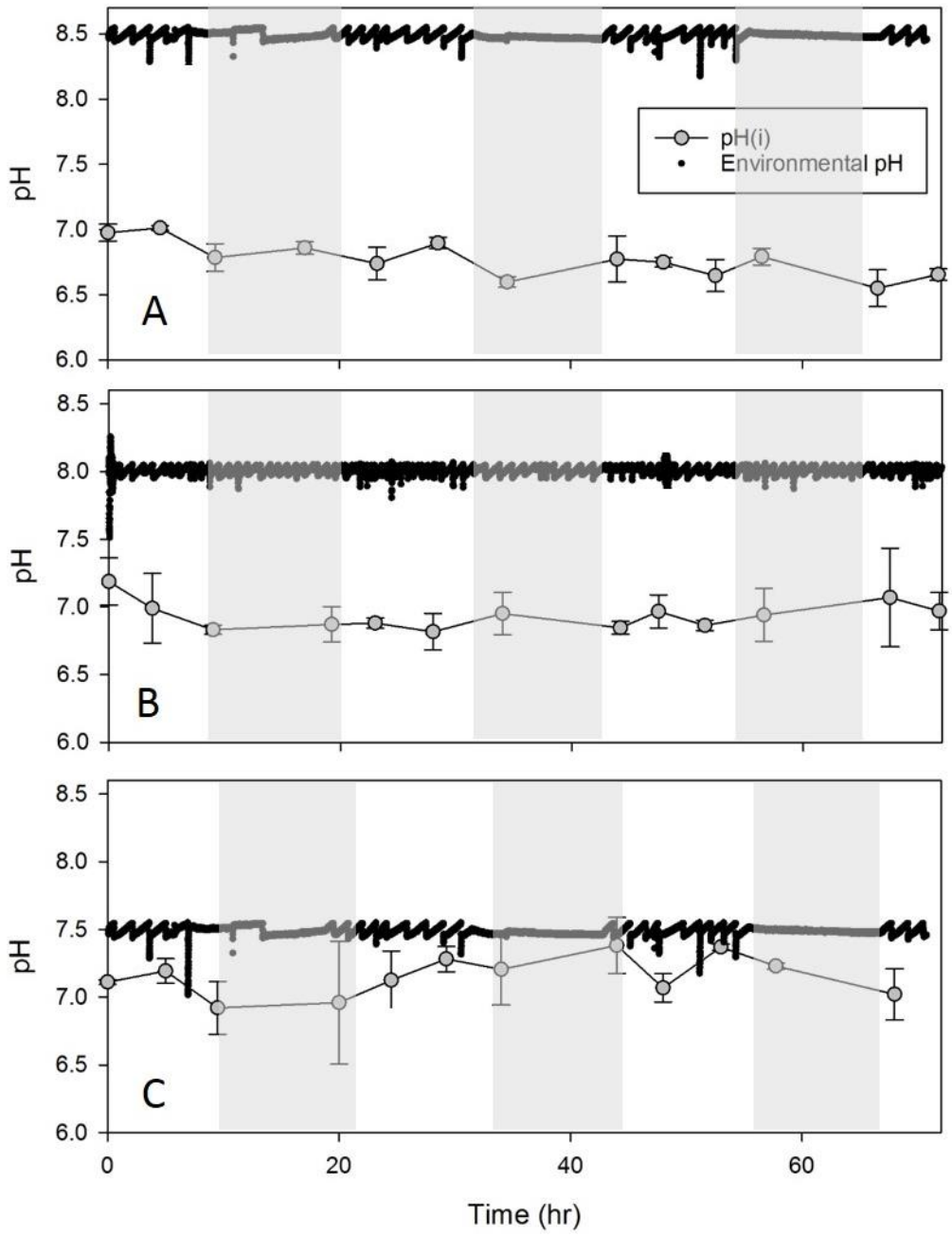

Figure 4.1: Representative figures from 72 h experiments under steady state conditions. (A) pH = 8.5, (B) pH = 8.0, (C) pH = 7.5. Black dots indicate environmental pH, individual gray dots indicate intracellular pH (pH_i). Error bars represent ± one standard deviation of the mean of triplicate samples.

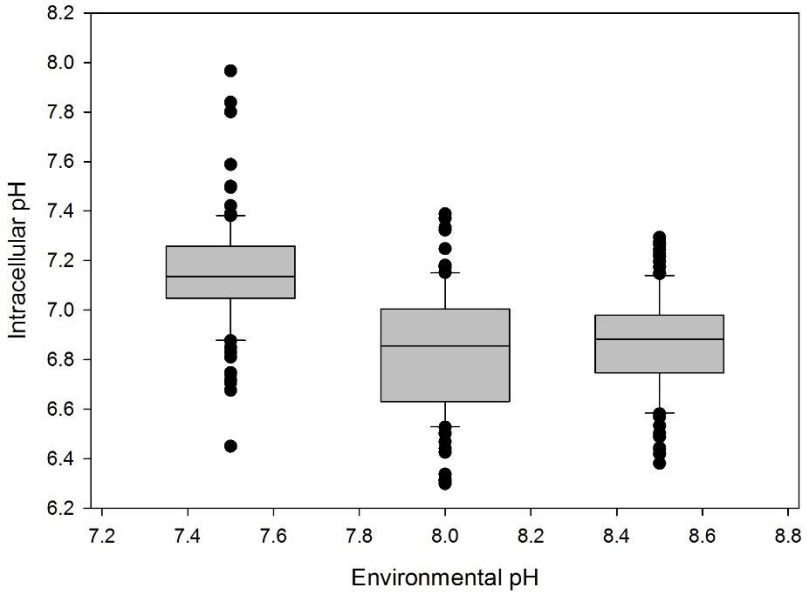

Figure 4.2. Intracellular pH (pH_i) for steady state treatments. Gray box plot indicates data in the interquartile range (IQR; between 1st and 3rd quartiles), black horizontal line within the box indicates the median pH_i value. Extended bars indicate statistically relevant maximum and minimum values. Black dots indicate statistical outliers. Environmental pH of 7.5 was significantly different than 8.0 and 8.5; no significant difference between 8.0 and 8.5 (significance threshold ≤ 0.05).

Comparison of *I. galbana* growth rates at different environmental pH levels showed that the growth rate at 8.5 (0.41 d^{-1}) is significantly higher than at 7.5 (0.24 d^{-1}; Fig. 4.3). Growth rate at 8.0 (0.33 d^{-1}) is not significantly different from either 8.5 or 7.5 ($P > 0.05$). Growth rate for cells from the coupled dynamic treatment (0.21 d^{-1}) was statistically different from the decoupled growth rate (0.33 d^{-1}), but similar to the growth rate at 7.5.

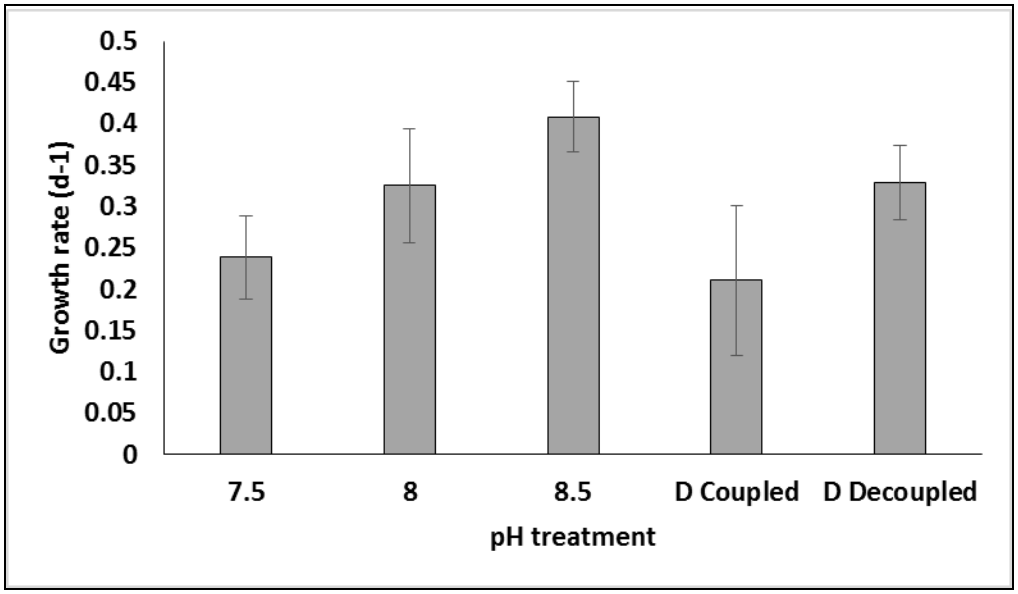

Figure 4.3. Comparison of *I. galbana* growth rate at different environmental pH levels. Growth rate at 8.5 was significantly different than 7.5 and the coupled dynamic pH treatment ($p < 0.05$). Error bars indicate standard deviation of triplicate samples.

Average esterase activity at pH_e 7.5 (0.54 fmol cell^{-1} min^{-1}) was significantly higher than in the other two treatments (pH_e 8.0 and 8.5, esterase activity 0.33, 0.44 fmol cell^{-1} min^{-1}, respectively); no significant difference was observed between pH_e 8.0 and 8.5 (Fig. 4.4; $p < 0.05$). Esterase activity was negatively correlated to the quantum yield of photosystem II (F_v/F_m) ($R = -0.53$, $p < 0.01$; Table 4.2, Fig. 4.5).

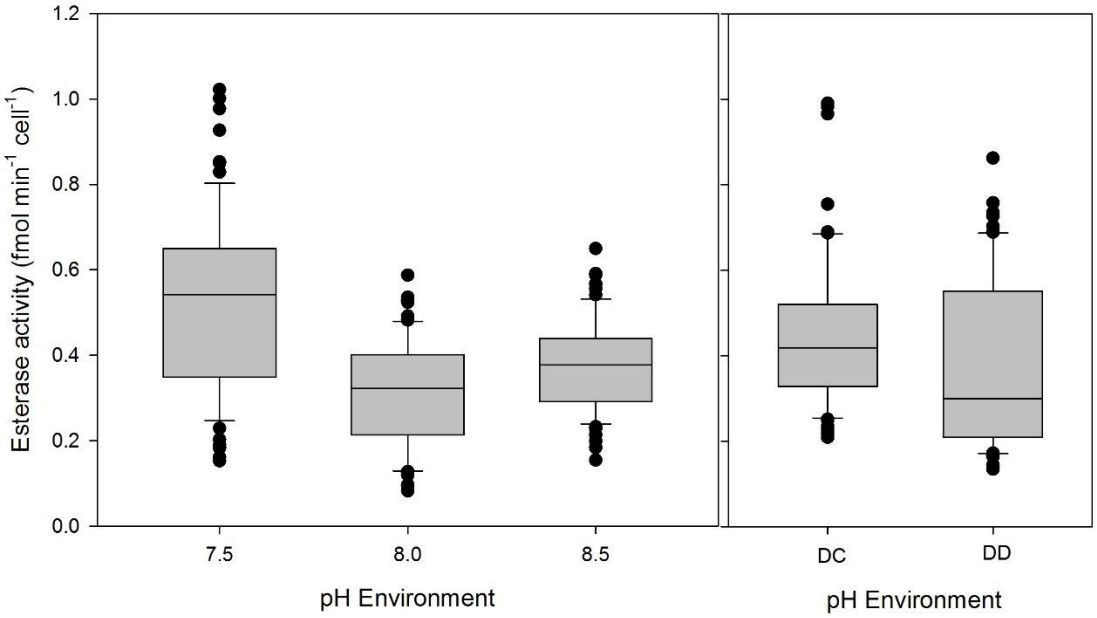

Figure 4.4: Esterase activity for steady state (left) and dynamic (right) treatments. Gray box plot indicates data in the interquartile range (IQR; between 1st and 3rd quartiles), black horizontal line within the box indicates the median esterase activity value. Extended bars indicate statistically relevant maximum and minimum values. Black dots indicate statistical outliers. DC = dynamic, coupled, DD = dynamic, decoupled.

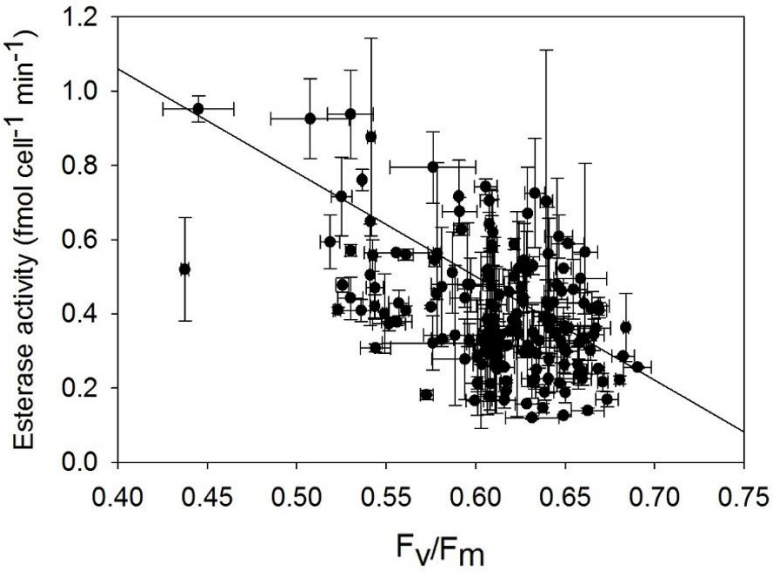

Figure 4.5. Relationship between esterase activity and maximum quantum efficiency of PS(II) (F_v/F_m) for all treatments. Data points indicate means of each value; error bars indicate standard deviation. $R^2 = 0.28$.

Table 4.2: Results of Pearson correlation and linear regression analyses of esterase activity versus maximum quantum yield (F_v/F_m).

pH treatment	r	R^2	P < 0.01?	n
7.5	-0.655	0.43	Yes	30
8.0	-0.726	0.53	Yes	34
8.5	-0.537	0.29	Yes	35
D. Coupled	-0.140	0.02	No	36
D. Decoupled	-0.485	0.024	Yes	35

There was a strong positive correlation between F_v/F_m and pH_i during the steady state runs pH_e 8.0 ($R = 0.77$, $p < 0.01$) and pH_e 7.5 ($R = 0.59$, $p < 0.01$). There was no significant correlation between F_v/F_m and pH_i for the 8.5 run. According to an analysis of variance (ANOVA), F_v/F_m of cells grown at pH_e 8.5 was significantly higher when pH_e was 8.0 or 7.5 ($p < 0.01$; Fig. 4.6). There was no significant difference in F_v/F_m values between pH_e 8.0 and 7.5.

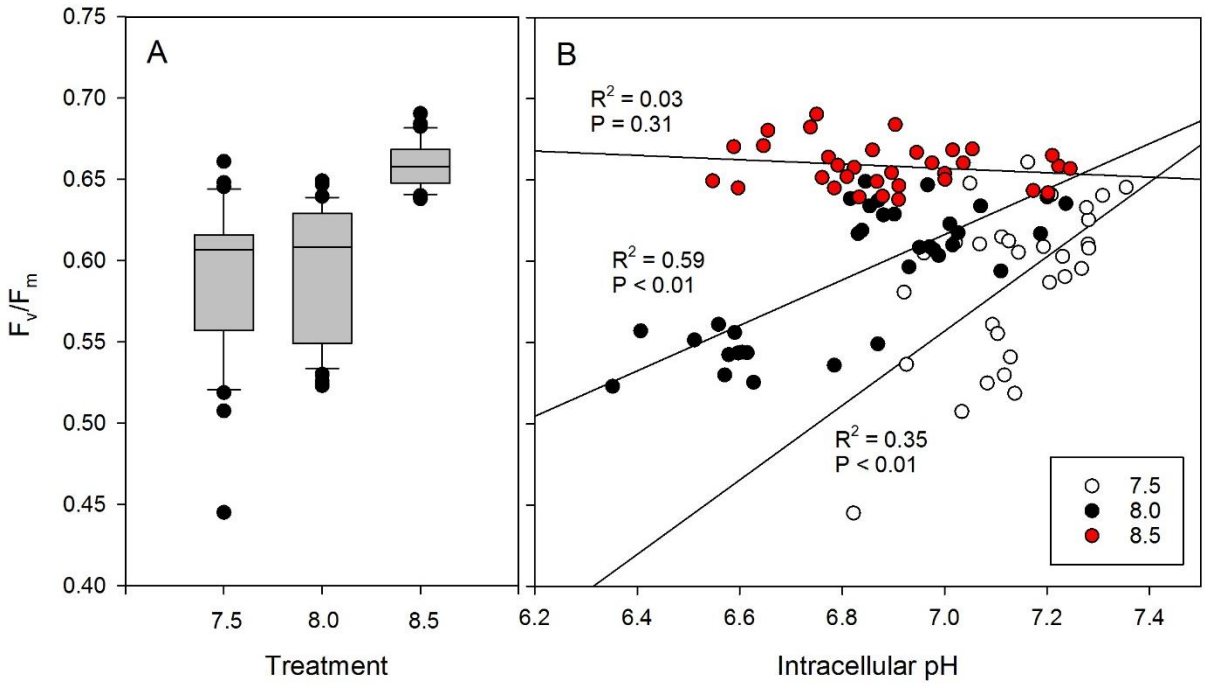

Figure 4.6: (A) Box-and-Whisker plots showing F_v/F_m for steady state pH_e treatments. Maximum quantum yield of PSII (F_v/F_m) of cells grown at pH_e 8.5 was significantly higher than at pH_e 7.5 or 8.0 ($p < 0.05$). (B) Linear regression of F_v/F_m vs intracellular pH at the three pH levels.

4.4.2 Dynamic conditions

In contrast to observations under steady state, pH_i varied inversely with pH_e over the course of each 24 h period when environmental pH was dynamic (Fig. 4.7). In the coupled runs, the difference in pH_i between dark and light was -0.3 ± 0.29 pH units, while for the decoupled run the change was +0.24 ± 0.10 pH units. The range of pH_i values observed for decoupled runs (1.15 pH units) was nearly twice as large compared to coupled runs (0.62 pH units).

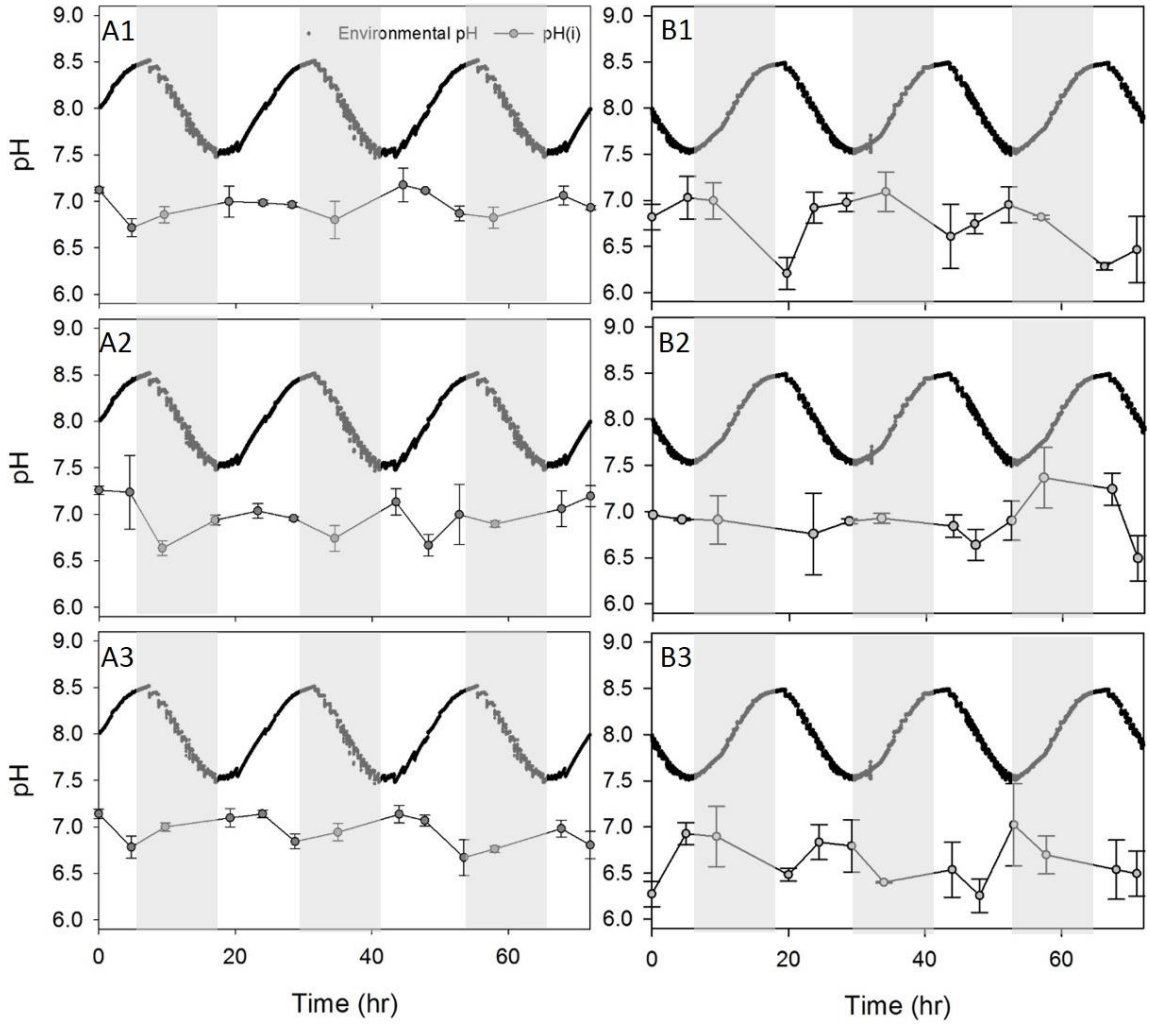

Figure 4.7: Dynamic pH experiments; (A) external pH when increasing pH_e is coupled to the light/dark cycle (i.e., pH drops at night, rises during the day), triplicate experiments; (B) external pH is decoupled from the light/dark cycle decoupled, triplicate experiments. Intracellular pH (pH_i) is indicated by gray circles, environmental pH (pH_e) is indicated by black circles; lines are included to illustrate the patterns of pH_i. Error bars represent ± one standard deviation of the mean of triplicate samples.

There was a significant relationship between environmental pH and pH_i, regardless of light periodicity (Fig. 4.5; $p < 0.01$). There was a positive relationship between pH_i and environmental pH when light cycles were coupled with a natural periodicity of external pH; however, a negative relationship emerged between pH_i and environmental pH when light cycles are decoupled from pH cycles (Fig. 4.8). Statistical uncertainty was determined by calculating standard error of the regressions; these were found to be 0.15 and 0.24 for coupled and decoupled, respectively. Graphical analysis of environmental pH versus calculated free energy transfer (ΔG_t) indicated that the environmental pH at which passive diffusion of H^+ ions effectively ceases ($\Delta G_t = 0$) increases with increasing pH_i (Fig. 4.9). X-intercepts occurred respectively for pH_i 6.6, 6.8, 7.2, and 7.5 at pH_e 7.65, 7.85, 8.25, and 8.55. Regression modeling showed that ΔG_t decreases with increasing pH_i. X-intercept occurred at pH 8.05, indicating that diffusion of H^+ ions decreases with increasing intracellular pH, effectively ceasing at approximately pH_i 8.0 (Fig. 4.10). Comparison of pH_i and ΔG_t dynamics showed that ΔG_t of the cells increases following periods of sustained darkness, and decreases after periods of sustained photosynthesis. This occurred regardless of pH_i (Fig. 4.11).

The average esterase activity of cells grown under the coupled dynamic conditions was statistically similar to the steady state experiments when pH_e was 7.5 (Fig. 4.4; $p < 0.05$). Both of these were significantly higher than the activities determined for pH_e 8.0 and 8.5. In contrast, esterase activity determined in the dynamic decoupled runs was statistically similar to pH_e 8.0 and 8.5 and significantly lower than at pH_e 7.5. However, esterase activities for cells grown in decoupled vs. coupled light/pH cycles were not significantly different ($p > 0.05$). There was no significant correlation between F_v/F_m and pH_i for either of the dynamic runs (data not shown).

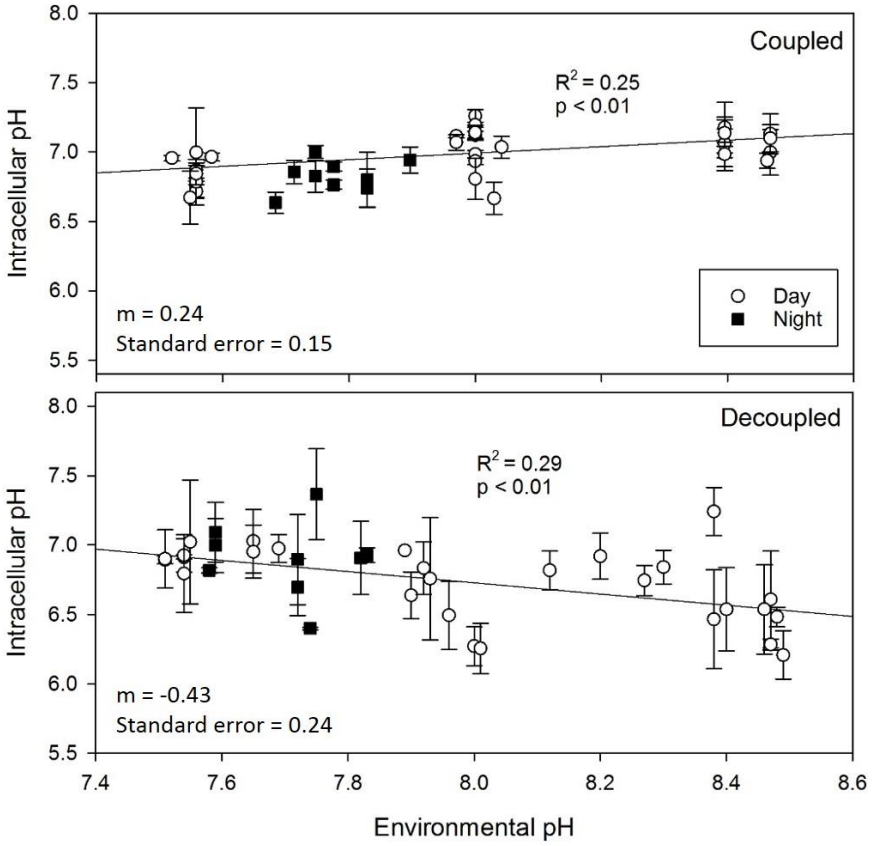

Figure 4.8. Comparison of relationships between environmental pH and pH_i in *I. galbana* between coupled and decoupled dynamic runs. Black squares indicate samples taken at night, white circles are samples taken during the day. Solid lines show linear regression of means, Coupled: m (slope) = 0.24, standard error = 0.15, $R^2 = 0.25$, $p < 0.01$; Decoupled: m = -0.43, standard error = 0.24, $R^2 = 0.29$, $p < 0.01$.

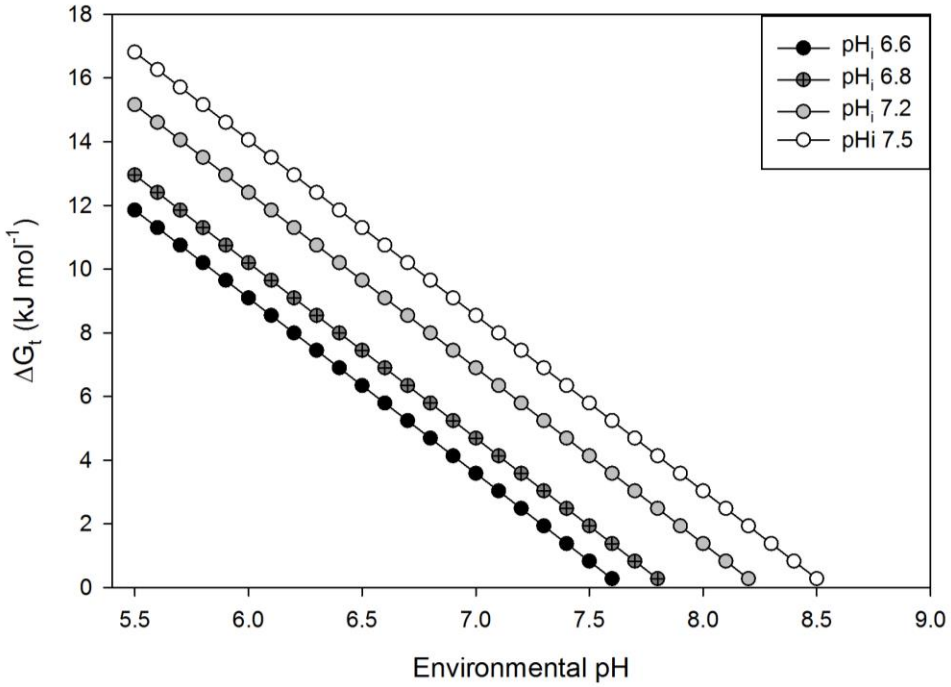

Figure 4.9: Environmental pH versus ΔG_t, with individual plots indicating individual intracellular pH. X-intercepts occur respectively for pH_i 6.6, 6.8, 7.2, and 7.5 at pH_e 7.65, 7.85, 8.25, and 8.55.

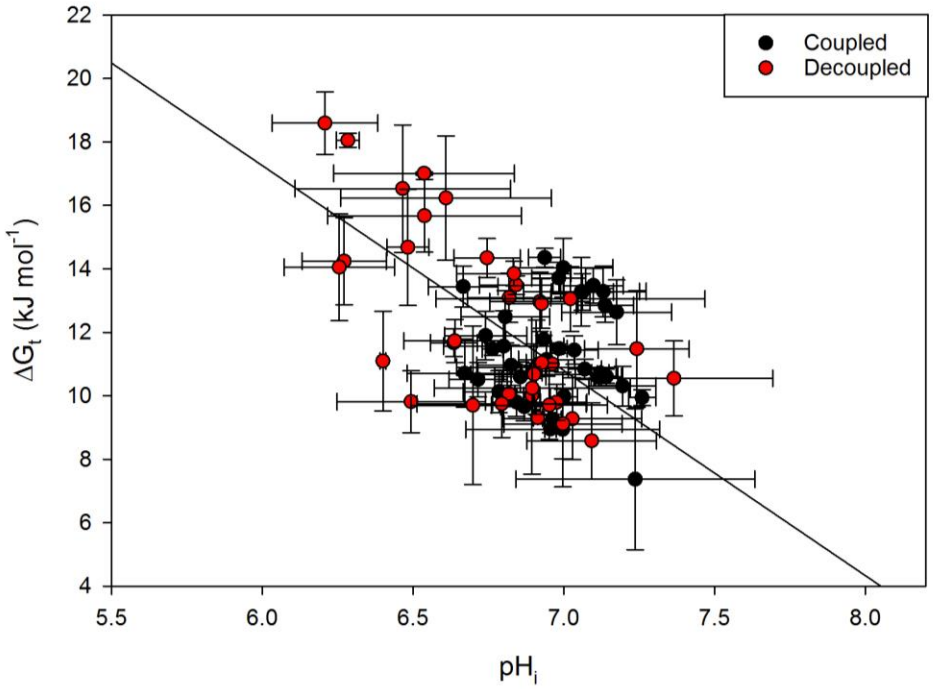

Figure 4.10: Regression model showing relationship between pH_i and free energy transfer across cell membrane (ΔG_t). X-intercept at 8.05; $R^2 = 0.45$; error bars represent ± one standard deviation of the mean of triplicate samples.

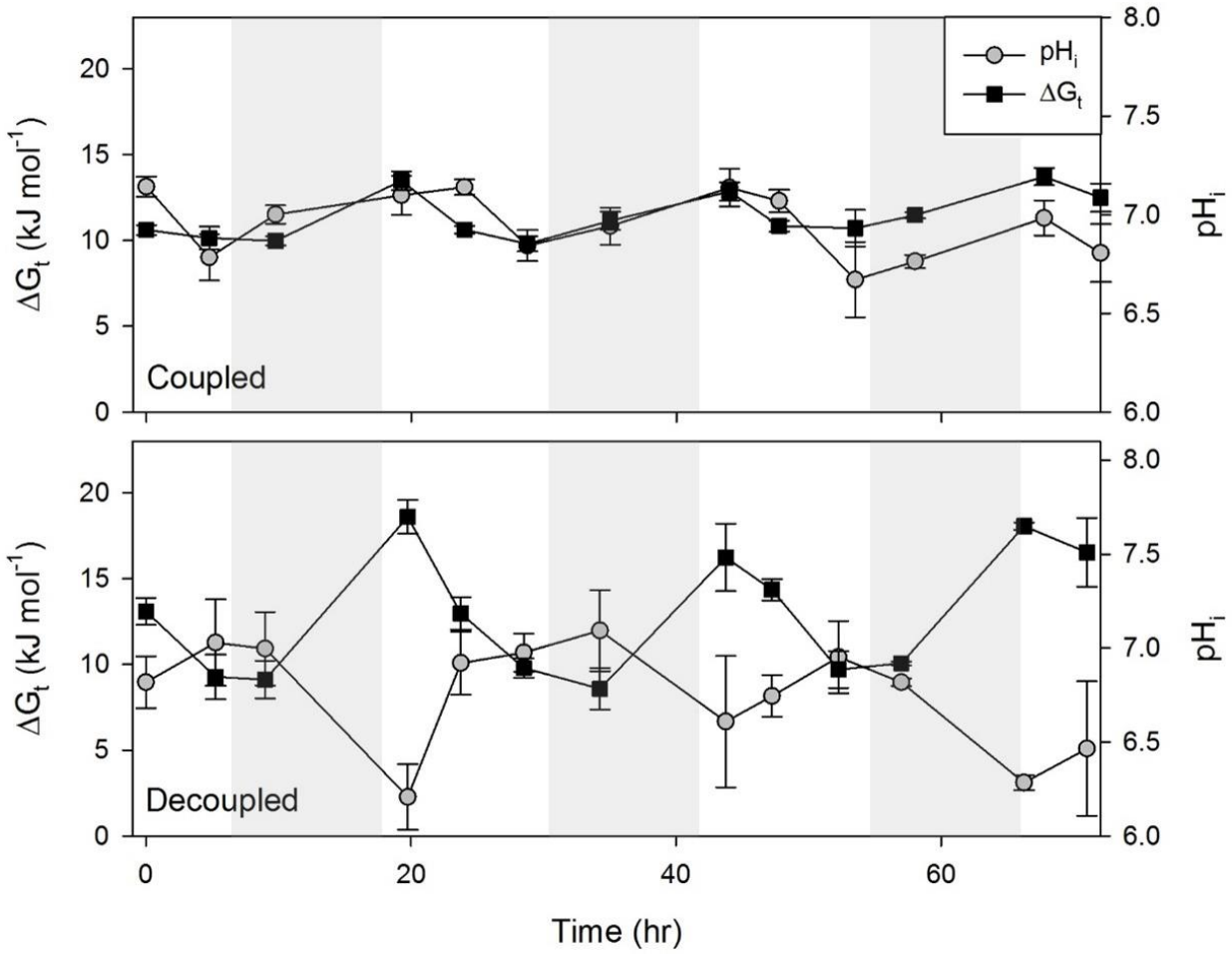

Figure 4.11: Representative dynamic experimental runs showing that ΔG_t increases at night, and becomes less negative during light periods. Shaded gray columns indicate dark periods. Error bars represent ± one standard deviation of the mean for triplicate samples .

4.5 Discussion

In environments where external pH fluctuates, regulation of pH_i is critical for achieving optimal growth (McCulloch et al., 2012), as transitory changes in pH often drive changes in normal cellular functions, for example in signaling or to initiate a shift in metabolism (Busa and Crowe, 1983; Karagiannis and Young, 2001). Although the exact mechanisms by which phytoplankton cells maintain pH_i homeostasis are unclear (Gibbin et al., 2014; Taylor et al., 2012), pH_i generally remains close to a mean of approximately 7.2 (Roos and Boron, 1981; Taylor et al., 2012), which is significantly more acidic than the average pH of seawater (~8.1–

8.2). The difference (ΔpH) between intracellular and extracellular pH supports an electrochemical gradient that provides the driving force for cellular transport of ions, termed proton motive force (PMF; Carter et al., 1967). The proton electrical gradient (E_h) specifically influences passive diffusion of H^+ ions into the cell, which in turn directly influences pH_i. Increasing E_h causes the electrical potential across the membrane to become more negative, presenting a more favorable environment for positive H^+ ions to passively cross the cell membrane (Nimer et al. 1994). This may explain why pH_i values varied inversely to pH_e, since PMF drives passive changes to pH_i (Carter et al. 1967). The favorability of ion transport is a balance between diffusive and electrical potential across membranes. This can be quantified by calculating ΔG_t. When ΔG_t increases, passive ion transport becomes more energetically favorable. As ΔG_t decreases towards zero, passive movement of ions becomes progressively less favorable, with effectively no ion exchange occurring at $\Delta G_t = 0$. When ΔG_t is plotted against environmental pH (Fig 4.9), the pH_e at which $\Delta G_t = 0$ (i.e., the x-intercept of ΔG_t) increases as pH_i increases. This means that as intracellular concentrations of H^+ drop with increasing pH_i, the external pH (i.e., concentration of H^+ ions outside the cell) at which diffusive potential equals zero also increases, allowing for sufficient ΔpH to maintain PMF across the cell membrane.

Passive transport across the cell membrane is more strongly favored at night, as ΔG_t becomes more positive during periods of sustained respiration. During the day ΔG_t becomes less positive with the increase of pH_i due to photosynthetic fixation of carbon. This change appears to be dependent on photoperiodicity, not changes in pH, as demonstrated by the continued coupled of ΔG_t to light/dark cycles, even after decoupling pH cycles from standard photoperiods. Previous research has shown that light-driven changes to PMF can influence ion distribution based on changes in the rate of ATP synthesis due to light-coupled reactions, as PMF drives ATP

synthesis (Cruz et al. 2005; Berg et al. 2002; Jagendorf and Uribe 1966). The connection between PMF and pH was further supported by regression analysis of pH_i and ΔG_t. These data show that as pH_i increases, ΔG_t decreases. This indicates that passive diffusion of H^+ was less favorable with increasing pH_i in environments with dynamic pH_e. Thus, PMF plays an important role in pH_i homeostasis relative to changing environmental pH.

Assuming a transmembrane potential of $V_m \approx$ -60 mV, the equilibrium, or Nernst, potential for H^+ (E_h) would be, according to the laws of electrochemistry (Boron 2004; Nimer et al., 1994):

$$E_h = 2.3RT/F * \log10([H^+]_o/[H^+]_i) \qquad \textit{Equation 4.3}$$

and

$$Eh = V_m (pH_i - pH_e) \qquad \textit{Equation 4.4}$$

approximately -18, -48, and -60 mV for pH_e of 7.5, 8.0, and 8.5, respectively, where V_m is the transmembrane potential ($V_m \approx$ -60 mV; Nimer et al., 1994), R is the universal gas constant, T is temperature in degrees Kelvin, and F is the Faraday constant. Since the voltage inside the cell is much less negative than the transmembrane potential, the electrical potential across the membrane favors passive influx of H^+ at all pH_i measured. However, this influx is weaker at pH 7.5 than at 8.0 and 8.5. Thus, at pH_e 7.5, more energy would be required to maintain pH homeostasis; it is possible that the lower F_v/F_m values and lower growth rate observed in this treatment are related to energy re-allocation for this purpose. This relationship has been seen previously in the acid-intolerant chlorophyte, *Scenedesmus quadricauda*, which showed reduced photosynthetic activity when exposed to an acidic environment (relative to pH 8.2), with a 50% decrease in the rate of oxygen evolution at pH 5.5 relative to higher pH levels

(7.0 and 8.0) due to energy reallocation from photosynthesis to the maintenance of internal pH (Lane and Burris, 1981). As ΔG_t decreases with decreasing pH_i, it may be necessary for the cell to reroute energy to active transport of H^+ ions into the cell in order to maintain the electrochemical gradient. This re-distribution of energy means that less energy is available for growth and cellular reproduction, resulting in reduced growth rates. A reduction in growth rate in response to changes in pH has also been observed in *Emiliania huxleyi* (Nimer et al., 1994), in muscle cells of the marine worm, *Sipunculus nudus* (Reipschläger and Pörtner, 1996), and in the colonial cyanobacterium, *Trichodesmium* (Hong et al. 2017).

Mechanisms involved in pH regulation differ based on the time scale of the perturbation. Short-term, or acute, changes in pH are generally neutralized using intracellular buffer systems, including phosphate, amino acids, and short-term modifications to inorganic carbon partitioning (Casey, Grinstein, and Orlowski 2010; Roos and Boron 1981). Buffer production and transport can be an energetically expensive cellular process (Casey, Grinstein, and Orlowski 2010; Dietz et al. 2001); thus, while buffering is used to modulate sudden changes in pH, acid/base transporters ultimately regulate pH_i dynamics within the cell (Boron 2004). Acid/base transporters are always working in conflict with one another—a necessary but energetically expensive balancing act (Boron 2004). There was a smaller range of diel variability in pH_i in *I. galbana* under steady state compared to dynamic conditions. Under steady state, the cells were exposed to a set pH for an extended period of time (4-6 weeks), and thus the cells had time to reach a state of equilibrium by upregulating acid extruders to achieve pH homeostasis.

Under dynamic conditions, pH_i did not track directly with pH_e, but was instead inversely related to pH_e in both coupled and decoupled treatments. It is likely that daily adjustments to maintain pH homeostasis were achieved by buffering. Boyarsky et al. (1990) showed that the

buffering system of rat mesangial cells tends to overcompensate for any perturbations in pH_i. After artificially suppressing activity of acid importers and exporters, a single chemically-mediated pH spike of +0.3 pH units was engineering in the cells, which used chemical buffering to compensate for the perturbation. The cell overshot the original pH_i significantly, dropping pH_i by -1.1 pH units within two minutes; it took five minutes to finally regain pH_i equilibrium. The resulting equilibrium pH was 0.4 pH units lower than the starting resting pH_i. The may be due to the initial acidic buffer production response of the cell, which consumed ambient basic buffering molecules, resulting in a lower resting pH_i. This correlates with our observation that under steady state conditions, pH_i at pH_e 7.5 was higher than at pH_e 8.0 or 8.5. This is in contrast to other studies where pH_i tracked pH_e (Dason and Colman 2004; Hong et al. 2017; Taylor et al. 2011).

Activity of intracellular esterases is related to metabolic activity, with suppression of esterase activity being an indicator that normal cell metabolism is being inhibited (Jiao et al. 2015). Aside from their functions during normal cellular metabolism, esterases are used by the cell to access stored energy reserves through lipid hydrolysis (Fojan et al., 2000). When not in need of extra energy to deal with an environmental perturbation, phytoplankton store most of their energy in the form of polysaccharide starches, which can be quickly broken down and used as energy (Johnson & Alric, 2013; Obata et al., 2013). However, phytoplankton subjected to stressful conditions have been shown to preferentially store energy in the form of lipids; even when not under stress, phytoplankton always store a portion of energy as short-chain fatty acids (Converti et al., 2009; Johnson and Alric, 2013). The energetic potential of these lipids is higher than that of polysaccharides, with a yield of 6.7 ATP equivalents per carbon atom, as opposed to 5.3 ATP equivalents from glucose oxidation (Johnson and Alric 2013). The energy in these lipids

is accessed by increasing esterase activity, as esterases and lipases (a subset of esterases) hydrolyze short chain fatty acids (Fojan et al., 2000).

The negative correlation between esterase activity and quantum yield of PSII indicates that esterase activity increases as energetic yield of photosynthesis falls. Energy captured through photosynthesis is used to synthesize lipids within the chloroplast, which are then distributed throughout the cell (Eltgroth et al., 2005). A decrease of photosynthetic efficiency leaves the cell with an energy deficit that can be remedied by actively upregulating esterases for fatty acid hydrolysis to meet the metabolic needs of the cell. This is supported by previous work; elevated CO_2 and decreased pH has been shown to reduce overall the fatty acid composition of the diatom *Thalassiosira pseudonana* (Rossoll et al. 2012), affecting energy potential in the cell. The changing fatty acid profile observed by Rossoll *et al*. (2012) in *T. pseudonana* may have been the result of a change in esterase activity in response to decreased pH. This idea is buttressed by results from Hong et al. (2017), which showed that an increase in ATP production partially mitigated the effect reduced environmental pH for the colonial cyanobacterium, *Trichodesmium*.

It is important to note that esterase activity is a multi-faceted parameter. First, increased esterase activity could also be the result of upregulation of the genes responsible for producing esterases, and thus increased activity is due to the increased availability of the enzyme. However, esterase activity is sensitive to pH (Bunting and Kabir 1978). Increased activity could be the result of an environment in which the catalytic efficiency of selected esterase enzymes is increased by a more favorable pH environment (Devonshire and Field 1991). Further, it is possible that the proportions of various esterases available changes, with specific enzymes being upregulated in the changing internal environment. Although many esterases can be promiscuous

with regard to substrate binding (Devamani et al., 2016; Fojan et al., 2000; Gould & Tawfik, 2005), substrate/enzyme specificity may cause the apparent overall esterase activity to change, depending on the substrate used in the assay (Goullet & Picard, 1995; Lomolino et al., 2005). General enzyme/substrate affinity has been shown to vary widely among phytoplankton, for example, in the highly structurally conserved enzyme Rubisco, substrate specificity varied up to a factor of 25 (Badger et al., 1998; Tortell, 2000). The esterase activity measurements taken during these experiments were accomplished with FDA as a substrate; although this is a widely accepted method for characterizing non-specific esterase activity, it is important to note that apparent esterase activity may change if another, more "preferable" substrate is used.

4.5.1 Conclusions

Average surface pH of the global open ocean is expected to decline to 7.8 by the year 2100 (Solomon et al. 2007). Any changes in phytoplankton physiology resulting from ocean acidification will have broad implications for primary and net biological production of coastal and open-ocean systems (Raven et al., 2011; Collins et al., 2013). A growing body of literature underscores the importance of pH as a variable controlling phytoplankton physiology, independent of changes in pCO_2 or alkalinity (Chen and Durbin, 1994; Eberlein et al., 2014).

This work highlights the complex inter-relationships of pH, photosynthetic efficiency, and esterase activity (Fig. 4.12). pH_i in *Isochrysis galbana* varied widely in response to changes in external pH. The changes observed in pH_i were found to be correlated to photosynthetic efficiency, with a significant positive relationship between pH_i and maximum quantum yield of PSII at lower steady state pHs. Due to the effect of internal pH changes on passive proton diffusion across the cell membrane, as well as the corresponding response of PSII observed in

the steady state experiments, it is arguable that the amount of energy required to maintain pH_i homeostasis in the face of changing external pH may be a limiting factor to phytoplankton growth at the lower pH environments observed in these experiments. This is reflected in the growth rates calculated for *I. galbana* over the course of the experiments where the growth rate the 7.5 treatment was significantly lower than that at pH 8.5. The calculated Nernst potential of H^+ ions was found to be progressively more negative with increasing external pH, nearing the transmembrane potential and thus requiring less energy to maintain pH_i homeostasis. However, these increased energetic needs, as well as the loss of energetic yield from photosynthesis, may be partially mitigated by increased availability of energy from fatty acid hydrolysis. Increased esterase activity allows the cells to make adjustments to pH_i, even as energetic input from the photosystem II declines at lower pH. However, this is done at the expense of growth and reproduction. For example, ocean acidification has been shown to reduce the fatty acid content of diatoms in laboratory cultures. This reduction in stored fatty acids reduced the nutritional potential of the phytoplankton, having a negative effect on predatory zooplankton (Koussoroplis et al. 2017; Rossoll et al. 2012), some of which in turn showed a reduction of total stored fatty acids (Garzke et al. 2016).

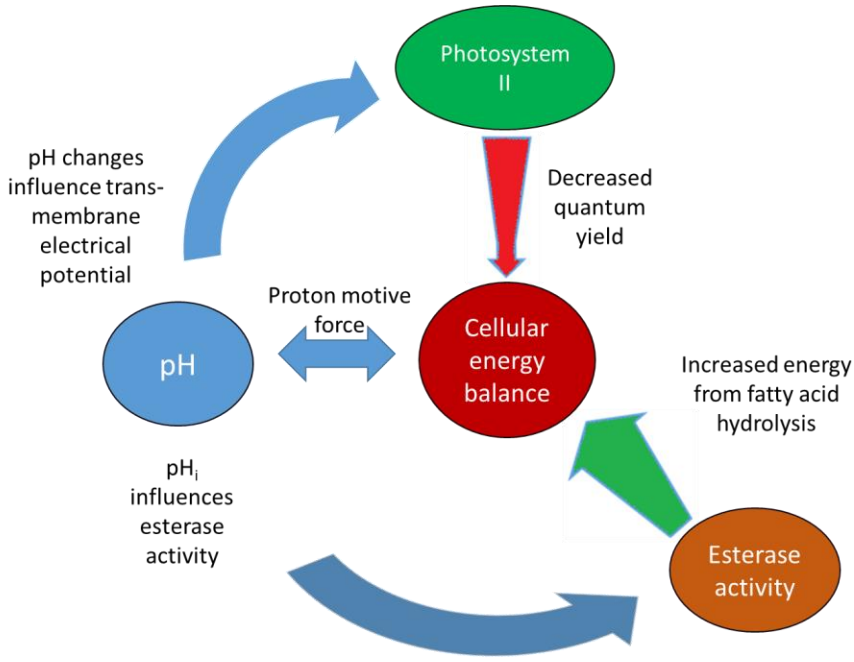

Figure 4.12: Conceptual diagram illustrating interrelationships between pH, esterase activity, PSII, and overall cellular energy demands and balance.

CHAPTER 5

Summary and Conclusions

In this era of unprecedented anthropogenically-driven changes to the world's oceans, it is important to understand the effects that changing pH will have on phytoplankton physiology. As the base of nearly all aquatic food webs, and the largest contributors to ocean trophic networks, changes to phytoplankton physiology necessarily results in changes to food web dynamics through bloom ecology, carbon uptake and transport and nutrient availability and dynamics. This research provides new tools for examining phytoplankton physiology in laboratory studies, as well as insight into phytoplankton pH dynamics and energetic potential.

In Chapter 2, the design for a novel pHstat system possessing both steady state and dynamic pH functionalities was presented, providing a reliable, flexible platform for future studies on phytoplankton response to varying pH environments. This system was shown to successfully and precisely simulate both steady state and cyclically dynamic pH variability within a controlled ecosystem. The use of reagents in conjunction with a self-modulating computer program successfully blended programmatic, electromechanical, and biological components to form an effective pH-regulating platform for culturing phytoplankton, with a precision of (±0.03 pH units). The development of this system presents an important new tool for OA research, allowing researchers to examine the combined effect of regular, diel fluctuations in pH with the small, long term changes to base pH that will be seen in future oceans as OA

worsens. This can give us valuable information on the more subtle effects of OA on dynamic systems such as estuaries or coastal ecosystems.

The experiments performed in Chapter 3 to assess SNARF efficacy as a pH_i indicator in phytoplankton prove it to be a valuable addition to the array of indicators available for measuring pH_i. It is an improvement on currently available dyes such as BCECF, which lack the more stable fluorescence measurements provided by the ratiometric fluorophore SNARF. The latter was shown to be an efficient pH_i indicator in a variety of phytoplankton, depending on the loading concentration of the fluorophore and the method of fluorescence detection. Fluorescence spectroscopy provided the most accurate fluorescence data for pH_i calculation. Esterase activity was shown to have a positive relationship with cell volume, influencing the detectability of SNARF in smaller cells. This, combined with autofluorescence from pigments within the cells, and a less than ideal fixed fluorescence detection wavelength, made flow cytometry a less accurate method of pH_i detection. However, SNARF's additional potential application of being used as a viability indicator keeps makes it a valuable tool for phytoplankton physiology studies.

Chapter 4 delved into the relationship between environmental pH and intracellular energy balance. The steady state pH levels described in Chapter 4 of this thesis are not outside of the range previously studied. Phytoplankton response to changes in environmental pH has been studied using a variety of organisms, and at pH levels far beyond the range of any that would be encountered in natural aquatic ecosystems, no matter how anthropogenically perturbed. The aim of this work was instead to examine long-term phytoplankton adaptation to changing pH, and observe their response to chronic, environmentally relevant pH environments. Intracellular pH in dynamic environments was found to inversely mirror external pH, with difference between environmental pH and pH_i (ΔpH) being strongest with the strengthening of the electrochemical

potential across the cell membrane. Varying external pH was also shown to correlate with esterase activity within the cell—a change that was correlated with decreasing photosynthetic yield. Photosynthetic efficiency declined in tandem with external pH at the lower steady state pH levels. Given that esterases are used in cellular metabolism to release energy stored as lipid reserves, these data suggest that esterase activity may somewhat mitigate the effect of acidification on the efficiency of PSII, and thus on overall cellular energy balance, a concept supported by related research regarding fatty acid storage and usage under OA conditions.

Future work should confirm decreasing lipid reserves in phytoplankton with increased esterase activity, and esterases should be characterized and measured with regard to relative abundance and specificity as these both affect bulk esterase activity. Changes in lipid/fatty acid reserves should be related to calorimetric measurements in order to quantify cellular energetics. Calorimetry can quantify the amount of energy available in a sample or system by measuring heat changes. Bomb calorimeters are often used for measuring bulk energy (Samuel et al. 2008; Weitkunat et al. 2015; Gidrewicz and Fenton 2014); gross energy content of the original sample can be calculated by combusting the sample and measuring the amount of heat energy released. Future work should also include an investigation into expression of the genes responsible for esterases. mRNA abundance would provide valuable data on esterase expression at different pH regimes. A closer examination of photosynthetic activity would be useful, and should include investigations regarding oxygen evolution, carbon fixation, and CCM activity in order to test the concept presented in this dissertation regarding carbon limitation due to reduced activity of carbonic anhydrase.

Insights into how pH_i is regulated could be reached by using ethylisopropylamide (EIPA) to block H^+ ion exchange in order to determine if short-term buffering or long-term upregulation

of acid/base transporters is the driving force behind the pH_i responses of *I. galbana* to fluctuating environmental pH. Finally, a broader group of organisms should be examined, as CCM activity, buffer capacity, and esterase activity vary among organisms (as shown in Chapter 3). Phytoplankton are highly diverse, and as such have varying responses to environmental stimuli. Now that a pHstat system is available with both steady state and dynamic capabilities, it is important to test the long-term effect of pH changes on a variety of phytoplankton. Of particular interest would be phytoplankton responsible for harmful algal blooms, as environmental stress has been linked to increased toxin production in numerous toxic dinoflagellate taxa (Grzebyk et al. 2003; Flynn et al. 1994).

REFERENCES

Agusti, Susana, and M. Carmen Sanchez. 2002. "Cell Viability in Nautral Phytoplankton Communities Quantified by a Membrane Permeability Probe." *Limnology and Oceanography* 47 (3): 818–28.

Agusti, Susana, Maria Paola Satta, Maria Paola Mura, and Esther Benavent. 1998. "Dissolved Esterase Activity as a Tracer of Phytoplankton Lysis: Evidence of High Phytoplankton Lysis Rates in the Northwestern Mediterranean." *Limnology and Oceanography* 43 (8): 1836–49.

Andersson, A.J., and F.T. Mackenzie. 2012. "Revisiting Four Scientific Debates in Ocean Acidification Research." *Biogeosciences* 9: 893–905.

Avendaño, Lizeth, Martha Gledhill, Eric P. Achterberg, Victoire M. C. Rérolle, and Christian Schlosser. 2016. "Influence of Ocean Acidification on the Organic Complexation of Iron and Copper in Northwest European Shelf Seas; a Combined Observational and Model Study." *Frontiers in Marine Science* 3: 58. doi:10.3389/fmars.2016.00058.

Aymerich, Ismael, Jaume Piera, Aureli Soria-Frisch, and Lluisa Cros. 2009. "A Rapid Technique for Classifying Phytplankton Fluorescence Spectra Based on Self-Organizing Maps." *Applied Spectroscopy* 63 (6): 716–26.

Badger, M.R., T.J. Andrews, S.M. Whitney, M Ludwig, D.C. Yellowlees, W Leggat, and G.D. Price. 1998. "The Diversity and Coevolution of RubisCO, Plastids, Pyrenoids, and Chloroplast Based CO2-Concentrating Mechansisms in Algae." *Canadian Journal of Botany* 76: 1052–71.

Badger, Murray. 2003. "The Roles of Carbonic Anhydrases in Photosynthetic CO2 Concentrating Mechanisms." *Photosynthesis Research* 77 (83).

Badger, Murray, and G. Dean Price. 1994. "The Role of Carbonic Anhydrase in Photosynthesis." *Annual Review of Plant Plhysiology and Plant Molecular Biology* 45: 369–92.

Baek, Seung, Seung Jung, and Kyoungsoon Shin. 2011. "Effects of Temperature and Salinity on Growth of Thalassiosira Pseudonana (Bacillariophyceae) Isolated from Ballast Water." *Journal of Freshwater Ecology* 26 (4): 547–52. doi:10.1080/02705060.2011.582696.

Baes, Charles, and Robert Mesmer. 1976. *The Hydrolysis of Cations*. New York, NY: John Wiley & Sons, Inc.

Barton, A.D., M.S. Lozier, and R.G. Williams. 2014. "Physical Control of Variability in North Atlantic Phytoplankton Communities." *Limnology and Oceanography* 60: 181–97.

Beaufort, L., I. Probert, T. de Garidel-Thoron, E. M. Bendif, D. Ruiz-Pino, N. Metzl, C. Goyet, et al. 2011. "Sensitivity of Coccolithophores to Carbonate Chemistry and Ocean Acidification." *Nature* 476 (7358): 80–83. doi:10.1038/nature10295.

Berdalet, Elisa. 1992. "Effects of Turbulence on the Marine Dinoflagellate Gymnodinium Nelsonii." *Journal of Phycology* 28: 267–72.

Berg, Jeremy, John Tymoczko, and Lubert Stryer. 2002. *Biochemistry*. 5th ed. New York, NY: W.H. Freeman.

Berge, Terje, Niels Daugbjerg, Bettina Andersen, and Per Juel Hansen. 2010. "Effect of Lowered pH on Marine Phytoplankton Growth Rates." *Marine Ecology Progress Series* 416: 79–91. doi:10.3354/meps08780.

Berges, J.A., D.J. Franklin, and P.J. Harrison. 2001. "Evolution of an Artificial Seawater Medium: Improvement in Enriched Seawater, Artificial Water over the Past Two Decades." *Journal of Phycology* 37: 1138–45.

Bockmon, E.E., C.A. Frieder, M.O. Navarro, L.A. White-Kershek, and A.G. Dickson. 2013. "Controlled Experimental Aquarium System for Multi-Stressor Investigation: Carbonate Chemistry, Oxygen Saturation, and Temperature." *Biogeosciences Discussions* 10: 3431–53.

Booth, Ian. 1985. "Regulation of Cytoplasmic pH in Bacteria." *Microbiological Reviews* 49 (4): 359–78.

Boron, Walter. 2004. “Regulation of Intracellular pH.” *Advanced Physiological Education* 28: 160–79.
Boyarsky, G, M B Ganz, E J Cragoe, and W F Boron. 1990. “Intracellular-pH Dependence of Na-H Exchange and Acid Loading in Quiescent and Arginine Vasopressin-Activated Mesangial Cells.” *Proceedings of the National Academy of Sciences of the United States of America* 87 (15): 5921–24.
Brauer, David, Joe Uknalis, Ruth Triana, and Shu-I Tu. 1996. “Subcellular Compartmentation of Different Lipophilic Fluorescein Derivatives in Maize Root Epidermal Cells.” *Protoplasma* 192 (1): 70–79.
Breeuwer, Pieter, Jean-Louis Drocourt, Frank Rombouts, and Tjakko Abee. 1994. “Energy-Dependent, Carrier-Mediated Extrusion of Carboxyfluorescein from Saccharomyces Cerevisiae Allows Rapid Assessment of Cell Viability by Flow Cytometry.” *Applied and Environmental Microbiology* 60 (5): 1467–72.
Bright, G.R., G.W. Fisher, J Rogowska, and D.L. Taylor. 1989. “Fluorescence Ratio Imaging Microscopy.” *Methods of Cell Biology* 30: 157–92.
Bunting, John, and Shaikh Kabir. 1978. “The pH-Dependence of the Non-Specific Esterase Activity of Carboxypeptidase A.” *Biochimica et Biophysica Acta (BBA) - Enzymology* 527 (1): 98–107.
Busa, W. B., and R. Nuccitelli. 1984. “Metabolic Regulation via Intracellular pH.” *American Journal of Physiology - Regulatory, Integrative and Comparative Physiology* 246 (4): R409.
Busa, William, and John Crowe. 1983. “Intracellular pH Regulates Trasitions between Dormancy and Development of Brine Shrimp (Artemia Salina) Embryos.” *Science* 221: 366–68.
Byreddy, Avinesh, Adarsha Gupta, Colin Barrow, and Munish Puri. 2015. “Comparison of Cell Disruption Methods for Improving Lipid Extraction from Thraustochytrid Strains.” *Marine Drugs* 13: 5111–27. doi:10.3390/md13085111.
Cai, Wei-Jun, Xinping Hu, Wei-Jen Huang, Li-Qing Jiang, Yongchen Wang, Tsung-Hung Peng, and Xin Zhang. 2010. “Alkalinity Distribution in the Western North Atlantic Ocean Margins.” *Journal of Geophysical Research: Oceans* 115 (C8): n/a-n/a. doi:10.1029/2009JC005482.
Campbell, Anna L., Stephanie Mangan, Robert P. Ellis, and Ceri Lewis. 2014. “Ocean Acidification Increases Copper Toxicity to the Early Life History Stages of the Polychaete Arenicola Marina in Artificial Seawater.” *Environmental Science & Technology* 48 (16): 9745–53. doi:10.1021/es502739m.
Carter, Norman, Floyd Rector, David Campion, and Donald Seldin. 1967. “Measurement of Intracellular pH of Skeletal Muscle with pH-Sensitive Glass Microelectrodes.” *Journal of Clinical Investigation* 46 (6): 920–33.
Casey, Joseph, Sergio Grinstein, and John Orlowski. 2010. “Sensors and Regulators of Intracellular pH.” *Nature Reviews Molecular Cell Biology* 11: 50–61. doi:doi:10.1038/nrm2820.
Chang, Ping-An, Yu-Ying Chen, Wen-zhen Qin, Ding-Xin Long, and Yi-Jun Wu. 2011. “The Role of Cell Cycle-Dependent Neuropathy Target Esterase in Cell Proliferation.” *Molecular Biology Reports* 38 (1): 123–30.
Chen, Celia, and Edward Durbin. 1994. “Effects of pH on the Growth and Carbon Uptake of Marine Phytoplankton.” *Marine Ecology Progress Series* 109: 83–94.
Chisti, Yusuf, and Murray Moo-Young. 1986. “Disruption of Microbial Cells for Intracellular Production.” *Enzyme and Microbial Technology* 8: 194–204.
Ciais, P, A.J. Dolman, A Bombelli, R Duren, A Peregon, P.J. Rayner, C Miller, et al. 2014. “Current Systematic Carbon-Cycle Observations and the Need for Implementing a Policy-Relevant Carbon Observing System.” *Biogeosciences* 11: 3547–3602.
Collins, Sinead, Björn Rost, and Tatiana Rynearson. 2013. “Evolutionary Potential of Marine Phytoplankton under Ocean Acidification Conditions.” *Evolutionary Applications* 7: 140–55.
Connell, Sean, Kristy Kroeker, Katharina Fabricius, David Kline, and Bayden Russell. 2013. “The Other Ocean Acidification Problem: CO2 as a Resource among Compettiors for Ecosystem Dominance.” *Philosophical Transactions of the Royal Soceity B* 368: 20120442.

Converti, Attilio, Alessandro Casazza, Erika Ortiz, Patrizia Perego, and Marco Del Borghi. 2009. "Effect of Temperature and Nitrogen Concentration on the Growth and Lipid Content of Nannochloropsis Oculata and Chlorella Vulgaris for Biodiesel Production." *Chemical Engineering and Processing: Process Intensification* 48 (6): 1146–51.

Cruz, Jeffrey, Atsuko Kanazawa, Nathan Treff, and David Kramer. 2005. "Storage of Light-Driven Transthylakoid Proton Motive Force as an Electric Field (Δψ) under Steady-State Conditions in Intact Cells of Chlamydomonas Reinhardtii." *Photosynthesis Research* 85 (2): 221–33.

Cyronak, Tyler, Kai Schulz, and Paul Jokiel. 2015. "The Omega Myth: What Really Drives Lower Calcification Rates in an Acidifying Ocean." *ICES Journal of Marine Science*. doi:10.1093/icesjms/fsv075.

Dai, M, Z Lu, W Zhai, B Chen, Z Cao, K Zhou, W.J. Cai, and C.T.A. Chen. 2009. "Diurnal Variations of Surface Seawater pCO2 in Contrasting Coastal Environments." *Limnology and Oceanography* 54: 735–45.

Dason, Jeffrey, and Brian Colman. 2004. "Inhibition of Growth in Two Dinoflagellates by Rapid Changes in pH." *Canadian Journal of Botany* 82 (4): 515–20.

Demaurex, Nicolas. 2002. "pH Homeostasis of Cellular Organelles." *Physiology* 17 (1): 1–5.

Devamani, Titu, Alissa M. Rauwerdink, Mark Lunzer, Bryan J. Jones, Joanna L. Mooney, Maxilmilien Alaric O. Tan, Zhi-Jun Zhang, Jian-He Xu, Antony M. Dean, and Romas J. Kazlauskas. 2016. "Catalytic Promiscuity of Ancestral Esterases and Hydroxynitrile Lyases." *Journal of the American Chemical Society* 138 (3): 1046–56. doi:10.1021/jacs.5b12209.

Devonshire, Alan, and Linda Field. 1991. "Gene Amplification and Insecticide Resistance." *Annual Review of Entomology* 36: 1–23.

Dietz, K.J., N Tavakoli, C Kluge, T Mimura, S.S. Sharma, G.C. Harris, A.N. Chardonnens, and D Golldack. 2001. "Significance of the V-Type ATPase for the Adaptation to Stressful Growth Conditions and Its Regulation on the Molecular and Biochemical Level." *Journal of Experimental Botany* 52 (363): 1969–80.

Doney, Scott. 2010. "The Growing Human Footprint on Coastal and Open-Ocean Biogeochemistry." *Science* 17: 1512–16.

Doney, Scott, William Balch, Victoria Fabry, and Richard Feely. 2009. "Ocean Acidification: A Critical Emerging Problem for the Ocean Sciences." *Oceanography* 22 (4): 16–25.

Doney, Scott, Victoria Fabry, Feely Richard, and Joan Kleypas. 2009. "Ocean Acidification: The Other CO2 Problem." *Annual Review of Marine Science* 1: 169–92.

Dorsey, Judy, Clarice Yentsch, Sara Mayo, and Colleen McKenna. 1989. "Rapid Analytical Technique for the Assessment of Cell Metabolic Activity in Marine Microalgae." *Cytometry* 10: 622–28.

Droop, M.R. 1975. "The Chemostat in Mariculture." *10th European Symposium on Marine Biology* 1: 71–93.

Duarte, Carlos, Iris Hendriks, Tommy Moore, Ylva Olsen, Alexandra Steckbauer, Laura Ramajo, and Jacob Carstensen. 2013. "Is Ocean Acidification an Open-Ocean Syndrome? Understanding Anthropogenic Impacts on Seawater pH." *Estuaries and Coasts*. doi:10.1007/s12237-013-9594-3.

Dufour, J.-P., P Malcorps, and P Silcock. 2008. "Control of Ester Synthesis during Brewery Fermentation." In *Brewing Yeast Fermentation and Performance*, 2nd ed., 213–33. John Wiley & Sons, Inc.

Eberlein, Tim, Dedmer Van de Waal, and Bjorn Rost. 2014. "Differential Effects of Ocean Acidification on Carbon Acquisition in Two Bloom-Forming Dinoflagellate Species." *Physiologia Plantarum* 151: 468–79.

Egleston, E.S., C.L. Sabine, and F.M. Morel. 2010. "Revelle Revisited: Buffer Factors That Quantify the Response of Ocean Chemistry to Changes in DIC and Alkalinity." *Global Biogeochemical Cycles* 24. doi:10.1029/2008GB003407.

Eltgroth, Matthew L., Robin L. Watwood, and Gordon V. Wolfe. 2005. "Production and Cellular Localization of Neutral Long-Chain Lipids in the Haptophyte Algae Isochrysis Galbana and

Emiliania Huxleyi." *Journal of Phycology* 41 (5): 1000–1009. doi:10.1111/j.1529-8817.2005.00128.x.
Espie, George, and Brian Colman. 1981. "The Intracellular pH of Isolated Photosynthetically Active Asparagus Mesophyll Cells." *Planta* 153: 210–16.
Fay, P, and S.A. Kulasooriya. 1973. "A Simple Apparatus for the Ccontinuous Culture of Photosynthetic Microorganisms." *British Phycological Journal* 8 (1): 51–57.
Feely, Richard, Simone Alin, Jan Newton, Christopher Sabine, Mark Warner, Allan Devol, Christopher Krembs, and Carol Maloy. 2010. "The Combined Effects of Ocean Acidification, Mixing, and Respiration on pH and Carbonate Saturation in an Urbanized Estuary." *Estuarine, Coastal and Shelf Science* 88: 442–49.
Feng, Yuanyuan, Mark Warner, Yaohong Zhang, Jun Sun, Fei-Xue Fu, Julie Rose, and David Hutchins. 2008. "Interactive Effects of Increased pCO2, Temperature and Irradiance on the Marine Coccolithophore Emiliana Huxleyi (Prymnesiophyceae)." *European Journal of Phycology* 43 (1): 87–98.
Fischer, R, T Anderson, H Hillebrand, and R Ptacnik. 2014. "The Exponentially Fed Batch Culture as a Reliable Alternative to Conventional Chemostats." *Limnology and Oceanography: Methods* 12: 432–40.
Flynn, Kevin, Jerry Blackford, Mark Baird, John Raven, Darren Clark, John Beardall, Colin Brownlee, Heiner Fabian, and Glen Wheeler. 2012. "Changes in pH at the Exterior Surface of Plankton with Ocean Acidification." *Nature Climate Change* 2: 510–13.
Flynn, Krystyna, Jose Franco, Pablo Fernandez, Beatriz Reguera, Manuel Zapata, Gareth Wood, and Kevin Flynn. 1994. "Changes in Toxin Content, Biomass and Pigments of the Dinoflagellate Alexandrium Minutum during Nitrogen Refeeding and Growth into Nitrogen or Phosphorus Stress." *Marine Ecology Progress Series* 111: 99–109.
Fojan, Peter, Per H. Jonson, Maria Petersen, and Steffen Petersen. 2000. "What Distinguishes an Esterase from a Lipase: A Novel Structural Approach." *Biochimie* 82: 1033–41.
French, C.S., James Smith, Hemming Virgin, and Robert Airth. 1956. "Fluorescence-Spectrum Curves of Chlorophyll.s, Pheophytins, Phycoerythrins, Phycocyanins and Hypericin." *Plant Physiology* 31 (5): 369–74.
French, C.S., and Violet Young. 1952. "The Fluorescence Spectra of Red Algae and the Transfer of Energy from Phycoerythrin to Phycocyanin and Chlorophyll." *The Journal of General Physiology* 35 (6): 873–90.
Frohlich, Donald. 1990. "Substrate Specificity of Esterases in a Solitary Bee, Megachile Rotundata (Hymenoptera: Megachilidae): Variability in Sex, Age and Life Stage." *Biochemical Systematics and Ecology* 18 (7–8): 539–47.
Frohnmeyer, Hanns, Alexander Grabov, and Michael Blatt. 1998. "A Role for the Vacuole in Auxin-Mediated Control of Cytosolic pH by Vicia Mesophyll and Guard Cells." *The Plant Journal* 13 (1): 109–16.
Fu, Jing, Erik Pacyniak, Marina Leed, Matthew Sadgrove, Lesley Marson, and Michael Jay. 2015. "Interspecies Differences in the Metabolism of a Multiester Prodrug by Carboxylesterases." *Journal of Pharmaceutical Sciences*. doi:10.1002/jps.24632.
Gao, Kunshan, and Yangqiao Zheng. 2010. "Combined Effects of Ocean Acidification and Solar UV Radiation on Photosynthesis, Growht, Pigmentation and Calicification of the Coralline Alga Corallina Sessilis (Rhodophyta)." *Global Change Biology* 16 (8): 2388–98.
Gao, Meng, Qinglian Hu, Guangxue Feng, Ben Tang, and Bin Liu. 2014. "A Fluorescent Light-up Probe with 'AIE+ESIPT' characteristics for Specific Detection of Lysosomal Esterase." *Journal of Materials Chemistry B*, no. 22: 3438–42. doi:10.1039/C4TB00345D.
Garcia-Arrazola, R, S.C. Siu, G Chan, I Buchanan, B Doyle, Titchener-Hooker, and F Baganz. 2005. "Garcia-Arrazola." *Biochemical Engineering Journal* 23 (3): 221–30.

Garvey, M., B. Moriceau, and U. Passow. 2007. “Applicability of the FDA Assay to Determine the Viability of Marine Phytoplankton under Different Environmental Conditions.” *Marine Ecology Progress Series* 352: 17–26.

Garzke, Jessica, Thomas Hansen, Stefanie Ismar, and Ulrich Sommer. 2016. “Combined Effects of Ocean Warming and Acidification on Copepod Abundance, Body Size and Fatty Acid Content.” *PLOS One* 11 (5). doi:10.1371/journal.pone.0155952.

Gattuso, J, and L Hansson. 2011. *Ocean Acidification*. New York, NY: Oxford University Press.

Gee, Christopher, and Krishna Niyogi. 2017. “The Carbonic Anhydrase CAH1 Is an Essential Component of the Carbon-Concentrating Mechanism in Nannochloropsis Oceanica.” *Proceedings of the National Academy of Science USA* 114 (17): 4537–42.

Gehl, Katharina, and Brian Colman. 1985. “Effect of External pH on the Internal pH of Chlorella Saccharophila.” *Plant Physiology* 77: 917–21.

Gerloff-Elias, Antje, Deepak Barua, Andreas Molich, and Spijkerman. 2006. “Temperature- and pH-Dependent Accumulation of Heat-Shock Proteins in the Acidophilic Green Alga Chlamydomonas Acidophila.” *FEMS Microbiology Ecology* 56 (3): 345–54. doi:10.1111/j.1574-6941.2006.00078.x.

Gibbin, Emma, Hollie Putnam, Simon Davy, and Ruth Gates. 2014. “Intracellular pH and Its Response to CO2-Driven Seawater Acidification in Symbiotic versus Non-Symbiotic Coral Cells.” *The Journal of Experimental Biology* 217: 1963–69. doi:doi: 10.1242/jeb.099549.

Gidrewicz, Dominica A., and Tanis R. Fenton. 2014. “A Systematic Review and Meta-Analysis of the Nutrient Content of Preterm and Term Breast Milk.” *BMC Pediatrics* 14 (1): 216. doi:10.1186/1471-2431-14-216.

Gledhill, Martha, Eric P. Achterberg, Keqiang Li, Khairul N. Mohamed, and Micha J.A. Rijkenberg. 2015. “Influence of Ocean Acidification on the Complexation of Iron and Copper by Organic Ligands in Estuarine Waters.” *Cycles of Metals and Carbon in the Oceans - A Tribute to the Work Stimulated by Hein de Baar* 177 (December): 421–33. doi:10.1016/j.marchem.2015.03.016.

Golda, Rachel, Mark Golda, Jacqueline Hayes, Tawnya Peterson, and Joseph Needoba. 2017. “Development of an Economical, Autonomous pHstat System for Culturing Phytoplankton under Steady State or Dynamic Conditions.” *Journal of Microbiological Methods* 136: 78–87.

Golda, Rachel, Mark Golda, Tawnya Peterson, and Joseph Needoba. 2017. “Graphical Coding Data and Operational Guidance for Implementation or Modification of a LabVIEW(R)-Based pHstat System.” *Data in Brief* 12: 463–70.

Gould, Stephen McQ., and Dan S. Tawfik. 2005. “Directed Evolution of the Promiscuous Esterase Activity of Carbonic Anhydrase II.” *Biochemistry* 44 (14): 5444–52. doi:10.1021/bi0475471.

Goullet, Philippe, and Bertrand Picard. 1995. “The Electrophoretic Polymorphism of Bacterial Esterases.” *FEMS Microbiology Reviews* 16: 7–31.

Gruber, Nicolas, Claudine Hauri, Zouhair Lachkar, Damian Loher, Thomas Frolicher, and Gian-Kasper Plattner. 2012. “Rapid Progression of Ocean Acidification in the California Current System.” *Science* 337: 220–23.

Grynkiewicz, G, M Poenie, and R.Y. Tsien. 1985. “A New Generation of Ca2+ Indicators with Greatly Improved Fluorescence Properties.” *Journal of Biological Chemistry* 260 (6): 3440–50.

Grzebyk, Daniel, Christian Bechemin, Clive Ward, Celine Verite, Geoffrey Codd, and Serge Maestrini. 2003. “Effects of Salinity and Two Coastal Waters on the Growth and Toxin Content of the Dinoflagellate Alexandrium Minutum.” *Journal of Plankton Research* 25 (10): 1185–99.

Han, Junyan, and Kevin Burgess. 2010. “Fluorescent Indicators for Intracellular pH.” *Chemical Reviews* 110: 2709–28.

Hansen, Per Juel, N Lundholm, and Björn Rost. 2007. “Growth Limitation in Marine Red-Tide Dinoflagellates: Effects of pH versus Inorganic Carbon Availability.” *Marine Ecology Progress Series* 334: 63–71.

Harrison, P.J., H.L. Conway, and R.C. Dugdale. 1976. “Marine Diatoms Grown in Chemostats under Silicate or Ammonium Limitation. I. Cellular Chemical Composition and Stead State Growth Kinetics of Skeletonema Costatum.” *Marine Biology* 35 (2): 177–86.
Harrison, P.J., R.E. Waters, and F.J.R. Taylor. 1980. “A Broad Spectrum Artificial Seawater Medium for Coastal and Open Ocean Phytoplankton.” *Journal of Phycology* 16: 28–35.
Haubner, Norbert, Peter Sylvander, Kristiina Vuori, and Pauline Snoeijs. 2014. “Abiotic Stress Modifies the Synthesis of Alpha-Tocopherol and Beta-Carotene in Phytoplankton Species.” *Journal of Phycology* 50: 753–59.
Havskum, Harry, and Per Juel Hansen. 2006. “Net Growth of the Bloom-Forming Dinoflagellate Heterocapsa Triquetra and pH: Why Turbulence Matters.” *Aquatic Microbial Ecology* 42: 55–62.
Hendriks, I.E., C.M. Duarte, and M Alvarez. 2010. “Vulnerability of Marine Biodiviersity to Ocean Acidification: A Meta-Analysis.” *Estuarine, Coastal and Shelf Science* 89: 186–90.
Herve, Vincent, Julien Derr, Stephane Douady, Michelle Quinet, Lionel Moisan, and Pascal Jean Lopez. 2012. “Multiparametric Analyses Reveal the pH-Dependence of Silicon Biomineralization in Diatoms.” *PLOS One* 7 (10): e46722.
Hinga, Kenneth. 2002. “Effects of pH on Coastal Marine Phytoplankton.” *Marine Ecology Progress Series* 238: 281–300.
Hoffmann, L.J., E Breitbarth, C McGraw, C.S. Law, K.I. Currie, and K.A. Hunter. 2013. “A Trace-Metal Clean, pH-Controlled Incubator System for Ocean Acidification Incubation Studies.” *Limnology and Oceanography: Methods* 11: 53–61.
Hong, Haizheng, Rong Shen, Futing Zhang, Zuozhu Wen, Siwei Chang, Wenfang Lin, Sven Kranz, et al. 2017. “The Complex Effects of Ocean Acidification on the Prominent N2-Fixing Cyanobacterium Trichodesmium.” *Science*. doi:10.1126/sciene.aal2981.
Hurd, Catriona, Christopher Hepburn, Kim Currie, John Raven, and Keith Hunter. 2009. “Testing the Effects of Ocean Acidification on Algal Metabolism: Consideration for Experimental Designs.” *Journal of Phycology* 45: 1236–51.
Iglesias-Rodriguez, M. Debora, Paul Halloran, Rosalind Rickaby, Ian Hall, Elena Colmenero-Hidalgo, John Gittins, Darryl Green, et al. 2008. “Phytoplankton Calcification in a High-CO2 World.” *Science* 320 (5874): 336–40.
Inoue, M, M Morikawa, M Tsuboi, and M Sugiura. 1979. “Species Difference and Characterization of Intestinal Esterase on the Hydrolizing Activity of Ester-Type Drugs.” *Japanese Journal of Pharmacology* 29 (1): 9–16.
Jagendorf, A T, and E Uribe. 1966. “ATP Formation Caused by Acid-Base Transition of Spinach Chloroplasts.” *Proceedings of the National Academy of Sciences of the United States of America* 55 (1): 170–77.
Jannasch, H.W. 1974. “Steady State and the Chemostat in Ecology.” *Limnology and Oceanography* 19 (4): 716–20.
Jayalakshmi, T., R. Nandakumar, B. Balaji Prasath, and P. Santhanam. 2016. “Effect of Acidification on Fatty Acids Profiling of Marine Benthic Harpacticoid Copepod Parastenhelia Sp.” *Annals of Agrarian Science* 14 (3): 278–82. doi:10.1016/j.aasci.2016.09.001.
Jiao, Yang, Hui-Ling Ouyang, Yu-Jiao Jiang, Xiang-Zhen Kong, Wei He, Wen-Xiu Liu, Bin Yang, and Fu-Liu Xu. 2015. “Toxic Effects of Ethyl Cinnamate on the Photosynthesis and Physiological Characteristics of Chlorella Vulgaris Based on Chlorophyll Fluorescence and Flow Cytometry Analysis.” *The Scientific World Journal* 2015: 107823. doi:10.1155/2015/107823.
Johnson, Carl, and David Epel. 1981. “Intracellular pH of Sea Urchin Eggs Measured by Dimtheyloxazolidinedione (DMO) Method.” *The Journal of Cell Biology* 89: 284–91.
Johnson, Xenie, and Jean Alric. 2013. “Central Carbon Metabolism and Electron Transport in Chlamydomonas Reinhardtii: Metabolic Constraints for Carbon Partitioning between Oil and Starch.” *Eukaryotic Cell* 12 (6): 776–93. doi:10.1128/EC.00318-12.

Kamendulis, L.M., M.R. Brzezinski, E.V. Pindel, W.F. Bosron, and R.A. Dean. 1996. “Metabolism of Cocaine and Heroin Is Catalyzed by the Same Human Liver Carboxylesterases.” *Journal of Pharmacology and Experimental Therapeutics* 279 (2): 713–17.

Kaplan, Drora, Zvi Cohen, and Aharon Abeliovich. 1986. “Optimal Growth Conditions for Isochrysis Galbana.” *Biomass* 9: 37–48.

Kar, Jayaranjan, and Reckha Singhal. 2015. “Investigations on Ideal Mode of Cell Disruption in Extremely Halophilic Actinopolyspora Halophila (MTCC 263) for Efficient Release of Glycine Betaine and Trehalose.” *Biotechnology Reports* 5: 89–97. doi:10.1016/j.btre.2014.12.005.

Karagiannis, Jim, and Paul Young. 2001. “Intracellular pH Homeostasis during Cell-Cycle Progression and Growth State Transition in Schizosaccharomyces Pombe.” *Journal of Cell Science* 114: 2929–41.

Kim, Ja-Myung, Kitack Lee, Kyoungsoon Shin, Jung-Hoon Kang, Hyun-Woo Lee, Miok Kim, Pung-Guk Jang, and Min-Chul Jang. 2006. “The Effect of Seawater CO2 Concentration on Growth of a Natural Phytoplankton Assemblage in a Controlled Mesocosm Experiment.” *Limnology and Oceanography* 51 (4): 1629–36.

Koo, Yeon, Eun Yoon, Jun Seo, Ju-Kon Kim, and Yang Choi. 2013. “Characterization of a Methyl Jasmonate Specific Esterase in Arabidopsis.” *Journal of the Korean Society for Applied Biological Chemistry* 56 (1): 27–33.

Kottmeier, Dorothee M, Sebastian D Rokitta, and Björn Rost. 2016. “Acidification, Not Carbonation, Is the Major Regulator of Carbon Fluxes in the Coccolithophore Emiliania Huxleyi.” *The New Phytologist* 211 (1): 126–37. doi:10.1111/nph.13885.

Kouser, Shereen, V Shakunthala, and S.N. Hegde. 2013. “Effect of Different Light Regimes on Esterase Isozyme Profiles of Three Species of Drosophila.” *Frontiers in Life Science* 7 (3–4): 148–54.

Koussoroplis, Apostolos-Manuel, Anke Schwarzenberger, and Alexander Wacker. 2017. “Diet Quality Determines Lipase Gene Expression and Lipase/esterase Activity in Daphnia Pulex.” *Biology Open* 6 (2): 210–16. doi:10.1242/bio.022046.

Krachler, Regina, Rudolf F. Krachler, Gabriele Wallner, Stephan Hann, Monika Laux, Maria F. Cervantes Recalde, Franz Jirsa, et al. 2015. “River-Derived Humic Substances as Iron Chelators in Seawater.” *Marine Chemistry* 174 (August): 85–93. doi:10.1016/j.marchem.2015.05.009.

Kranz, Sven A, Dieter Sultemeyer, Klaus-Uwe Richter, and Bjoern Rost. 2009. “Seawater Carbonate Chemistry and Processes during Experiments with Cyanobacterium Trichodesmium (IMS101), 2009.” *Supplement to: Kranz, SA et Al. (2009): Carbon Acquisition by Trichodesmium: The Effect of pCO2 and Diurnal Changes. Limnology and Oceanography, 54(2), 548-559, doi:10.4319/lo.2009.54.2.0548*, April. doi:10.1594/PANGAEA.736024.

Kroeker, Kristy, Rebecca Kordas, Ryan Crim, Iris Hendriks, Laura Ramajo, Gerald Singh, Carlos Duarte, and J Gattuso. 2013. “Impacts of Ocean Acidification on Marine Organisms: Quantifying Sensitivities and Interactions with Warming.” *Global Change Biology* 19: 1884–96.

Kroeker, Kristy, Rebecca Kordas, Ryan Crim, and Gerald Singh. 2010. “Meta-Analysis Reveals Negative yet Variable Effects of Ocean Acidification on Marine Organisms.” *Ecology Letters* 13: 1419–34. doi:10.1111/j.1461-0248.2010.01518.x.

Lane, Ann, and John Burris. 1981. “Effects of Environmental pH on the Internal pH of Chlorella Pyrenoidosa, Scenedesmus Quadricauda, and Euglena Mutabilis.” *Plant Physiology* 68: 439–42.

LaRoche, J, Björn Rost, and A Engel. 2010. “Bioassays, Batch Culture and Chemostat Experimentation, Approaches and Tools to Manipulate the Carbonate Chemistry. In: Guide for Best Practices in Ocean Acidification Research and Data Reporting.” In *Guide for Best Practices in Ocean Acidification Research and Data Reporting*, 81–92.

Lee, Kitack, Lan T. Tong, Frank J. Millero, Christopher L. Sabine, Andrew G. Dickson, Catherine Goyet, Geun-Ha Park, Rik Wanninkhof, Richard A. Feely, and Robert M. Key. 2006. “Global Relationships of Total Alkalinity with Salinity and Temperature in Surface Waters of the World’s Oceans.” *Geophysical Research Letters* 33 (19): n/a-n/a. doi:10.1029/2006GL027207.

Levitan, Orly, Jorge Dinamarca, Ehud Zelzion, Desmond S Lun, L Tiago Guerra, Min Kyung Kim, Joomi Kim, Benjamin A S Van Mooy, Debashish Bhattacharya, and Paul G Falkowski. 2015. "Remodeling of Intermediate Metabolism in the Diatom Phaeodactylum Tricornutum under Nitrogen Stress." *Proceedings of the National Academy of Sciences of the United States of America* 112 (2): 412–17. doi:10.1073/pnas.1419818112.

Lewis, Ceri, Robert P. Ellis, Emily Vernon, Katie Elliot, Sam Newbatt, and Rod W. Wilson. 2016. "Ocean Acidification Increases Copper Toxicity Differentially in Two Key Marine Invertebrates with Distinct Acid-Base Responses" 6 (February): 21554.

Li, Xianchun, Mary Schuler, and May Berenbaum. 2007. "Molecular Mechanisms of Metabolic Resistance to Synthetic and Natural Xenobiotics." *Annual Review of Entomology* 52: 231–53. doi:10.1146/annurev.ento.51.110104.151104.

Liu, Jixiang, Zhenjun Diwu, and Wai-Yee Leung. 2001. "Synthesis and Photophysical Properties of New Fluorinated Benzo[c]xanthene Dyes as Intracellular pH Indicators." *Bioorganic & Medicinal Chemistry Letters* 11: 2903–5.

Lloyd, D, D.J. Mason, and M.T.E. Suller. 2001. "Microbial Infections." In *Cytometric Analysis of Cell Phenotype and Function*. Cambridge, UK: Cambridge University Press.

Loiselle, Frederick, and Joseph Casey. 2003. "Measurement of Intracellular pH." In *Membrane Transporters: Methods and Protocols*, 311–31. Totowa, New Jersey: Humana Press.

Lomolino, Giovanna, Anna Lante, Corrado Rizzi, Paolo Spettoli, and Andrea Curioni. 2005. "Comparison of Esterase Patterns of Three Yeast Strains as Obtained with Different Synthetic Substrates." *Journal of the Institute of Brewing* 111 (2): 234–36.

Lund, Barbara. 1967. "A Study of Some Motile Group D Streptococci." *Journal of General Microbiology* 49: 67–80.

Maberly, Stephen C., Lucy A. Ball, John A. Raven, and Dieter Sültemeyer. 2009. "Inorganic Carbon Acquisition by Chrysophytes." *Journal of Phycology* 45 (5): 1052–61. doi:10.1111/j.1529-8817.2009.00734.x.

MacIntyre, H.L., and J.J. Cullen. 2005. "Using Cultues to Investigate the Physiological Ecology of Microalgae." In *Algal Culturing Techniques*. Burlington, MA: Elsevier Academic Press.

Mackinder, Luke, Glen Wheeler, Declan Schroeder, Ulf Riebesell, and Colin Brownlee. 2010. "Molecular Mechanisms Underlying Calcification in Coccolithophores." *Geomicrobiology Journal* 27 (6–7): 585–95.

MacLeod, C.D., H.L. Doyle, and K.I. Currie. 2015. "Technical Note: Maximising Accuracy and Minimising Cost of a Potentiometrically Regulated Ocean Acidification Simulation System." *Biogeosciences* 12: 713–21.

Masamoto, Kazumori, and Mitsuo Nishimura. 1977. "Estimation of Internal pH in Cells of Blue-Green Algae in the Dark and under Illumination." *Journal of Biochemistry* 82: 483–87.

Maxwell, Kate, and Giles Johnson. 2000. "Chlorophyll Fluorescence - a Practical Guide." *Journal of Experimental Botany* 51 (345): 659–68.

Mayerhoff, Z.D.V.L, T.T. Franco, and I.C. Roberto. 2008. "A Study of Cell Disruption of Candida Mogii by Glass Bead Mill for the Recovery of Xylose Reductase." *Separation and Purification Technology* 63: 706–9.

McCulloch, Malcolm, Jim Falter, Julie Trotter, and Paolo Montagna. 2012. "Coral Resilience to Ocean Acidification and Global Warming through pH up-Regulation." *Nature Climate Change* 2: 623–27. doi:10.1038/NCLIMATE1473.

McGraw, C.M., C.E. Cornwall, M.R. Reid, K.I. Currie, C.D. Hepburn, P Boyd, C.L. Hurd, and K.A. Hunter. 2010. "An Automated pH-Controlled Culture System for Laboratory-Based Ocean Acidification Experiments." *Limnology and Oceanography: Methods* 8: 686–94.

Miller, Charles. 2004. *Biological Oceanography*. Malden, MA: Blackwell Publishing.

Millero, F.J., and D.J. Hawke. 1992. "Ionic Interactions of Divalent Metals in Natural Waters." *Marine Chemistry* 40 (1–2): 19–48.

Millero, FRANK J., RYAN Woosley, BENJAMIN Ditrolio, and JASON Waters. 2009. "Effect of Ocean Acidification on the Speciation of Metals in Seawater." *Oceanography* 22 (4): 72–85.
Molecular Probes. 2003. "SNARF pH Indicators: Product Information."
Monod, J. 1950. "La Technique de Culture Continue. Theorie et Applications." *Annales de l'Institut Pasteur* 79: 390–410.
Montella, Isabela, Renata Schama, and Denise Valle. 2012. "The Classification of Esterases: An Important Gene Family Involved in Insecticide Resistance - a Review." *Memorias Do Instituto Oswaldo Cruz* 107 (4): 437–49.
Moroney, James, and Aravind Somanchi. 1999. "How Do Algae Concentrate CO2 to Increase the Efficiency of Photosynthetic Carbon Fixation?" *Plant Physiology* 119: 9–16.
Nakata, Eiji, Yoshijiro Nazumi, Yoshihiro Yukimachi, Yoshihiro Uto, Hiroshi Maezawa, Toshihiro Hashimoto, Yasuko Okamoto, and Hitoshi Hori. 2011. "Synthesis and Photophysical Properties of New SNARF Derivatives as Dual Emission pH Sensors." *Bioorganic & Medicinal Chemistry Letters* 21 (6): 1663–66.
Nakata, Eiji, Yoshihiro Yukimachi, Yoshijiro Nazumi, Yoshihiro Uto, Hiroshi Maezawa, Toshihiro Hashimoto, Yasuko Okamoto, and Hitoshi Hori. 2010. "A Newly Designed Cell-Permeable SNARF Derivative as an Effective Intracellular pH Indicator." *Chemical Communications* 46: 3526–28. doi:10.1039/C003167D.
Nakata, Eiji, Yoshihiro Yukimachi, Yoshijiro Nazumi, Maki Uwate, Hideaki Maseda, Yoshihiro Uto, Toshihiro Hashimoto, Yasuko Okamoto, Hitoshi Hori, and Takashi Morii. 2014. "A Novel Strategy to Design Latent Ratiometric Fluorescent pH Probes Based on Self-Assembled SNARF Derivatives." *RSC Advances* 4: 345–57.
Negulescu, Paul, and Terry Machen. 1990. "[4] Intracellular Ion Activities and Membrane Transport in Parietal Cells Measured with Fluorescent Dyes." *Methods in Enzymology* 192: 38–81.
Nimer, Nabil, Colin Brownlee, and Michael Merrett. 1999. "Extracellular Carbonic Anhydrase Facilitates Carbon Dioxide Availability for Photosynthesis in the Marine Dinoflagellate Prorocentrum Micans." *Plant Physiology* 120: 105–11.
Nimer, Nabil, Colin Brownlee, and M.J. Merrett. 1994. "Carbon Dioxide Availability, Intracellular pH and Growth Rate of the Coccolithophore Emiliana Huxleyi." *Marine Ecology Progress Series* 109: 257–62.
Novick, A, and L Szilard. 1950. "Description of the Chemostat." *Science* 112: 715–16.
Oakley, Clinton A., Brian M. Hopkinson, and Gregory W. Schmidt. 2012. "A Modular System for the Measurement of CO2 and O2 Gas Flux and Photosynthetic Electron Transport in Microalgae." *Limnology and Oceanography: Methods* 10 (12): 968–77. doi:10.4319/lom.2012.10.968.
Obata, Toshihiro, Alisdair R Fernie, and Adriano Nunes-Nesi. 2013. "The Central Carbon and Energy Metabolism of Marine Diatoms." *Metabolites* 3 (2): 325–46. doi:10.3390/metabo3020325.
Olariaga, Alejandro, Elisa F. Guallart, Verónica Fuentes, Àngel López-Sanz, Antonio Canepa, Juancho Movilla, Mar Bosch, Eva Calvo, and Carles Pelejero. 2014. "Polyp Flats, a New System for Experimenting with Jellyfish Polyps, with Insights into the Effects of Ocean Acidification." *Limnology and Oceanography: Methods* 12 (4): 212–22. doi:10.4319/lom.2014.12.212.
Olenina, Irina, Susanna Hajdu, Lars Edler, Agneta Andersson, Norbert Wasmund, Susanne Busch, Jeannette Gobel, et al. 2006. "Biovolumes and Size-Classes of Phytoplankton in the Baltic Sea." HELCOM Baltic Sea Environmental Proceedings. No 106.
Ores, Joana da Costa, Marina Campos Assumpção De Amarante, Sibele Santos Fernandes, and Susana Juliano Kalil. 2016. "Production of Carbonic Anhydrase by Marine and Freshwater Microalgae." *Biocatalysis and Biotransformation* 34 (2): 57–65. doi:10.1080/10242422.2016.1227793.
Palmer, Jeffrey. 1996. "Rubisco Surprises in Dinoflagellates." *The Plant Cell* 8 (343): 343–45.
Pancic, M, P.J Hansen, A Tammilehto, and N Lundholm. 2015. "Resilience to Temperature and pH Changes in a Future Climate Change Scenario in Six Strains of the Polar Diatom Fragilariopsis Cylindrus." *Biogeosciences* 12: 4235–44.

Paul, J, and P Fottrell. 1961. “Tissue-Specific and Species-Specific Esterases.” *Biochemical Journal* 78: 418–24.
Pick, Uri. 2002. “Adaptation of the Halotolerant Alga Dunaliella to High Salinity.” In *Salinity: Environment - Plants - Molecules*, edited by André Läuchli and Ulrich Lüttge, 97–112. Dordrecht: Springer Netherlands. http://dx.doi.org/10.1007/0-306-48155-3_5.
Radchenko, I, and L Il’yash. 2006. “Growth and Photosynthetic Activity of Diatom Thalassiosira Weissflogii at Decreasing Salinity.” *Plant Physiology* 33 (3): 242–47.
Radic, Sandra, and Branka Pevalek-Kozlina. 2010. “Differential Esterase Activity in Leaves and Roots of Centaurea Ragusina L. as a Consequence of Salinity.” *Periodicum Biologorum* 112 (3): 253–58.
Raven, John, Mario Giordano, and John Beardall. 2011. “Algal and Aquatic Plant Carbon Concentrating Mechanisms in Relation T Oenvironmental Change.” *Photosynthesis Research* 109: 281–96.
Regel, RH, FM Ferris, GG Ganf, and JD Brookes. 2002. “Algal Esterase Activity as a Biomeasure of Environmental Degradation in a Freshwater Creek.” *Aquatic Toxicology* 24 (59(3-4)): 209–23.
Riebesell, Ulf, and Philippe D. Tortell. 2011. “Effects of Ocean Acidification on Pelagic Organisms and Ecosystems.” In *Ocean Acidification*. New York, NY: Oxford University Press.
Riebesell, Ulf, I Zondervan, Björn Rost, Philippe D. Tortell, R.E. Zeebe, and Francois Morel. 2000. “Reduced Calcification of Marine Plankton in Response to Increased Atmospheric CO2.” *Nature* 407 (6802): 364–67.
Riegman, Roel. 2002. “The Use of Dissolved Esterase Activity as a Tracer of Phytoplankton Lysis.” *Limnology and Oceanography* 47 (3): 916–20.
Rink, T.J., Roger Tsien, and T Pozzan. 1982. “Cytoplasmic pH and Free Mg2+ in Lymphocytes.” *The Journal of Cell Biology* 95: 189–96.
Roos, Albert, and Walter Boron. 1981. “Intracellular pH.” *Physiological Reviews* 61 (2): 296–434.
Rossoll, Dennis, Rafael Bermúdez, Helena Hauss, Kai G Schulz, Ulf Riebesell, Ulrich Sommer, and Monika Winder. 2012. “Ocean Acidification-Induced Food Quality Deterioration Constrains Trophic Transfer.” Edited by Simon Thrush. *PLoS ONE* 7 (4): e34737. doi:10.1371/journal.pone.0034737.
Rost, Björn, Ulf Riebesell, and Steffen Burkhardt. 2003. “Carbon Acquisition of Bloom-Forming Marine Phytoplankton.” *Limnology and Oceanography* 48 (1): 55–67.
Russell, Bayden, J.I. Thompson, Laura Falkenberg, and Sean Connell. 2009. “Synergistic Effects of Climate Change and Local Stressors: CO2 and Nutrient-Driven Change in Subtidal Rocky Habitats.” *Global Change Biology* 15: 2153–62.
Samuel, Buck S., Abdullah Shaito, Toshiyuki Motoike, Federico E. Rey, Fredrik Backhed, Jill K. Manchester, Robert E. Hammer, et al. 2008. “Effects of the Gut Microbiota on Host Adiposity Are Modulated by the Short-Chain Fatty-Acid Binding G Protein-Coupled Receptor, Gpr41.” *Proceedings of the National Academy of Sciences* 105 (43): 16767–72. doi:10.1073/pnas.0808567105.
Santos, I.R., R.N. Glud, D. Maher, D Erler, and B.D. Eyre. 2011. “Diel Coral Reef Acidificaiton Driven by Porewater Advection in Permeable Carbonate Sands.” *Geophysical Research Letters* 38: L03604.
Shi, Dalin, Yan Xu, Brian M. Hopkinson, and François M. M. Morel. 2010. “Effect of Ocean Acidification on Iron Availability to Marine Phytoplankton.” *Science* 327 (5966): 676. doi:10.1126/science.1183517.
Shi, D, Y Xu, and Francois Morel. 2009. “Effects of the pH/pCO2 Control Method on Medium Chemistry and Phytoplankton Growth.” *Biogeosciences* 6: 1199–1207.
Siu, Gavin, Maria Young, and D.K.O Chang. 1997. “Environmental and Nutritional Factors Which Regulate Population Dynamics and Toxin Production in Teh Dinoflagellate Alexandrium Catenella.” *Hydrobiologia* 352: 117–40.
Solomon, S, D Qin, M Manning, Z Chen, M Marquis, K.B. Averyt, M Tignor, and H.L. Miller, eds. 2007. “Summary for Policymakers.” In *Climate Change 2007: The Physical Science Basis*,

Contribution of Working Group I to the Fourth Assessment Report of the Intergovernmental Panel on Climate Change, 1–18. Cambridge, UK: Cambridge University Press.
Steeman Nielsen, E. 1975. *Marine Photosynthesis with Special Emphasis on the Ecological Aspects*. Amsterdam, Netherlands: Elsevier.
Sunda, William G. 2012. "Feedback Interactions between Trace Metal Nutrients and Phytoplankton in the Ocean." *Frontiers in Microbiology* 3: 204. doi:10.3389/fmicb.2012.00204.
Sunda, William, and Susan Huntsman. 1997. "Interrelated Influence of Iron, Light and Cell Size on Marine Phytoplankton Growth." *Nature* 390: 389–92.
Tagawa, K, and D.I. Arnon. 1962. "Ferredoxins as Electron Carriers in Photosyntehsis and in the Biological Production and Consumption of Hydrogen Gas." *Nature* 195 (4841): 537–43.
Talmage, Stephanie C., and Christopher J. Gobler. 2010. "Effects of Past, Present, and Future Ocean Carbon Dioxide Concentrations on the Growth and Survival of Larval Shellfish." *Proceedings of the National Academy of Sciences* 107 (40): 17246–51. doi:10.1073/pnas.0913804107.
Taylor, Alison, Colin Brownlee, and Glen Wheeler. 2012. "Proton Channels in Algae: Reasons to Be Excited." *Trends in Plant Science* 17 (11): 675–84.
Taylor, Alison, Abdul Chrachri, Glen Wheeler, Helen Goddard, and Colin Brownlee. 2011. "A Voltage-Gated H+ Channel Underlying pH Homeostasis in Calcifying Coccolithophores." *PLOS Biology* 9 (6): e1001085. doi:10.1371/journal.pbio.1001085.
Thomas, H., L.-S. Schiettecatte, K. Suykens, Y. J. M. Koné, E. H. Shadwick, A. E. F. Prowe, Y. Bozec, H. J. W. de Baar, and A. V. Borges. 2009. "Enhanced Ocean Carbon Storage from Anaerobic Alkalinity Generation in Coastal Sediments." *Biogeosciences* 6 (2): 267–274. doi:10.5194/bg-6-267-2009.
Thomas, R.C. 1974. "Intracellular pH of Snail Neurones Measured with the New pH-Sensitive Glass Micro-Electrode." *Journal of Physiology* 238 (1): 159–80.
Tortell, P.D. 2000. "Evolutionary and Ecologiccal Perspectives on Carbon Acquisition in Phytoplankton." *Limnology and Oceanography* 45 (3): 744–50.
Tortell, Philippe D., Christopher D. Payne, Yingyu Li, Scarlett Trimborn, Björn Rost, Walker O. Smith, Christina Riesselman, Robert B. Dunbar, Pete Sedwick, and Giacomo R. DiTullio. 2008. "CO2 Sensitivity of Southern Ocean Phytoplankton." *Geophysical Research Letters* 35 (4): n/a-n/a. doi:10.1029/2007GL032583.
Trimborn, S, N Lundholm, S Thoms, KU Richter, PJ Hansen, and Björn Rost. 2008. "Inorganic Carbon Acquisition in Potentially Toxic and Non-Toxic Diatoms: The Effect of pH-Induced Changes in Seawater Carbonate Chemistry." *Physiologia Plantarum* 133 (1): 92–105. doi:10.1111/j.1399-3054.2007.01038.x.
Uete, Tetsuo, Kumiko Masui, and Machiko Miyauchi. 1985. "Comparison of Substrates for Measuring Serum Choline Esterase Activity in Hepato-Biliary Disease." *Journal of Clinical Chemistry and Clinical Biochemistry* 23: 669–75.
Venn, A.A., Eric Tambutte, S. Lotto, D Zoccola, Denis Allemand, and Sylvie Tambutte. 2009. "Imaging Intracellular pH in a Reef Coral and Symbiotic Anemone." *PNAS* 106 (39): 16574–79.
Waddell, William, and Thomas Butler. 1959. "Calculation of Intracellular pH from the Distribution of 5,5-Dimethyl-2,4-Oxazolidinedione (DMO). Application to Skeletal Muscle of a Dog." *Journal of Clinical Investigation* 38 (5): 720–29.
Waldbusser, George, Elizabeth Brunner, Brian Haley, Burke Hales, Christopher Langdon, and Frederick Prahl. 2013. "A Developmental and Energetic Basis Linking Larval Oyster Shell Formation to Acidification Sensitivity." *Geophysical Research Letters* 40 (10): 2171–76.
Waldbusser, George, and Joseph Salisbury. 2014. "Ocean Acidification in the Coastal Zone from an Organism's Perspective: Multiple System Parameter, Frequency Domains, and Habitats." *Annual Review of Marine Science* 6: 221–47.
Wang, Guizhi, Wenping Jing, Shuling Wang, Yi Xu, Zhangyong Wang, Zhouling Zhang, Quanlong Li, and Minhan Dai. 2014. "Coastal Acidification Induced by Tidal-Driven Submarine Groundwater

Discharge in a Coastal Coral Reef System." *Environmental Science & Technology* 48 (22): 13069–75. doi:10.1021/es5026867.
Weitkunat, Karolin, Sara Schumann, Klaus Jürgen Petzke, Michael Blaut, Gunnar Loh, and Susanne Klaus. 2015. "Effects of Dietary Inulin on Bacterial Growth, Short-Chain Fatty Acid Production and Hepatic Lipid Metabolism in Gnotobiotic Mice." *The Journal of Nutritional Biochemistry* 26 (9): 929–37. doi:10.1016/j.jnutbio.2015.03.010.
Welschmeyer, Nicholas. 1994. "Fluorometric Analysis of Chlorophyll a in the Presence of Chlorophyll B and Pheopigments." *Limnology and Oceanography* 39 (8): 1985–92.
White, A. W. 1976. "Growth Inhibition Caused by Turbulence in the Toxic Marine Dinoflagellate Gonyaulax Excavata." *Journal of the Fisheries Research Board of Canada* 33 (11): 2598–2602. doi:10.1139/f76-306.
Whiteley, Marvin, Erin Brown, and Robert J.C. McLean. 1997. "An Inexpensive Chemostat Apparatus for the Study of Microbial Biofilms." *Journal of Microbiological Methods* 30 (2): 125–32. doi:10.1016/S0167-7012(97)00054-7.
Williams, F.M. 1985. "Clinical Significance of Esterases in Man." *Clinical Pharmacokinetics* 10 (5): 392–403.
Wood, A.M., R.C. Everroad, and L.M. Wingard. 2005. "Measuring Growth Rates in Microalgal Cultures." In *Algal Culturing Techniques*, 269–85. Burlington, MA: Elsevier Academic Press.
Wray, S. 1988. "Smooth Muscle Intraccellular pH: Measurement, Regulation, and Function." *American Journal of Physiology - Cell Physiology* 254 (2): C213–25.
Wu, MM, J Llopis, JM McCaffery, MS Kulomaa, TE Machen, HP Moore, and RY Tsien. 2000. "Organelle pH Studies Using Targeted Avidin and Fluorescein-Biotin." *Chemistry & Biology* 7 (3): 197–209.
Wynn-Edwards, C, R King, S Kawaguchi, A Davidson, S Wright, P.D. Nichols, and P Virtue. 2014. "Development of a Continuous Phytoplankton Culture System for Ocean Acidification Experiments." *Water* 6: 1860–72.
Xu, Sen, and Raj Mutharasan. 2011. "Cell Viability Measurement Using 2′,7′-Bis-(2-Carboxyethyl)-5-(and-6)-Carboxyfluorescein Acetoxymethyl Ester and a Cantilever Sensor." *Analytical Chemistry* 83 (4): 1480–83. doi:10.1021/ac102757q.
Xu, Yan, Dalin Shi, Ludmilla Aristilde, and Francois M. M. Morel. 2012. "The Effect of pH on the Uptake of Zince and Cadmium in Marine Phytoplankton: Possible Role of Weak Complexes." *Limnology and Oceanography* 57 (1): 293–304.
Yang, Zhou, and Fanxiang Kong. 2011. "Enhanced Growth and Esterase Activity of Chlorella Pyrenoidosa (Chlorophyta) in Response to Short-Term Direct Grazing and Grazing-Associated Infochemicals from Daphnia Carinata." *Journal of Freshwater Ecology* 26 (4): 553–61.
Ying, Kezhen, D James Gilmour, and William Zimmerman. 2014. "Effects of CO2 and pH on Growth of the Microalga Dunaliella Salina." *Microbial and Biochemical Technology* 6 (3): 167–73. doi:10.4172/1948-5948.1000138.

APPENDIX A[4]

The front panel and block diagrams constituting the LabVIEW® Virtual Instrument (VI) are shown (Figs. A1–A4) to demonstrate the software/programmatic component of the pHstat system. Figs. A1 and A2 depict the front panel of the two functionalities of the VI. The front panel is the portion of the VI with which the user interacts during an experiment or whenever the VI is running.

The block diagrams contain the actual graphical code for running the LabVIEW® VI (Figs. A3 and A4)., Figs. A3.1–A3.4 and A4.1–A4.3 show the graphical code blocks separated broadly by function. Details on connecting this code language to the electromechanical portion of the pHstat can be found in Golda *et al.* (2017). The figures are followed by operational instructions for using the VI as it operates according to the coding blocks presented in Figs. A3, A4, A3.1–A3.4, and A4.1–A4.3.

Fig. A5 shows the detailed schematic of the electromechanical portion of the pHstat system, the conditioning **g** **e**lectronically **o**perated **r**elay **g**rouping (GEORG).

[4] Reproduced (with edits) with permission from Golda, R., Peterson, and T., Needoba, J. Graphical coding data and operational guidance for implementation or modification of a LabVIEW®-based pHstat system for the cultivation of microalgae. 2017. *Data in Brief*. 12:463-470.

Figure A1: Front panel of virtual instrument (VI) for producing a steady state pH environment.

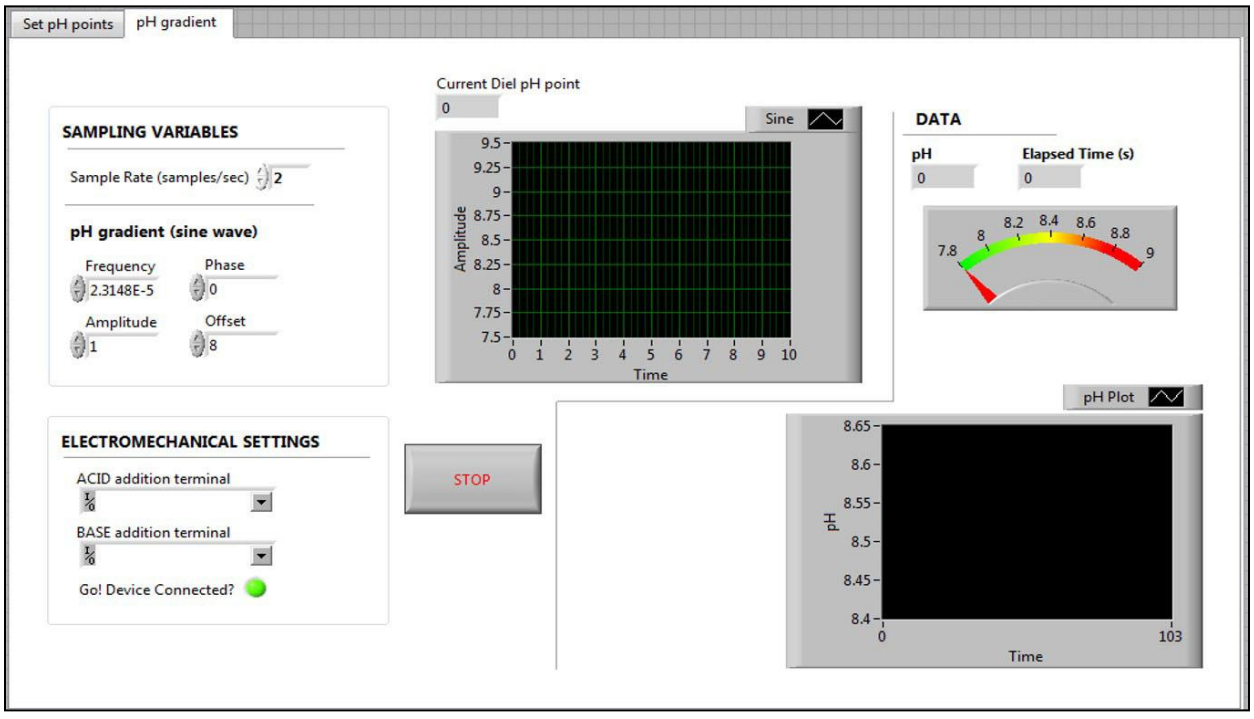

Figure A2: Front panel of virtual instrument (VI) for producing a dynamic pH environment based on a sine wave.

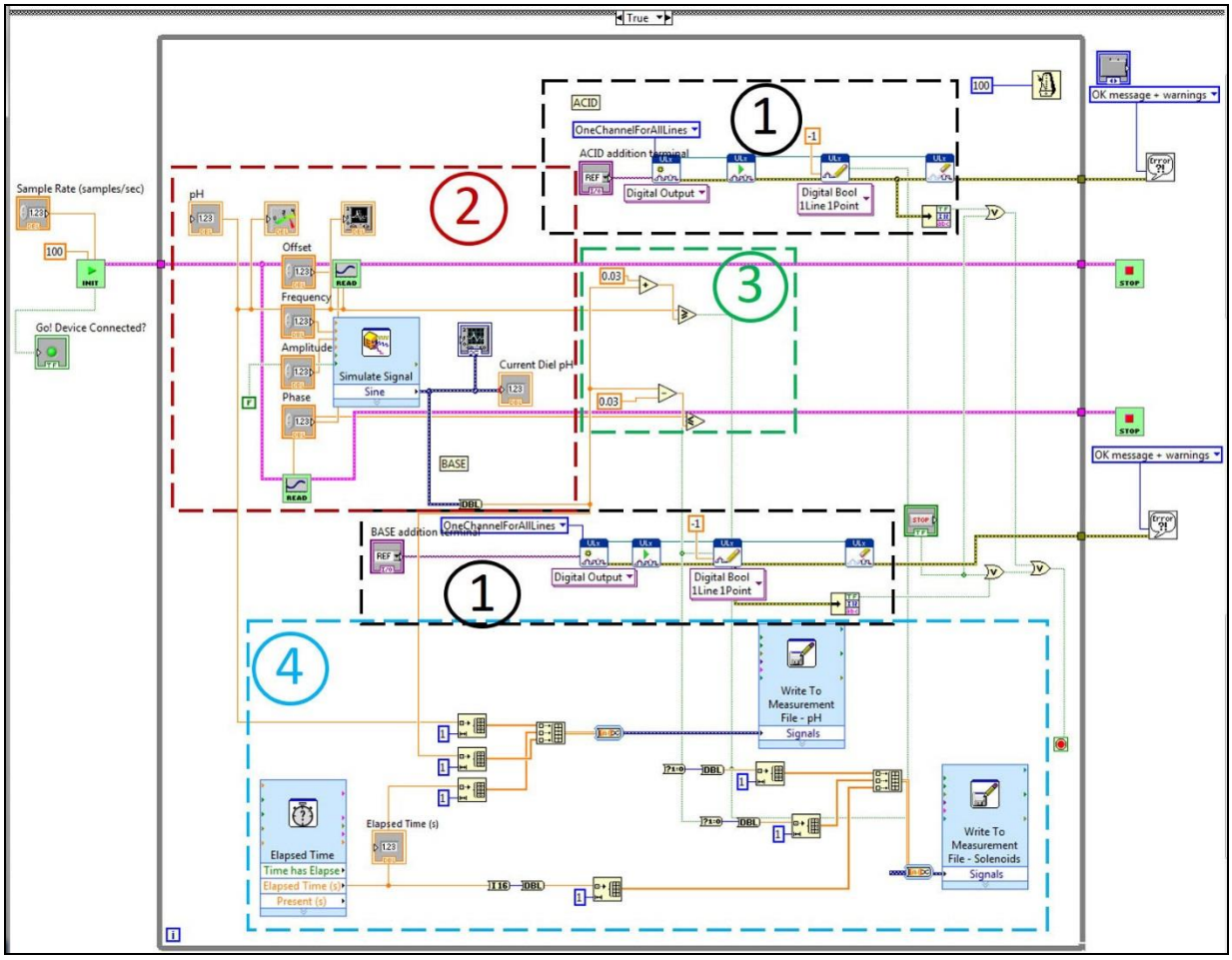

Figure A3: Block diagram for VI showing graphical code for dynamic pH functionality. Sections 1, 2, 3, and 4 match up to Figs. A3.1, A3.2, A3.3, and A3.4, respectively.

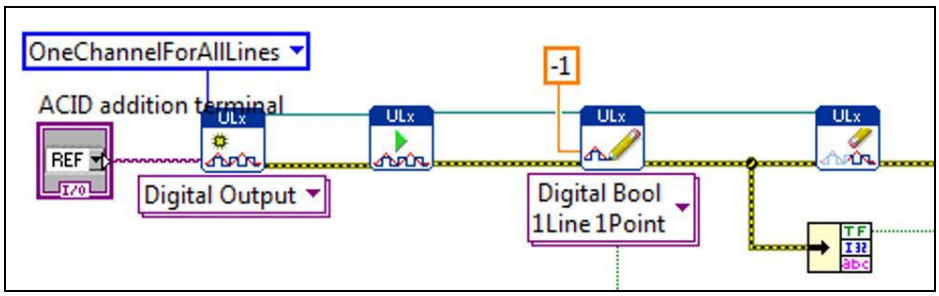

Fig. A3.1: Section 1 from Fig. A3 expanded to show programmatic detail. Depicts graphical code for connecting the MC control board to the pHstat system.

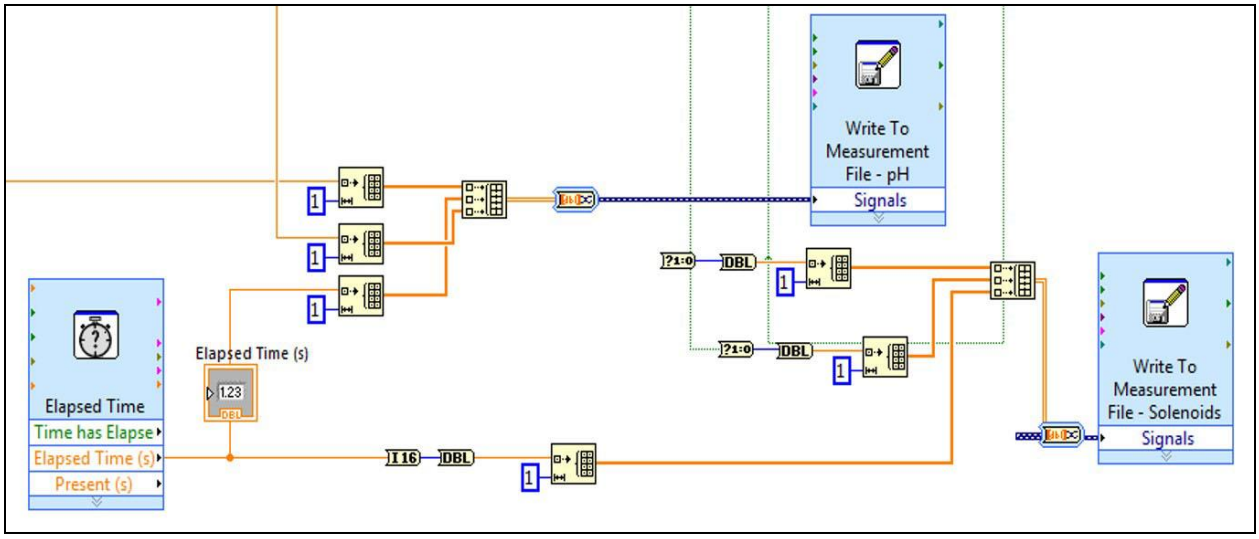

Fig. A3.2: Section 2 from Fig. A3 expanded to show programmatic detail. Depicts graphical code for generating and recording data from the subVIs "Elapsed Time," "Write to Measurement File – pH," and "Write to Measurement File – Solenoids."

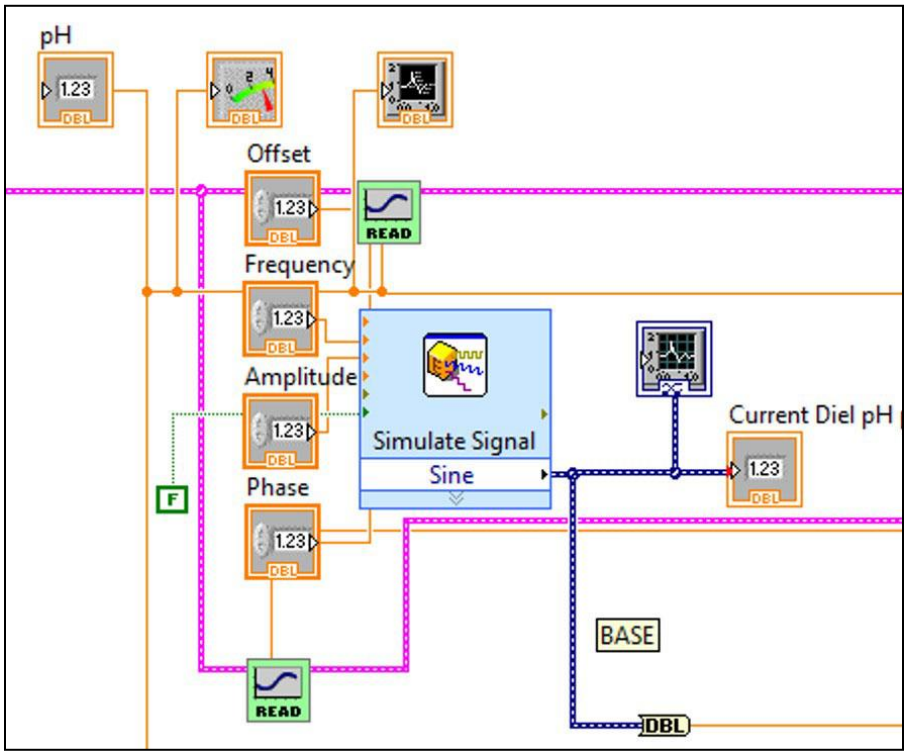

Fig. A3.3: Section 3 from Fig. A3 expanded to show programmatic detail. Shows subVI for providing the guide pH for the dynamic functionality of the pHstat. Guide pH is generated using a sine wave, with the user setting the frequency, offset, amplitude, and phase in order to time the wave to start at a desired pH.

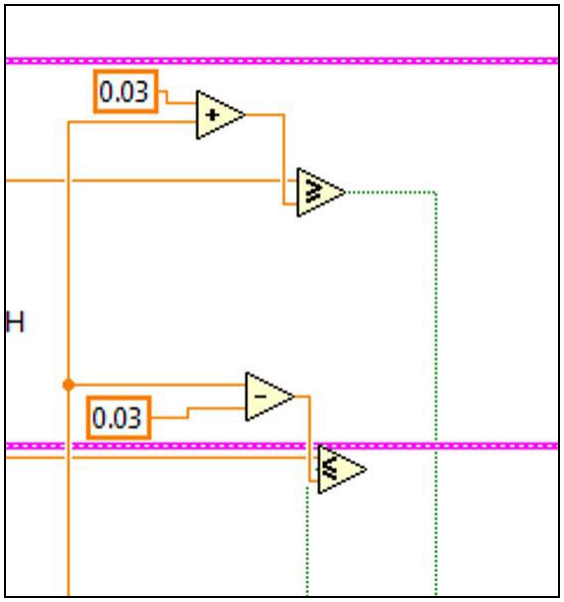

Fig. A3.4: Section 4 from Fig. A3 expanded to show programmatic detail. Depicts programmatic element of pH control using Boolean operators to maintain pH thresholds within a set pH points of the guide pH at any given time.

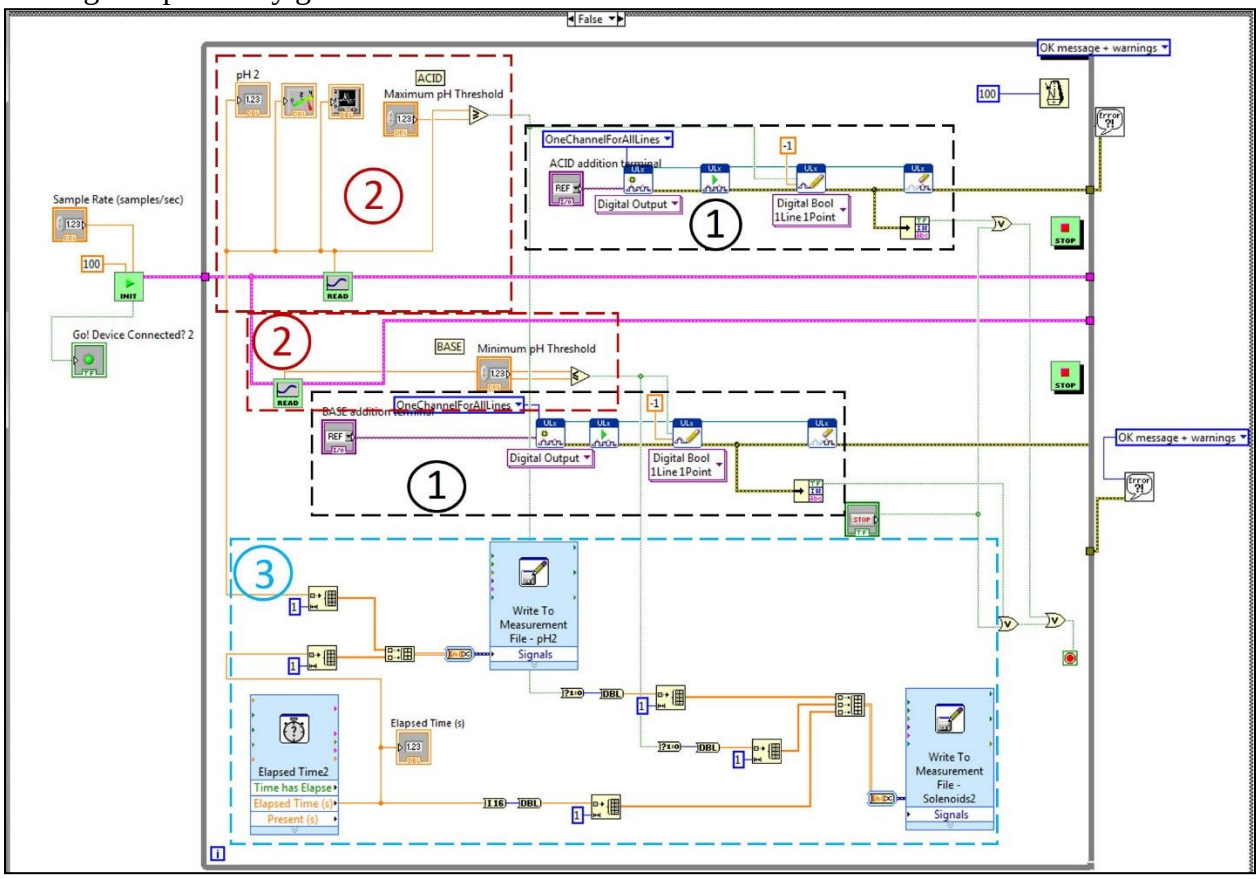

Figure A4: Block diagram for VI showing graphical code for steady state pH functionality. Sections 1, 2, and 3 match up to Figs. A4.1, A4.2, and A4.3, respectively.

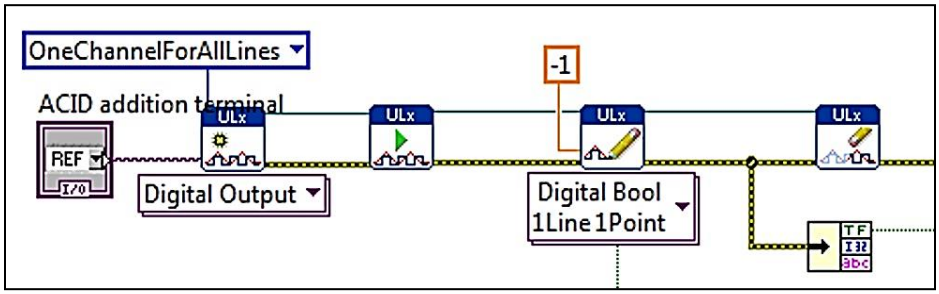

Figure A4.1: Section 1 from Fig. A4 expanded to show programmatic detail. Depicts graphical code for connecting the MC control board to the pHstat system.

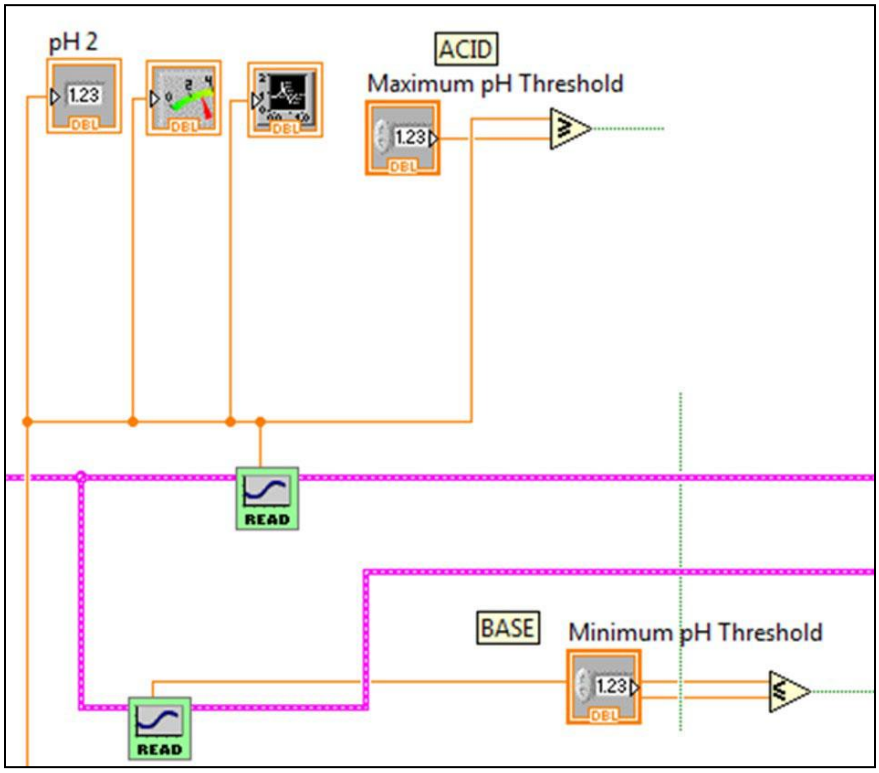

Figure A4.2: Section 2 from Fig. A4 expanded to show programmatic detail. Depicts programmatic element of pH control using front panel indicators to maintain pH within thresholds. Broken wires connect to other elements, which were deleted for clarity.

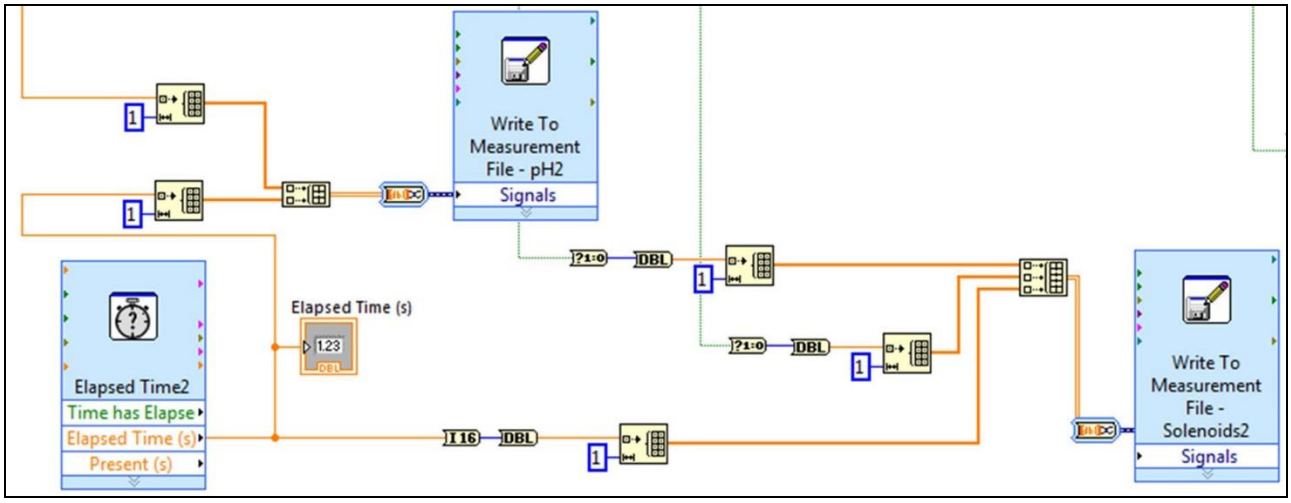

Figure A4.3: Section 3 from Fig. A4 expanded to show programmatic detail. Depicts graphical code for generating and recording data from the subVIs "Elapsed Time," "Write to Measurement File – pH," and "Write to Measurement File – Solenoids."

Operation of the VI

This section describes how to operate the virtual instrument (VI) that runs the pHstat system. We recommend that the user disable the "Sleep" and "Hibernate" settings on their computer when using the VI, as these functions interrupt VI continuity.

A) Setting up the system

IMPORTANT: Due to the risk of electrical shock, whenever the user is setting up or handling the electronic or electromechanical portions of this system, they should ensure that the system is not connected to any power supply. This includes computer connections and wall sockets. All connections to power sources should be made after the user has completed hands-on work with the system.

1) Install drivers and necessary software for pH probe and digital input/output (I/O) device.
2) Connect the pH probe to the computer (if using a Go!Link (Vernier), connect the probe to the Go!Link, then connect the Go!Link to the computer).

3) Connect the relay array (GEORG) to the digital I/O device by inserting the appropriate wires into the screw terminals of the I/O device. A pinout diagram of the screw terminals should be available in the manual for the I/O device. We used a USB-1024LS digital I/O device (Measurement Computing Corporation, Norton, MA) as an interface between the VI and the relay array. NOTE: This device is sensitive to electrostatic discharge (ESD). We suggest the operator grounds himself/herself prior to touching this device.
4) Connect GEORG to the pH modification manifolds using the custom input/output cables. Make sure that each relay for GEORG is connected to the appropriate solenoid valve on the modification manifold. Use Figure 3 for relay orientation.
5) Connect the digital input/output device to the computer using the provided universal serial bus (USB) connector cable.
6) Connect GEORG's power supply to the wall.

B) Operating the VI during an experiment
1) Complete setup steps detailed in section A of this appendix.
2) ELECTROMECHANICAL SETTINGS
    a. These terminals correspond to the screw terminals chosen to activate the acid/base solenoids on the pH modification manifolds.
    b. Use the pinout diagram associated with the digital I/O device to choose the appropriate terminals.
3) SAMPLING VARIABLES
    a. Select VI functionality (front panel). Default setting is Steady-state; press button labeled "pH Gradient (ON/OFF)" to switch to a dynamic pH regime.

b. Use tabs at top of screen to set parameters for pH regime.

c. FOR STEADY-STATE PH

i. Set minimum pH threshold.

ii. Set maximum pH threshold.

iii. Set sample rate. NOTE: If using the reagent manifold do not set the sample rate for more than 2 samples per second; this will cause the system to overcompensate and result in loss of pH control.

d. FOR DYNAMIC PH

i. Set sample rate.

ii. Set parameters for guide pH, "pH gradient (sine wave)," including frequency, amplitude and offset (mid-point pH).

4) Press "Run" button (arrow at top left corner).

5) Save data when prompted. There will be two save prompts; one is for the pH data, the other is for the solenoid activity data. If the user doesn't want to save their data click "Cancel" for each save prompt and confirm "Do not save."

6) To stop the experiment, press the "STOP" button.

7) Real-time data is shown on the right side of the screen. pH data is displayed as a numerical value, on a scale meter and as a waveform chart. Elapsed time is given in seconds. Solenoid activity data is not displayed, and must be accessed directly from the saved data.

8) Data is saved as a .lvm file.

C) Data Processing

1) Data is saved as a .lvm file.

2) This file type can be opened using Microsoft® Excel or Notepad.

3) Data is given in column format. The first column is blank for both data types.

4) For the pH data sets, column 2 is pH data, column 3 is elapsed time in seconds.

For the solenoid activity data, column 2 is the activity data for the acid-dispensing solenoid, column 3 is the activity data for the base-dispensing solenoid, and column 4 is the elapsed time in seconds.

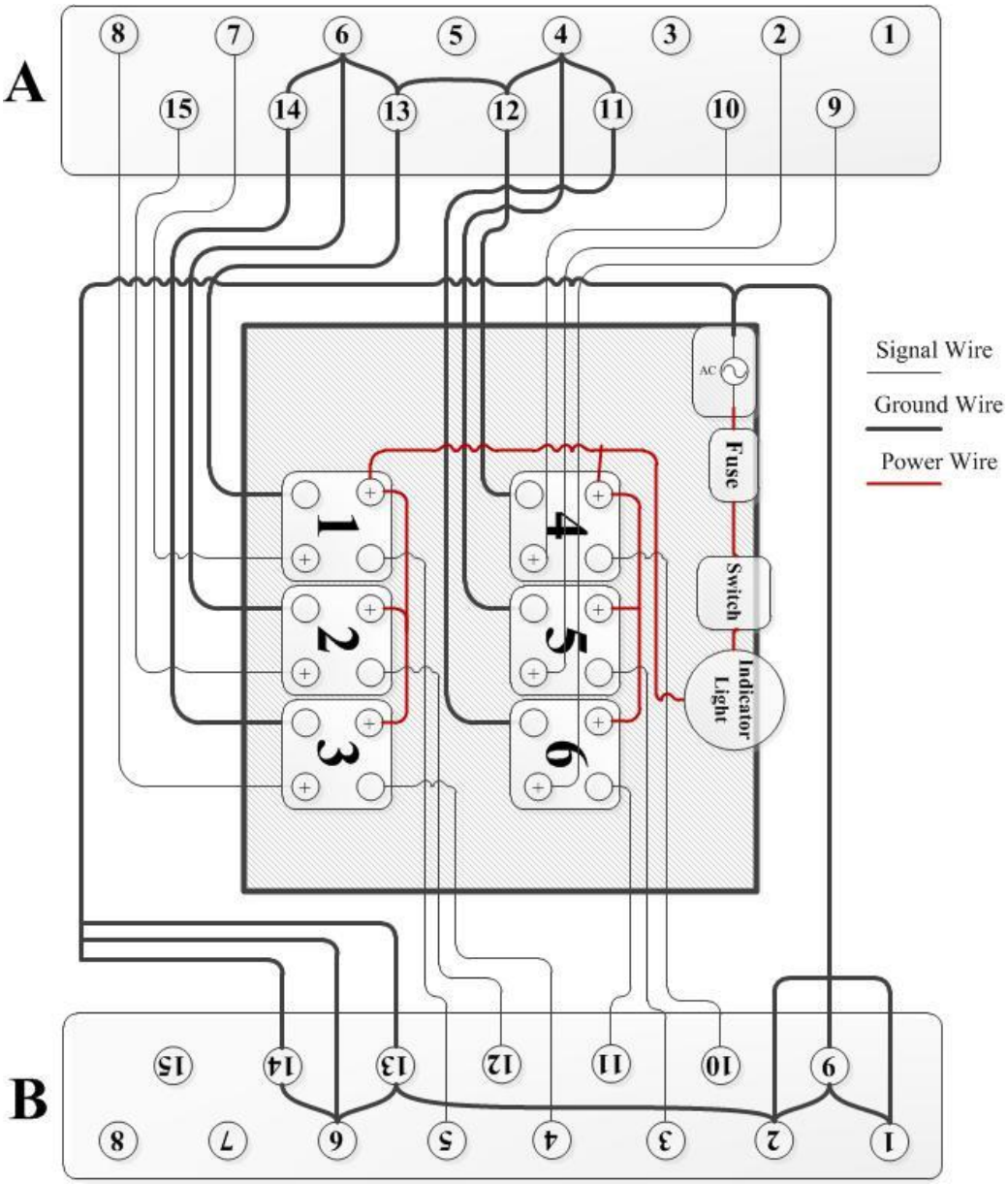

Figure A5: Schematic of GEORG, with wiring diagram for DB15 (D-subminiature, 15 pin) connectors mounted on the box. A and B indicate DB15 connectors that provide signal transfer to and from GEORG, respectively. A is a male DB15 that receives signals from the computer; B is a female DB15 that transmits signals to the pH modification manifolds. Connector cables from the digital input/output device and to the pH-modification manifolds must be customized to match these DB15 connectors. Red lines indicate power supply wires, bold black lines indicate ground wires, thin black lines indicate signal wires running from the computer.

APPENDIX B

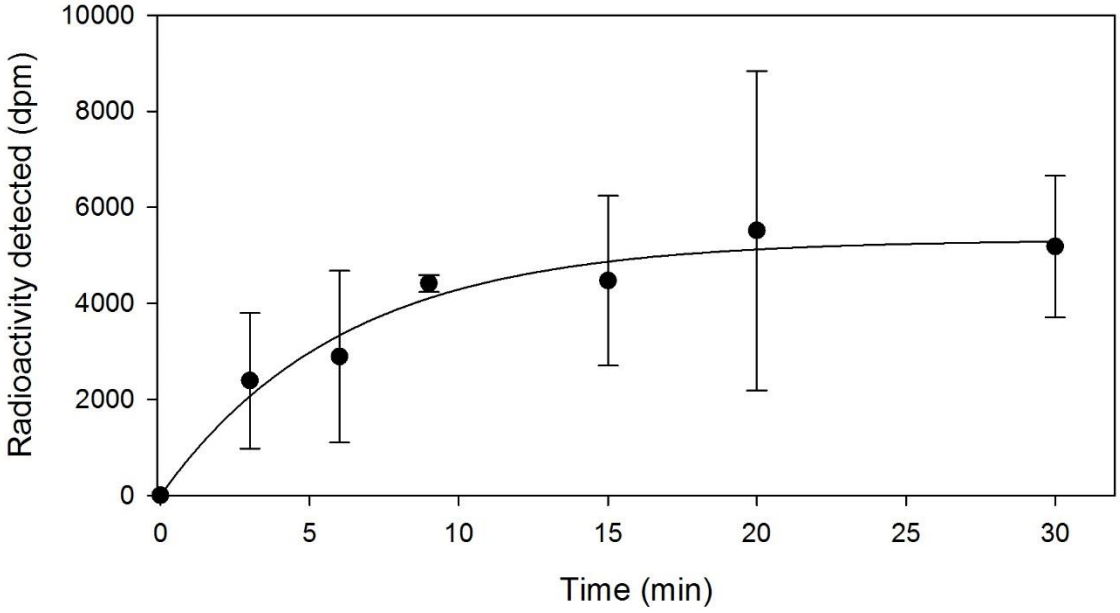

Figure B1: Uptake curve for ^{14}C-DMO. Error bars indicate standard deviation.

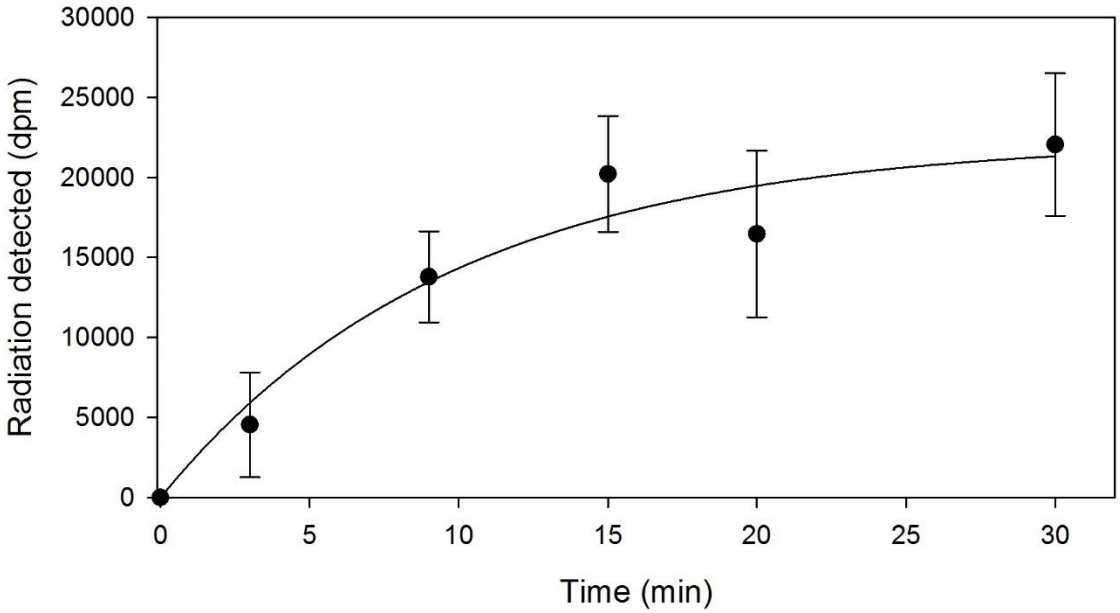

Figure B2: Uptake curve for tritiated water. Error bars indicate standard deviation.

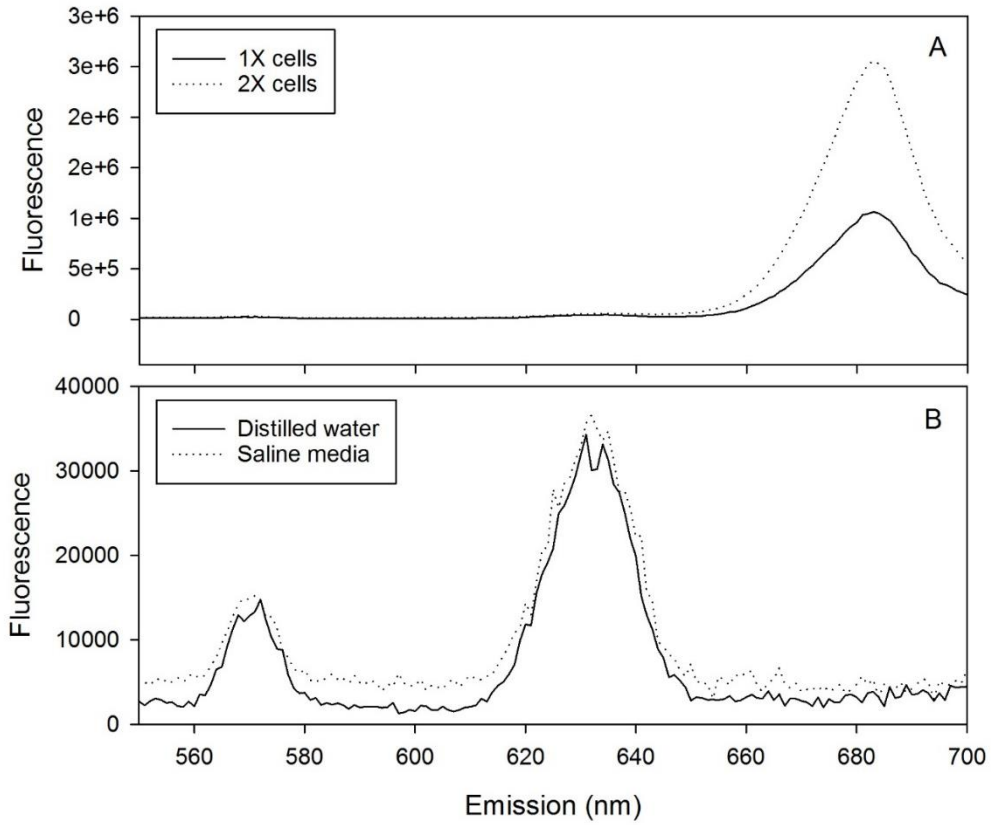

Figure B3**:** Fluorescence spectra for two concentrations of cells (A), and distilled water, saline media (ESAW) overlaid (B).

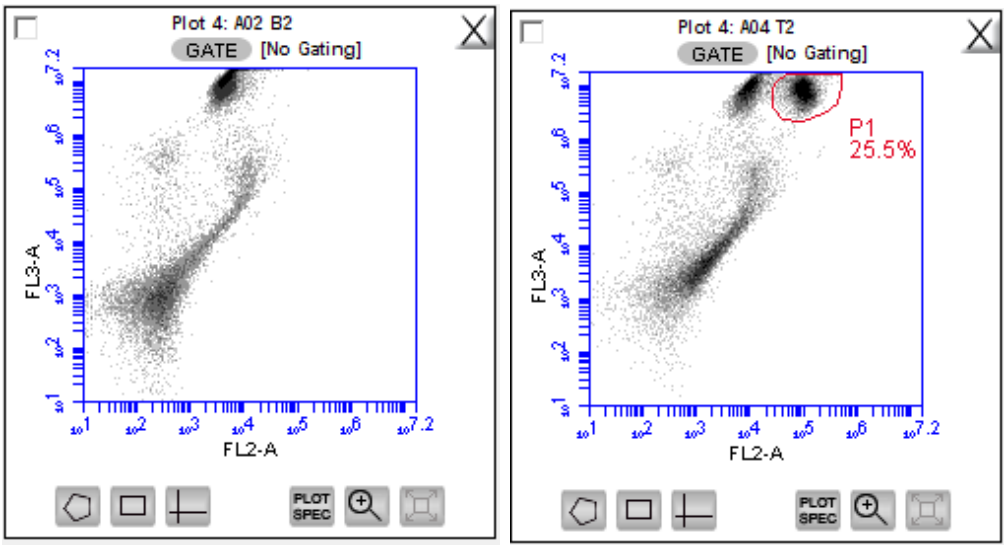

Figure B4: Cytograms from flow cytometric analysis of *Alexandrium tamarense*. Excitation: 488 nm. Emission: 670 nm . Note the gated region (P1) showing the population of cells exhibiting increased fluorescence in the SNARF-treated cells on the right, as compared to the cells not exposed to SNARF (left).

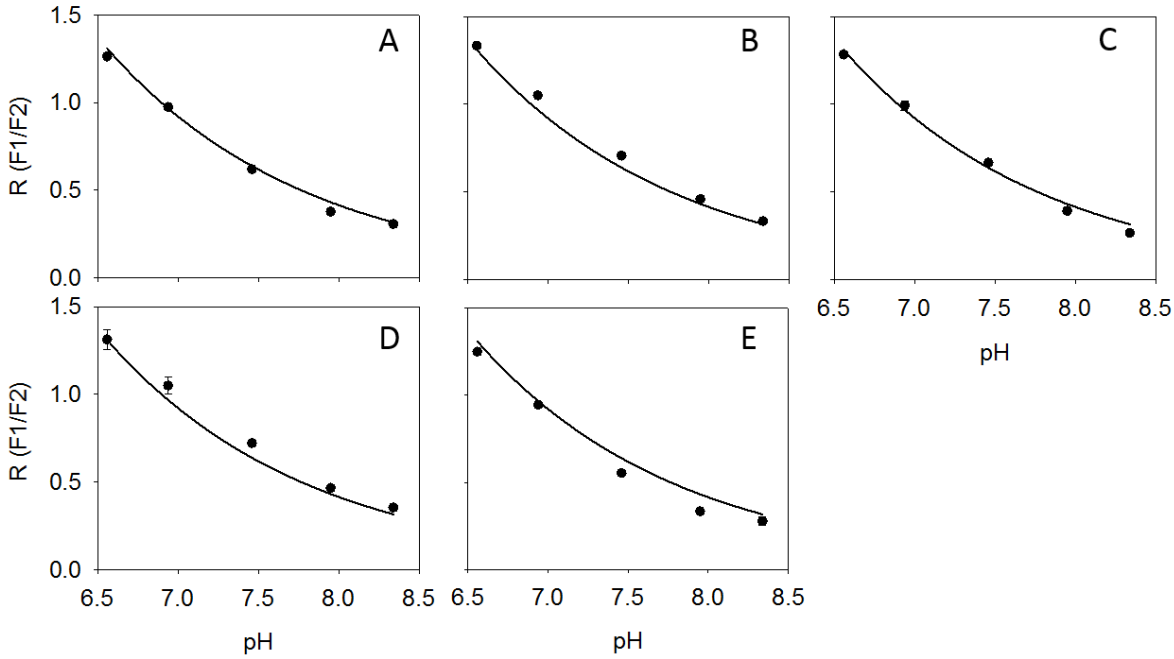

Figure B5: Fluorescence spectroscopy calibration curves for A) *Alexandrium tamarense*, B) *Isochrysis galbana*, C) *Thalassiosira weissflogii*, D) *Dunaliella salina*, E) *Thalassiosira pseudonana*. Error bars indicate standard deviation

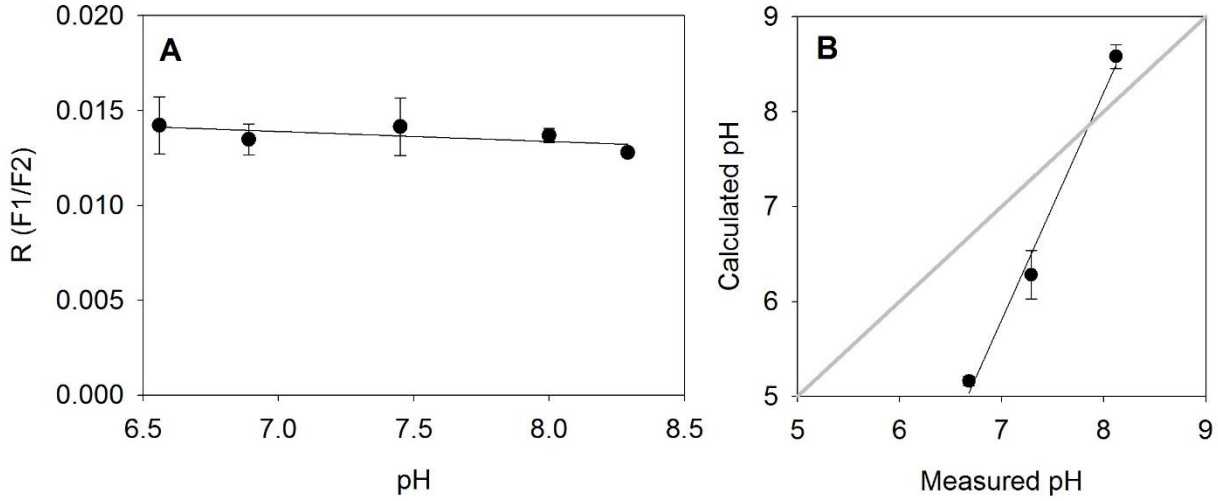

Figure B6: (A) Calibration curve for pH(i) in *Alexandrium tamarense* determined using flow cytometric detection of SNARF. R is the ratio of mean fluorescence emission intensity of the SNARF peaks (F1, F2). Error bars represent ± standard deviation from mean R values. (B) Calculated pH vs. measured pH determined following addition of nigericin in *Alexandrium tamarense*.

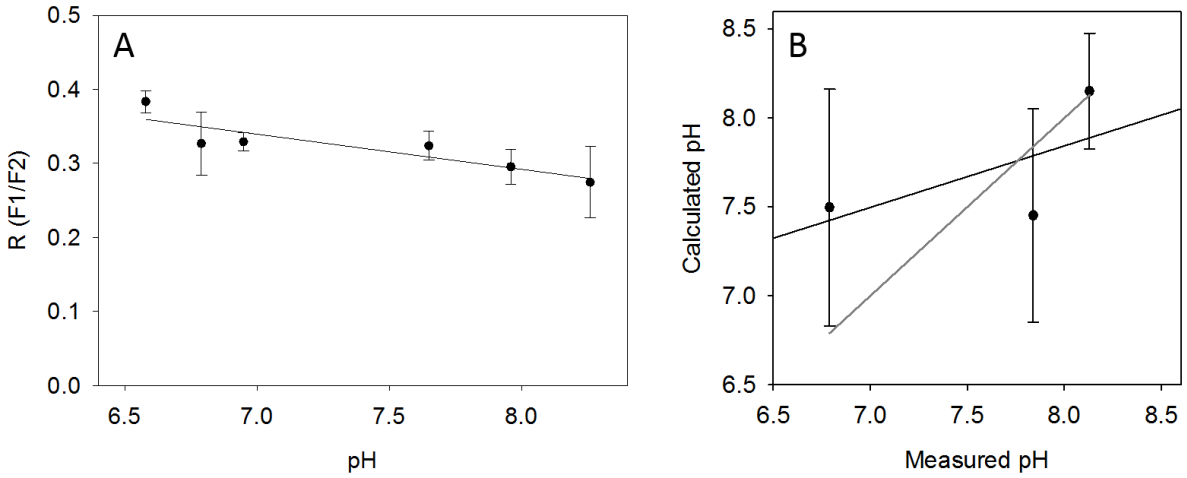

Figure B7: (A) Calibration curve for pH(i) in *T. weissflogii* determined using flow cytometric detection of SNARF. R is the ratio of mean fluorescence emission intensity of the SNARF peaks (F1, F2). Error bars represent ± standard deviation from mean R values. (B) Calculated pH vs. measured pH determined following nigericin equilibration of *T. weissflogii.*

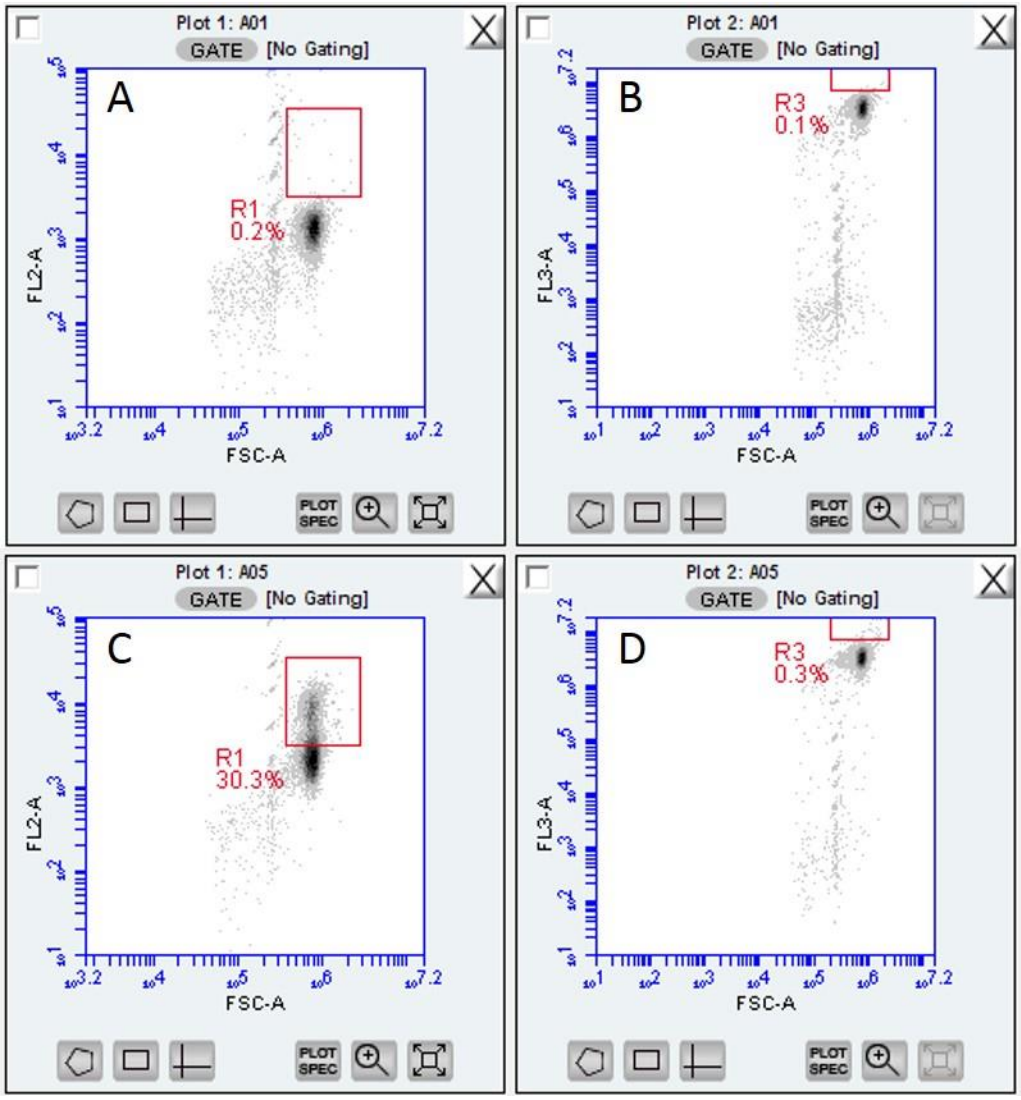

Figure B8: Gating for SNARF at peak F1 (A,C) and peak F2 (B,D). Note the significant shift for F1 peak.

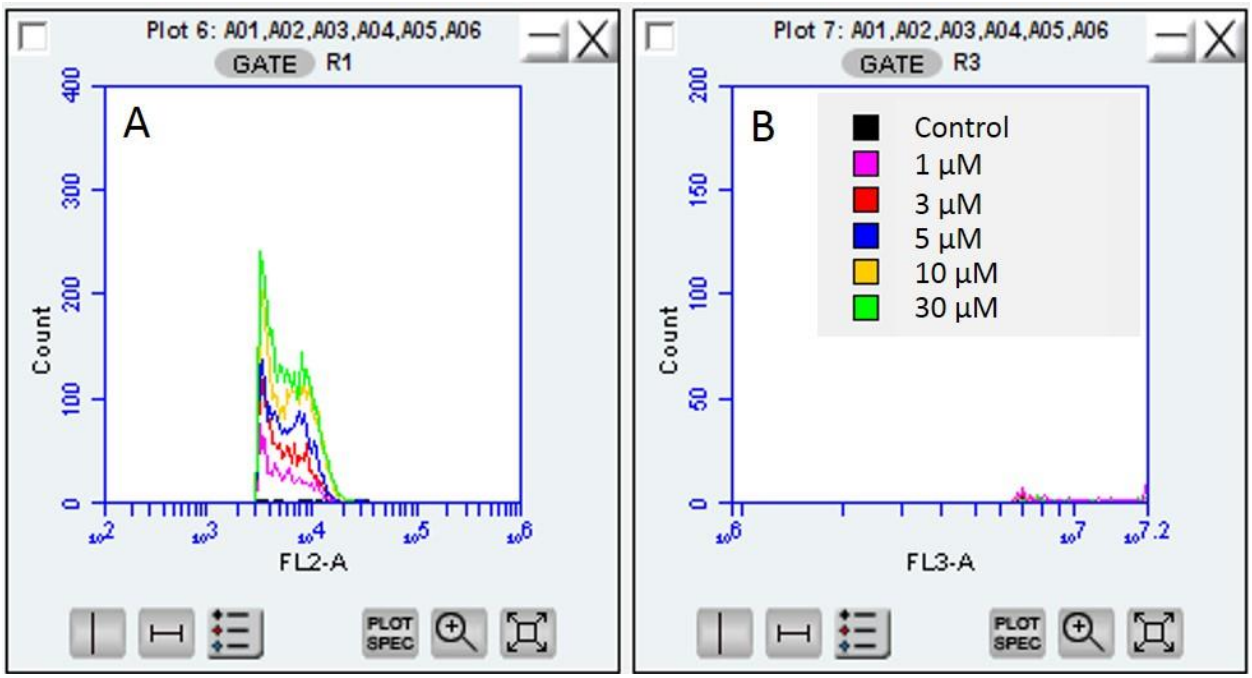

Figure B9: Plots showing distribution of SNARF fluorescent cells for F1 peak (A) and F2 peak (2). While the F1 peak showed increasing fluorescence corresponding with increasing dye concentration, the F2 peak showed no virtually no SNARF fluorescence, regardless of dye concentration.

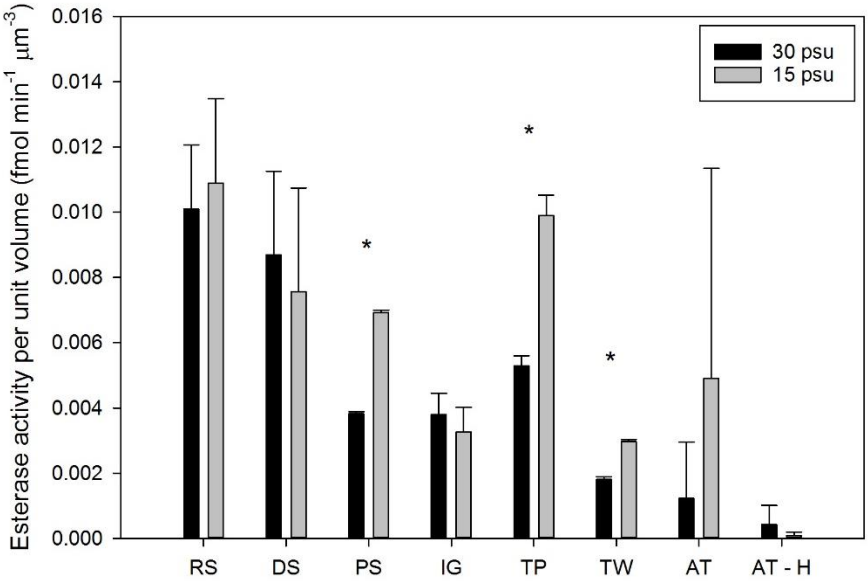

Figure B10: Comparisons of esterase activity per unit of cellular volume (μm^3) when exposed to varying salinities. Esterase activity per unit cellular volume (fmol min^{-1} μm^{-3}) was corrected for vacuole volume. Column pairs with a (*) indicate organisms for which the esterase activity was significantly different ($p \leq 0.05$) between the 30 PSU and 15 PSU treatments. Error bars represent ± 1 standard deviation. RS = *R. salina*, DS = *D. salina*, PS = *Phytomonas* sp., IG = *I. galbana*, TP = *T. pseudonana*, TW = *T. weissflogii*